SIMULATION AND DESIGN OF ELECTRON GUN FOR TRAVELLING WAVE TUBE WITH PARTICLE IN CELL CODE

A THESIS SUBMITTED TO
THE GRADUATE SCHOOL OF NATURAL AND APPLIED SCIENCES
OF
MIDDLE EAST TECHNICAL UNIVERSITY

BY

FİLİZ ECE SAĞCAN

IN PARTIAL FULLFILLMENT OF THE REQUIREMENTS
FOR
THE DEGREE OF MASTER OF SCIENCE
IN
ELECTRICAL AND ELECTRONICS ENGINEERING

MAY 2014

Approval of the thesis:

SIMULATION AND DESIGN OF ELECTRON GUN FOR TRAVELLING WAVE TUBE WITH PARTICLE IN CELL CODE

submitted by **FİLİZ ECE SAĞCAN** in partial fulfillment of the requirements for the degree of **Master of Science in Electrical and Electronics Engineering Department, Middle East Technical University** by,

Prof. Dr. Canan Özgen
Dean, Graduate School of **Natural and Applied Sciences** _____

Prof. Dr. Gönül Turhan Sayan
Head of Department, **Electrical and Electronics Eng.** _____

Prof. Dr. Şimşek Demir
Supervisor, **Electrical and Electronics Eng. Dept., METU** _____

Examining Committee Members:

Prof. Dr. Canan Toker
Electrical and Electronics Eng. Dept., METU _____

Prof. Dr. Şimşek Demir
Electrical and Electronics Eng. Dept., METU _____

Prof. Dr. Altunkan Hızal
Electrical and Electronics Eng. Dept., METU _____

Prof. Dr. Sencer Koç
Electrical and Electronics Eng. Dept., METU _____

Ahmet Kırlılar, M.Sc.
Manager, ASELSAN _____

Date: 26/05/2014

I hereby declare that all information in this document has been obtained and presented in accordance with academic rules and ethical conduct. I also declare that, as required by these rules and conduct, I have fully cited and referenced all material and results that are not original to this work.

Name, Last name: Filiz Ece SAĞCAN

Signature :

ABSTRACT

SIMULATION AND DESIGN OF ELECTRON GUN FOR TRAVELLING WAVE TUBE WITH PARTICLE IN CELL CODE

Sağcan, Filiz Ece

M. Sc., Department of Electrical and Electronics Engineering

Supervisor: Prof. Dr. Şimşek Demir

May 2014, 117 pages

Vacuum tubes are widely used microwave devices in many applications such as radar and telecommunication. Electron gun is very important component of a vacuum device since it generates electron beam into the device to interact with electromagnetic waves. Electron gun structures vary according to application and type of vacuum device. In order to design and simulate electron gun, Particle in Cell codes which solves the problems with charged particle motion, are used.

In this thesis, various types of electron gun for Travelling Wave Tube are investigated. First, Pierce gun parametrical simulation is performed by CST PS Tracking Solver. Effects of simulation parameters are compared with respect to beam current, perveance, beam waist radius and beam waist position. After Pierce gun simulation, electron guns having special usage are simulated and optimized according to Pierce gun results. In this simulation, Pinto-Xavier-Motta, dual anode and annular beam electron gun was constructed and simulated in CST PS and their electron beam characteristics are examined.

Keywords: Vacuum tube, Electron gun, Particle-in-Cell code, Travelling wave tube

ÖZ

HÜCREDE PARÇACIK KODU İLE YÜRÜYEN DALGA TÜPÜ İÇİN ELEKTRON TABANCASI BENZETİMİ VE TASARIMI

Sağcan, Filiz Ece
Yüksek Lisans, Elektrik ve Elektronik Mühendisliği Bölümü
Tez Yöneticisi: Prof. Dr. Şimşek Demir
May 2014, 117 sayfa

Vakum tüpleri radar ve telekomünikasyon gibi alanlarda sıkça kullanılan mikrodalga cihazlardır. Elektron tabancası vakum tüp içerisinde elektromanyetik dalgayla etkileşecek elektron huzmesini oluşturur, bu sebeple vakum tüplerinin önemli bir elemanıdır. Elektron tabancası mimarisi uygulamaya ve vakum cihazının tipine göre değişiklik gösterir. Bir elektron tabancası tasarlamak ve benzetimini yapmak için hareket halindeki yüklü parçacık problemlerini çözebilen Hücrede Parçacık kodlarının kullanılması gerekmektedir.

Bu tezde, Yürüyen Dalga Tüplerinde kullanılabilinecek farklı tiplerdeki elektron tabancaları incelenmiştir. İlk olarak, Pierce tabancasının parametrik benzetimi CST PS Tracking Solver kullanılarak gerçekleştirilmiştir. Elektron tabancası parametrelerinin etkileri huzme akımı, perveance, huzme bel yarıçapı ve huzme bel pozisyonuna göre karşılaştırılmıştır. Pierce tabancası benzetiminden sonra, özel kullanımlara sahip elektron tabancaları Pierce tabancası benzetiminden elde edilen sonuçlara göre simüle edilmiş ve eniyilenmiştir. Bu benzetimde Pinto-Xavier-Motta, ikili anotlu ve halka huzmeli elektron tabancası CST PS benzetim ortamında oluşturulup benzetimi yapılmıştır ve huzme özellikleri incelenmiştir.

Anahtar Kelimeler: Vakum tüp, Elektron tabancası, Hücrede Parçacık kodu, Yürüyen Dalga Tüpü

To my family,

Aysel Sağcan,

Yusuf Vefa Sağcan,

Gülseli Sağcan,

Emre Kafa,

and

to my love,

Tayfun Filci

ACKNOWLEDGEMENTS

First of all, I would like to express my deepest gratitude to my family Aysel Sağcan, Vefa Sağcan, Gülseli Sağcan and Emre Kafa for their loving and continued support.

I cannot express enough thanks to my advisor, Prof. Dr. Şimşek Demir for his excellent guiding, caring, patience and encouragement throughout the thesis. I had an outstanding research activity under his supervision.

I am grateful to ASELSAN Electronic Industries for giving me opportunity to improve my engineering capabilities and for providing me every kind of hardware, software and financial support.

I would like to thank my home mates Fatma Nesrin Ergin, Meltem Haykır and Servet Çağlayan and my precious friends, Emine Demiryapan, Esra Savari and Funda Çoktaş, Nagihan Usturalı, Ceyda Kuzuoğlu and Berçin Özteke for their helping and patience. In addition, I would also thank my colleagues in ASELSAN.

I would like to extend my special appreciation to my love Tayfun Filci for his support, patience, and kindness throughout my graduate study.

TABLE OF CONTENTS

LIST OF TABLES

TABLES

LIST OF FIGURES

FIGURES

LIST OF ABBREVIATIONS

A_c	: Control Anode
A_i	: Ion Barrier Anode
A_g	: Ground Anode
AM	: Amplitude Modulation
BWO	: Backward Wave Oscillator
CST PS	: Computer Simulation Technology Particle Studio
CW	: Continuous Wave
DC	: Direct Current
EM	: Electromagnetic
FM	: Frequency Modulation
FDTD	: Finite Difference Time Domain
HPM	: High Power Microwave
METU	: Middle East Technical University
PEC	: Perfect Electric Conductor
PIC	: Particle-in-Cell
PM	: Particle Monitor
PPM	: Periodic Permanent Magnet
RF	: Radio Frequency
SLAC	: Stanford Linear Accelerator Center
SWS	: Slow Wave Structure
TWT	: Travelling Wave Tube
TWTA	: Travelling Wave Tube Amplifier
TV	: Television
Vircator	: Virtual Cathode Oscillator

CHAPTER 1

INTRODUCTION

Historically the first microwave active device is a vacuum tube. Magnetron being the first RF generator appeared in the 1920s. Then on, a number of different versions of vacuum tubes are designed and used. Following the invention of semiconductor transistors, the popularity of the vacuum tubes decreased. Nevertheless, due to certain reasons, the use of the tubes never ceased out and its technology and application areas become more widespread including High Power Microwaves and micro-vacuum electronic devices.

Microwave vacuum tubes have been used in many applications as an oscillator or a high power amplifier. Contemporary vacuum tube applications cover the 300 MHz to 100 GHz frequency range even reaching to THz band. Although transistor and integrated circuit technologies are developing extremely fast, microwave tubes technology continues its improvement and it is still an important constituent of RF technology today.

Application areas of microwave tubes are very wide; many of them are used in short wave radio, AM and FM radio broadcasting, TV and satellite communication. In addition, microwave tubes are used mostly in radar and military system, especially airborne. Industrial, scientific and medical applications may also require microwave tubes [1], [2].

There are many different types of microwave vacuum tubes designed for various reasons. Nevertheless, operation principle of vacuum tubes is basically the same;

electron beam injected by an electron gun interacts with the RF wave, consequently amplification or oscillation occurs according to the tube geometry. Microwave tubes differ according to this interaction mechanism, which are detailed in Chapter 2. Klystrons, inductive output tube, travelling wave tube, backward wave oscillator, magnetron and cross field amplifiers are some of the widely used microwave tubes.

Among the other vacuum tubes, Travelling Wave Tube (TWT) has the highest commercial market; it represents over 50% of all sales of microwave vacuum electronic devices. TWT is a linear beam microwave tube whose power level may range from a few watts to several tens of MW and its frequency ranges from 1 GHz to 100 GHz. Until recently, they are used in nearly all communications satellites, radar system and electronic countermeasures systems as an amplifier [3]. All TWTs consists of an electron gun, a slow wave circuit and a collector. The elements of RF generation are electron beam formation and acceleration in the electron gun, power transfer from the electron beam to the amplified RF wave in an interaction section and collection of the spent electron beam in a collector [1]. RF input and output couplers and magnetic beam focusing system are additional elements in a TWT.

TWT design can be split into two as the design of DC and RF circuits. The DC TWT circuit is composed of an electron gun, a drift tube and an electron collector [4]. Electron gun plays a crucial role in the TWT DC circuit design, because the electron gun provides an electron beam in an appropriate shape and intensity to interact RF wave travelling along the slow wave structure. Thermionic cathode is the most common electron gun in TWTs.

In thermionic cathodes, electron beam is generated by heating the cathode to sufficiently high temperatures to decrease the work function and then applying a high electric potential difference between anode and cathode [4]. The quality of the electron beam can be expressed with various parameters which are explained in the following chapters. In order to create high quality and non-divergent beam, some focusing elements can be added to the electron gun design. The electron gun should provide desired electron beam current and beam quality to obtain linear, reliable and long-lived TWT. Therefore, the design of electron gun becomes very important.

There are various parameters which affect the beam quality and should be taken into account in electron gun design. Electrical design parameters are focusing electrode biasing voltage and potential difference between cathode and anode. On the other hand, mechanical parameters such as cathode radius, anode height, cathode anode distance and focusing electrode angle should be selected properly. In order to reduce cost and time and obtain optimal electron gun design, simulation programs are used widely.

Although, there had been some electron gun applications in the literature, the first analytical solution of electron gun was expressed by J. R. Pierce. Moreover, he proposed electron gun which corrects deficiencies of previous guns and this electron gun was called Pierce electron gun. Therefore, today's electron gun design is based on mostly Pierce electron gun.

In this thesis work, Pierce electron gun designs are carried out and the role of each electrical and mechanical parameters of Pierce electron gun is investigated. For this purpose, electron beam and field interaction formulations are examined and numerical solution methods are elaborated.

There are various methods such as beam tracking and PIC (Particle-in-Cell) and various software such as TRAK, KARAT, EGUN, MAGIC, and CST Particle Studio. For understanding the vacuum tubes, due to availability limitations, CST Particle Studio and MAGIC software are used within the context of this thesis. Moreover, CST Particle Studio is used extensively for parametric analysis of the Pierce Gun designs of the thesis studies.

The parametric analysis enabled us the understanding of how each design parameter of electron gun affects each beam parameter, namely beam current, beam waist radius and beam waist position. In addition, various electron gun geometries in literature are studied and based on the available information specific designs are carried out. On these designs, parametric analysis are performed for gaining insight in the operation of the electron gun.

Based on the above mentioned content, this thesis is organized as follows. Initially, Chapter 1 will describe briefly the vacuum electronic device, travelling wave tubes and electron gun. Previous work in literature about electron gun is also given in Chapter 1. In Chapter 2, electron beam parameters will be introduced and the analytical analysis of planar and cylindrical Pierce gun will be given. In Chapter 3, PIC codes and CST Particle Studio simulation tool is briefly mentioned. Moreover, detailed parametric analysis of Pierce gun will be given. In Chapter 4, electron gun parameter for TWT will be discussed and present electron gun designs will be simulated by CST. Finally, the thesis work is ended by giving summary, conclusion and future work.

CHAPTER 2

LITERATURE RESEARCH

2.1 Microwave Tubes

Microwave tubes are used as oscillators and powerful amplifiers for more than 60 years and their frequency range is from 300 MHz to several hundreds of GHz [1]. They can be classified according to working principle, frequency or output power. The frequency - power relationship of various microwave tubes for CW and peak power is shown in Figure 1.

A microwave tube is vacuum device in which electrons and electromagnetic waves interact. In the tube, electron beam give up some of the energy to electromagnetic energy, thus generation or amplification of electromagnetic wave occurs. Vacuum tube geometry and interaction procedure decide type of microwave tubes.

Microwave tubes can be divided to three groups according to their electron and wave interaction, namely O-type, M-type and Space Charge. O-type source has external H field parallel to the electron beam. Travelling wave tube, backward wave oscillator and klystrons are examples of O-type sources. M-type source has E and H field perpendicular to electron beam like magnetron. Space charge source type microwave tubes include space charge distribution and interaction of the electrons each other. Vircator is one of the examples of space charge sources.

In history, the first vacuum device was diode which is discovered by J. A. Fleming in 1904. It was used to detect electromagnetic waves by H.R. Hertz. In 1906, Lee de

Forest added 3rd electrode and developed triode which was called Audion and it became very attractive amplifier in broadcasting in 10 years [1], [5].

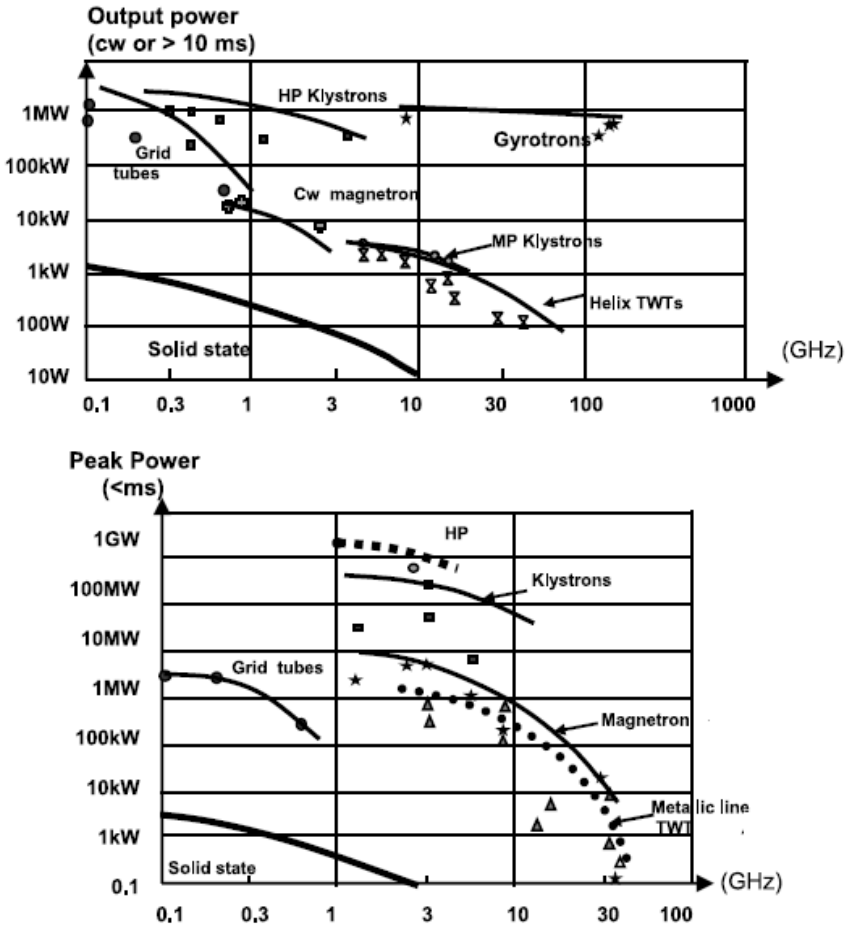

Figure 1 Peak and CW power of various microwave tubes [1]

In 1920, H. Barkhausen invented retarded-field tube (reflex triode), which is known as first transit time tube. In 1921, magnetron was developed by A.W. Hull followed by E. Habann and A. Zacek [1]. H.A.H. Boot and J.T. Randall used klystron type resonator in 1939. During World War II, magnetron played very crucial role and took its present state, due to urgent need for high power microwave generators for radars. However, magnetron and triode were not high frequency and large gain amplifiers. Therefore, some researches were carried out to have high power at high frequency. For example, Varian introduced multicavity klystron which gave 50 W at 3 GHz with 30 dB gain. After klystrons developments, reflex klystrons made great contributions in local oscillators. Afterwards, in 1942, Kompfner described

travelling wave interaction and one year later, he developed first TWT with helix as a delay line. In 1946, J. R. Pierce introduced theory of microwave tubes and how to compress parasitic oscillations [1]. With the help of Pierce theoretical analysis, TWT evolution gained speed. In 1950, coupled cavity TWT was discovered. In 1953, cross field amplifier was introduced by W.C. Brown. At the same time, backward wave oscillator or carcinotron was developed [1]. Until today, microwave tubes technology has been developed according to military and civilian needs. In the last 40 years, mass production of magnetron started for microwave ovens [1]. In the meantime, helix production technologies also have been improved such that brazed, pressed and variable pitch helix TWTs were used in radar transmitters with higher efficiency. In addition to that, various cathode types were developed such as gridded electron gun and impregnated cathodes [1]. In the same time, depressed and radiating collector was developed for TWT. From 1962, TWTA has been used on satellites while tunable klystrons have been used in TV and communications. Between 1960 and 1980, multibeam, medium power klystrons were used in Soviet countries. Vapor cooled collectors and 300 kV pulsed electron guns were developed for high power microwave tubes [1]. High efficiency (>65%), high pulsed power (tens of MW) and CW (>1.3 MW) klystrons and multibeam high power klystrons have been used since 1995. The gyrotrons were invented, they can deliver very high power (MW) at very high frequencies (>100GHz) [1]. Today, researches and developments in microwave tube technology still continue to achieve better performance, higher frequency and higher power.

2.2 Travelling Wave Tubes

The travelling wave tube (TWT) is a linear beam and O-type microwave device as mentioned before. Frequency range of TWT is starting from 1 GHz and reaching to 100 GHz. Power values range from few watts to 10 MWs while spanning 40 to 70 dB gain interval for small signal drive [2], [3].

TWTs are used as final amplifier in almost all communications satellites, which is most important application of them. Moreover, in many radar systems, TWTs are used as high power amplifier transmitting RF pulse. Besides, TWT can be used

driver amplifier for other high power RF amplifier. Another large application of TWTs is electronic countermeasures systems [6].

Electron beam and electromagnetic wave interaction concept was introduced by Hoeff in 1933. Hoeff discovered the possibility of travelling wave interaction between electron beam and RF circuits. In his devices, RF signal propagates on helical structure to deflect nearby hollow electron beam. However, amplification of travelling RF wave was not considered in Hoeff work [3]. In 1935, Posthumus built a cavity type magnetron oscillator and described interaction between electron beam and tangential components of a travelling RF wave. Thus, electron energy is converted to amplification of the RF wave by this interaction [3]. Lindenblad explained helix travelling wave amplifiers which is similar to helix TWT in 1940. It was the first explanation for synchronous interaction between electron beam and the RF wave on a helix in order to produce amplification of a signal on the helix [3].

After Lindenblad works, Kompfner in England stated that the basic growing wave principle of the magnetron could be used for amplification of RF signals. In 1943, Kompfner developed first travelling wave tube [3]. In June 27 and 28, 1946, at the Fourth Institute of Radio Engineer's Electron Tube Conference at Yale, public announcement of helix TWT was made first time. At the same conference, J.R. Pierce and L.M. Field from Bell Telephone Laboratories described their work in United States [3]. In Pierce TWT, there were longitudinal insulating rods to support and position the helix and uniform magnetic field to focus the electron beam. Pierce also suggested a method to suppress backward wave oscillations [3]. After World War II, many studies carried on TWT to explain operation of TWT. In addition to Pierce's works, A. Blanc-Lapierre and P. Lapostolle in France contributed the analysis of TWT [3].

Mainly two different RF circuits are used for electron beam and electromagnetic wave interaction namely coupled cavity and helix. These structures became advantageous in specific applications such that while helix is used for broadband application, coupled cavity is used for high power application. For helix TWTs, two

octaves and more can be achievable and for coupled cavity TWTs bandwidths are in 10-20% range [6]. In Figure 2, the Pierce helical TWT is shown.

Main components of TWT are electron gun, slow wave structure (helix or coupled cavity) magnetic focusing structure, RF input and output port and collector. These components are shown in Figure 3. Electron gun, electron beam and collector are common in all microwave tube devices, interaction circuits differ.

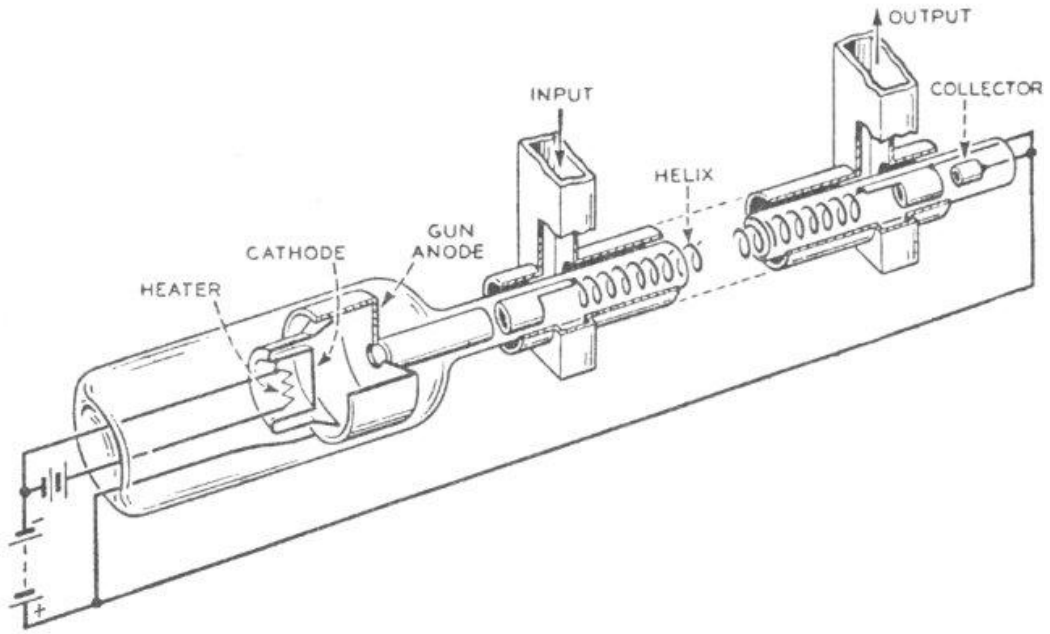

Figure 2 Schematic view of helical travelling wave tube [7]

The operation principle of TWT can be summarized as follows. The electron beam generated by electron gun enters the slow wave structure. Normally in a vacuum tube, electron beam travels at the speed of light, thus RF wave and electron beam interaction cannot be occurred. Slow wave structure slows down the RF wave thus, RF signal and electron beam travels at approximately same speed. While electron travels in the SWS, electrons in positive portion of RF accelerate and electrons in negative portion of RF decelerate. Then electron bunches are created and alternating current occurs on the beam current. This alternating current generates amplification of RF signal.

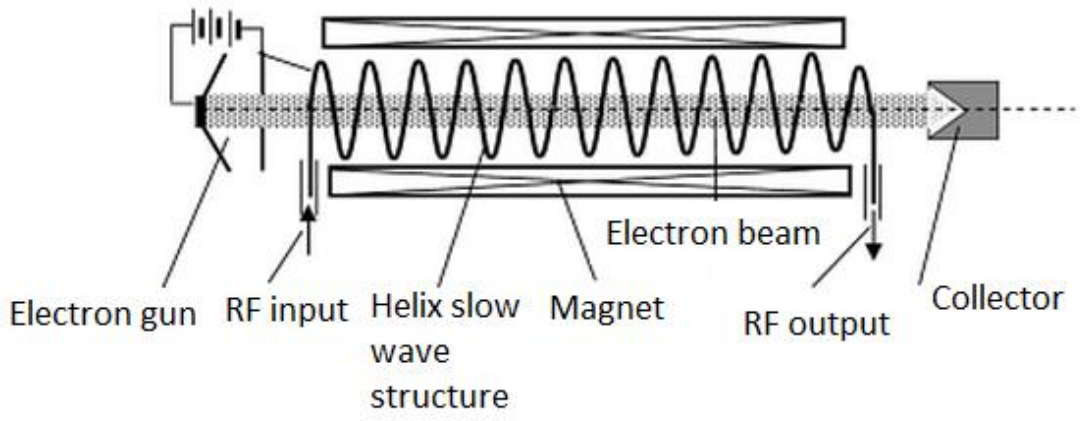

Figure 3 Basic elements of travelling wave tube [5]

Electron gun generates high current density electron beam to interact the travelling RF wave along slow wave structure. Typically, electrons are emitted from cathode and converged to proper beam by focus electrode. It is important to obtain high quality beam for efficient amplification in TWT. For high quality beam, electron gun performance is crucial. The slow wave structure in TWT allows interaction of electron beam and RF wave. Electron beam travels at almost the same velocity by the slow wave structure, thus gives its energy to the RF wave. Electron beam should not diverge and cross section of beam should be kept in same dimension along slow wave structure to have efficient interaction. In order to satisfy these conditions, magnetic focusing system is used. After travelling interaction circuit, spent electron beam reaches the collector and remaining beam energy is dissipated at collector.

2.3 Electron Gun

Electron gun produces narrow, collimated electron beam in all types of vacuum tubes. They were used initially in cathode ray tubes, older televisions, computer displays and oscilloscopes. Today, they are used in microwave vacuum tubes such as klystrons, TWTs and gyrotrons. In scientific, they have usage such as electron microscopes and particle accelerators.

The electron gun is important for all linear beam devices including TWTs. Operating principle of electron gun for all devices are almost the same; the differences are size and operating voltage and current [6]. The electron beam in a microwave tube is used

to generate electrons from cathode into a suitable beam to interact with microwave circuit. J. R. Pierce proposed electron gun geometry for linear microwave tubes to solve basic problems in electron gun design. In an electron beam, beam generated electric force cause the beam to diverge and the required current density in electron beam is far greater than the emission density that the cathode can supply [6]. These two problems were solved with Pierce gun design, thus these guns were called Pierce gun. In Figure 4, the gun described by Pierce is illustrated.

Pierce gun consists of three parts namely cathode, anode and focusing electrode. The electrons are extracted from spherical cathode and flow toward the center of the cathode curvature by focusing electrode. Then the electrons are accelerated by the anode potential and leave the acceleration region from anode aperture. In this process, electrons start to transport under the space charge forces.

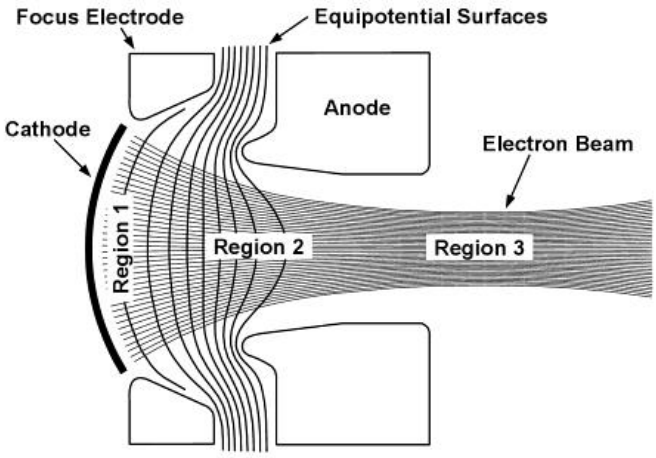

Figure 4 Overview of Pierce gun [6]

After basic Pierce gun design, some researchers studied on specific cases. For example, Pierce gun focusing electrode design could not be sufficient to obtain desired equipotential lines for some cathode geometry. Therefore, shape of focus electrode should be modified. In 1947, P. Helm, K. Spangerberg and L.M. Field published "Cathode design procedure for electron beam tubes" and investigated many possible shapes of focusing electrode [3].

Equipotential profiles are also distorted near the anode extraction gap and perveance of electron gun, which will be investigated in detail in further sections, is an important parameter for anode perturbation. While for low perveance gun, perturbation is not strong, for high perveance gun distortion becomes serious. In 1957, G.R. Brewer proposed modification of focus electrode and reduced distortion of equipotential lines in “Formation of high density electron beams". In addition, K. Amboss gave treatment of the effect of anode aperture in 1962 [3]. In the same time, Frost, Purl and Johnson were able to correct lens aberration for high perveance guns by modifying the sphere radius of the cathode in 1962 [3]. Moreover, there are other factors that affect the electron gun performance were investigated. For example, in C.C. Cutler and M. E. Hines’s "Thermal velocity effect in electron gun" study, published in 1955, analyzed the effects of thermal velocities [3]. Beam current control is another consideration in gun design and it is required in all microwave tubes. There are generally four methods to control the beam current, which can be observed from Figure 5. In cathode modulation, cathode is pulsed in negative direction and full beam voltage has to be switched. Anode modulation is similar to cathode modulation; however, few percent of beam current should be switched [2**]**. When focus electrode is biased negatively with respect to cathode, beam can be turned off. Focus electrode beam controlling method is advantageous since focus electrode has no current and implementation is easier [2**]**. Grid is placed in front of the cathode. When grid potential switched with 5% of cathode voltage beam can be modulated.

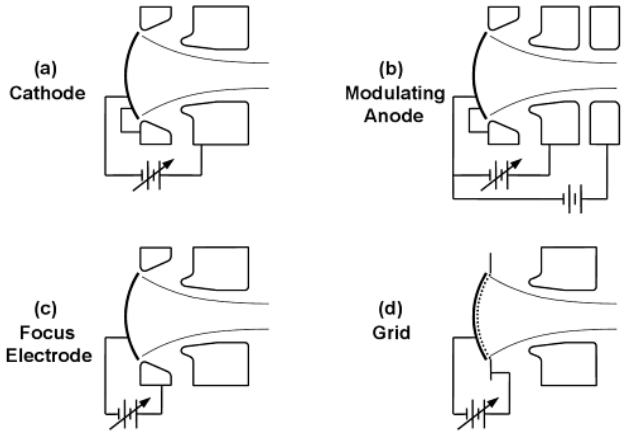

Figure 5 Techniques for current control in an electron gun [6]

Grid control is widely used method in TWTs. Single grid element has been used since the invention of vacuum tube. In 1960, Wolkstein proposed methods for design of grids for Pierce gun. After that different grid structures have been introduced by researchers to improve control of beam current. Drees's shadow grid, True and Laycock's tapered grid, Miram and Lien's bonded grid are the examples of different grid structures [3**]**.

Design of electron gun is very complicated task and includes iterative process to optimize the gun. Therefore, many computer simulation tools have been developed for this purpose. Today, simulation programs such as EGUN [8], TRAK, and KARAT are widely used in designing the electron gun. Simulation of guns provides more accurate and simple design and they are much more time saving. Also, researchers try to develop simulation codes for gun simulation like COLLGUN which is 3D Finite Element Simulator for the design of TWTs electron guns and multistage collectors [9]. Besides them, CST Particle Studio is one of the useful tools to simulate charged particle dynamics in 3D electromagnetic fields [10].

In present, with the help of simulation programs, analysis and optimization of electron gun becomes easier and various gun geometries could be designed and introduced to literature for different purpose. C.C.Xavier and C.C. Motta proposed design of gridded electron gun with EGUN in 2009 and analyzed effects of geometrical parameters of the gun in [11]. Their gridded gun geometry is given in Figure 6. Then in 2011, the same researchers with M.N. Pinto described electron gun design procedure in [4] in 2011 based on EGUN code simulation. They analyzed the geometrical parameter of electron gun in [11] without grid and optimized geometry parameters by simulation.

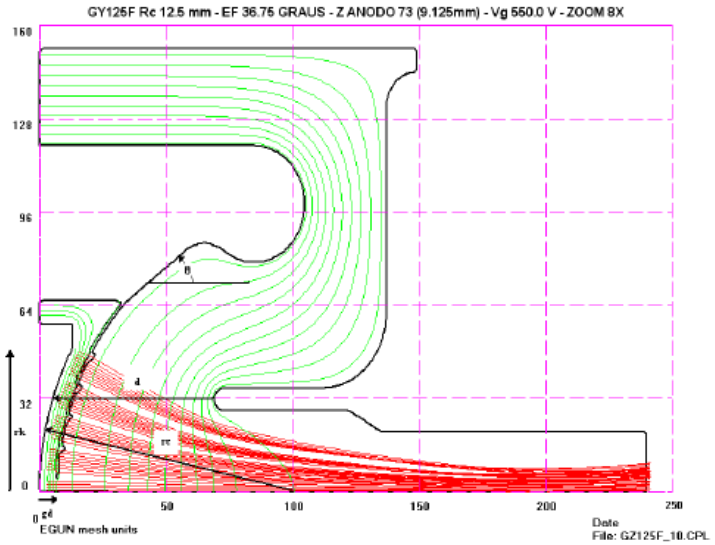

Figure 6 Gridded electron gun in [11]

In addition to solid beam electron gun, there are annular beam electron guns to produce higher beam current. In 2001, M. Fazio, B. Carlsten, C. Fortgang, K. Habiger and E. Nelson developed annular beam klystron whose power is 1GW [12]. Moreover, J. Elton, M. Yean and S. Park designed annular beam electron gun which is shown in Figure 7 for high power microwave source like relativistic BWO in 2003 [13].

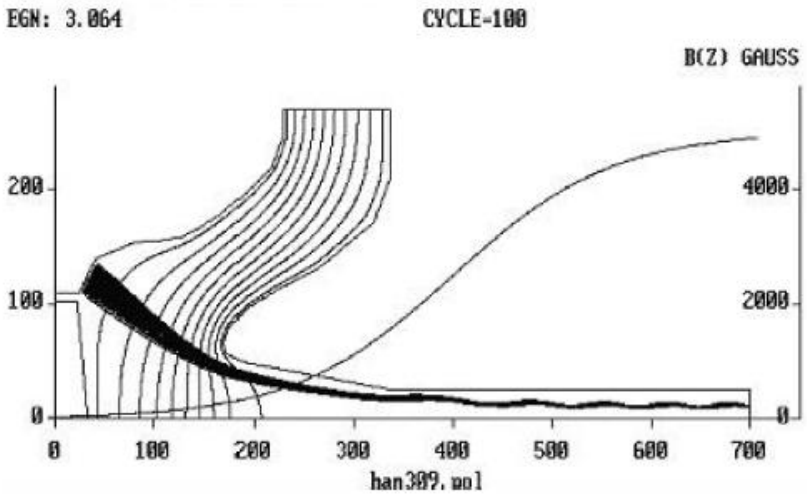

Figure 7 Geometrical model of the annular beam gun in [13]

Furthermore, in literature there are dual beam or multibeam electron gun designs. David A. Zalavid developed dual beam dual mode TWTA in [14] which consists of an annular hollow beam cathode, concentric and co-planar with a solid beam cathode which is shown in Figure 8.

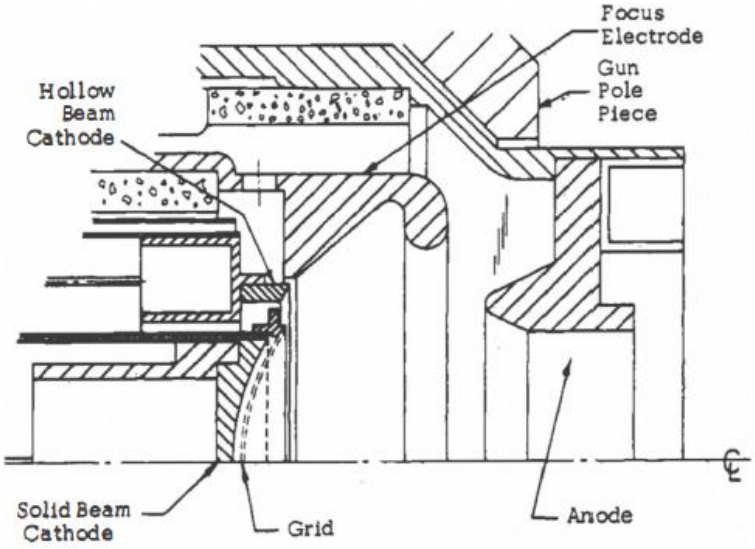

Figure 8 Cross -sectional view of dual beam in [14]

In addition to that, W. Czarczynski and J. Sabonski proposed multibeam electron gun design for coupled cavity TWT in [15]. The electron trajectories in a multibeam gun are illustrated in Figure 9.

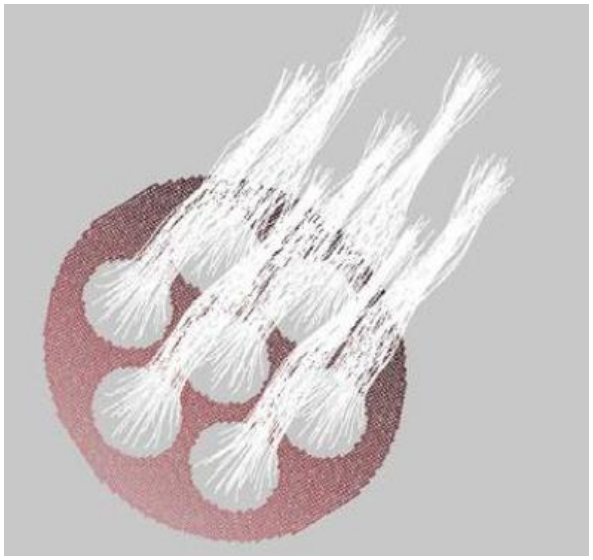

Figure 9 Electron trajectories in a multibeam gun [15]

Another geometry in literature is dual anode electron gun. Choundhury and Sharma introduced 140W Ku band dual anode electron gun to fulfill the requirement of long life and high reliability of TWT in 2003 [16]. Then they continued their dual anode research on Ka band and Ku band dual electron gun and PPM focusing system in [17], [18] and [19]. The dual anode geometry is given in Figure 10.

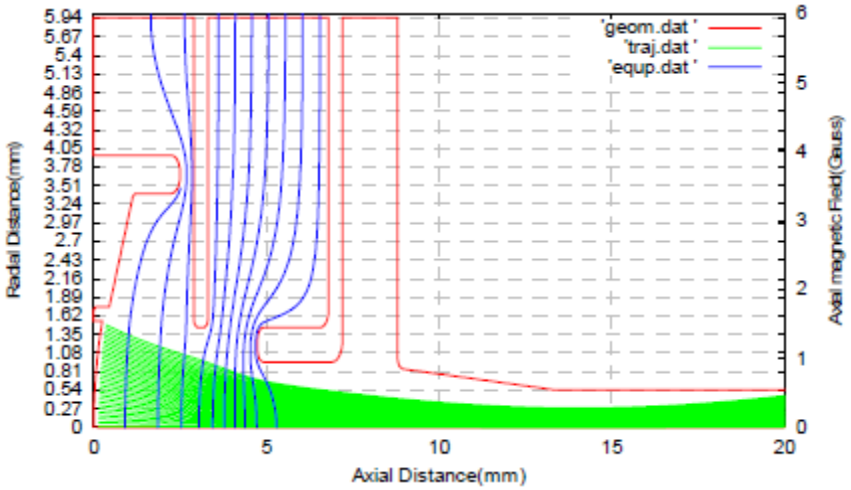

Figure 10 Dual anode geometry [17]

CHAPTER 3

THEORY OF OPERATION

3.1 Electron beam

Electron beam is flow of free electrons generated by heat, bombardment of charged particles or atoms, or strong electric fields in a direction [5**]**, [20**]**. The electron beam is important part of TWT because it interacts the RF field in the slow wave structure. Electron beam is generated by electron gun in microwave tubes. In TWT, mostly, thermionic emission mechanism occurs. According to TWT design, electron beam should have some properties such as beam current, perveance, beam radius. Therefore, electron gun is designed to satisfy these parameters.

In electron gun design, beam physics should be well understood. Charged particles interact each other and electric and magnetic fields are generated by these interactions. Beam generated fields limit transportable beam current **[7]**. The longitudinal limit can be determined by Child law. Child law gives maximum current density which can be extracted from a particle source. The effects of beam generated source and Child law derivation based on derivation in **[7]** will be given following section of this chapter.

3.2 Electric and Magnetic Fields of Beam

In order to analyze the electric and magnetic fields of beam, simplified geometry can be chosen. Thus, ideal sheet beam, showed in Figure 11, is used to derive beam generated forces.

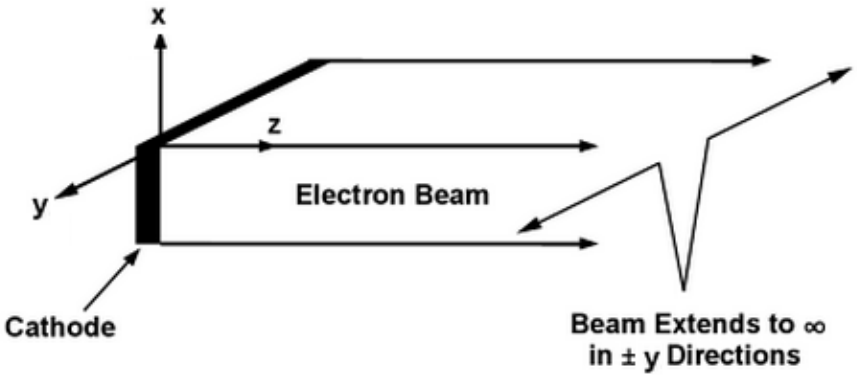

Figure 11 Geometry of sheet beam of infinite width in the y-direction propagating in the z-direction [6]

In Figure 11, beam extends infinitely in y and z direction and average particle motion is parallel to z-direction. Particles are contained between $+x_0$ and $-x_0$.

$$\bar{\nabla} \cdot \bar{E} = \frac{\rho}{\epsilon_0} \tag{1}$$

Since particle density varies only in x-direction, Poisson equation in (1) reduces to (2).

$$\frac{\partial E_x}{\partial x} = \frac{qn(x)}{\epsilon_0} \tag{2}$$

For simplicity, electric field at the axis can be taken as zero. Then integration of (2) becomes as in (3).

$$E_x = \frac{q}{\epsilon_0} \int_0^x n(x')\, dx' \tag{3}$$

Magnetic field is related to the z-directed current density. Thus, (4) is reduced to (5).

$$\bar{\nabla} \times \bar{B} = \mu_0 \bar{J} \tag{4}$$

$$\frac{\partial B_y}{\partial x} = \mu_0 j_z(x) \tag{5}$$

In this derivation, it is assumed that axial velocity is constant over the beam cross section and beam has negligible transverse velocity components. Therefore, current density becomes as in (6).

$$j_z(x) = qn(x)v_z \tag{6}$$

Integration of (4) and substituting (5) into (4) gives (7).

$$B_y(x) = qv_z\mu_0\int_0^x n(x')dx' \tag{7}$$

If the particle density is uniform, $n(x)=n_0$, integrals in (3) and (7) can be calculated as in (8) and (9) respectively. Beam generated electromagnetic fields can be obtained by using (8) and (9) for sheet beam.

$$E_x = \frac{qn_0}{\epsilon_0}x \tag{8}$$

$$B_y = \mu_0 qn_0 v_z x \tag{9}$$

3.3 One Dimensional Child Law Derivation

Maximum current density of an electron gun can be limited by two ways, which are source limited and space charge limited electron gun. In this thesis, source limited electron gun will not be investigated. Thus, it is assumed that electron gun is space charge limited. Space charge limit results from longitudinal electric field of the beam space charge. The Child law gives the limit of maximum current density for charged particle extractor [7]. Figure 12 shows one dimensional anode cathode acceleration gap for Child law calculation.

In Figure 12, $-V_0$ is applied to cathode and source anode potential is set to 0. The distance between anode cathode gap has width d. It is assumed that particle rest mass is m_0 and charge $+Z_e$. If -1 is placed for $+Z_e$, the calculation becomes valid for the electron.

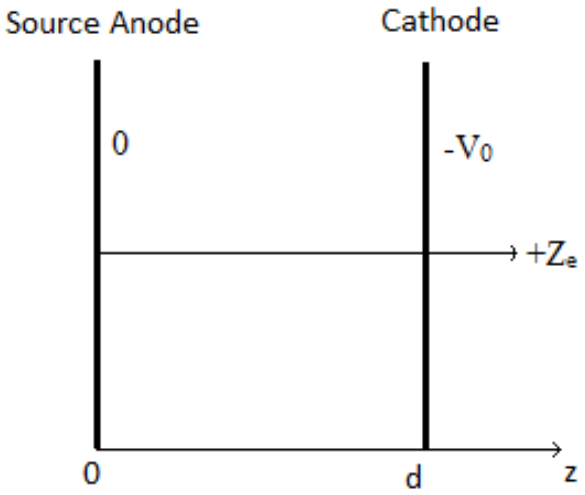

Figure 12 Geometry for the calculation of space charge limited particle flow

All particles will have eV_0 kinetic energy at cathode and exit from acceleration gap from ideally. In order to make the calculation easier, some assumption were made according to [7]. Firstly, the motion is non-relativistic. As mentioned before, particle flow is not source limited, only space charge limited. Transverse electric field and velocity is negligible compared to these values in z. Moreover, beam generated magnetic force is small compared to axial electric force, thus particles flow in a straight line. Finally, electric fields and space charge density at all positions are constant, thus particles flow continuously [7].

When the space charge limit is reached, charge density becomes constant in time. Thus the time derivative of charge density is zero as in (10).

$$\frac{\partial \rho}{\partial t} = 0 \tag{10}$$

$$\bar{\nabla} \cdot \bar{J} + \frac{\partial \rho}{\partial t} = 0 \tag{11}$$

Since second term in continuity equation in (11) is zero due to steady state condition, only the first term remains. The current density can be written in terms of particle charge (Z_e), particle density (n) and longitudinal velocity (v_z) as in (12).

$$J = Z_e n(z) v_z(z) \tag{12}$$

Therefore, (11) becomes (13), when (10) and (12) are substituted into (11).

$$\frac{\partial\left(Z_e n(z) v_z(z)\right)}{\partial z} = 0 \tag{13}$$

Equation (13) means that current density is the same at all positions in the gap. If the constant current density value is assigned as j_0, the particle density can be written as in (14).

$$n(z) = \frac{j_0}{Z_e v_z(z)} \tag{14}$$

It is assumed that electrostatic potential at the particle is zero, thus the kinetic and potential energy is related with (15).

$$\frac{m_0 v_z^2}{2} = -Z_e \phi \tag{15}$$

Equation (16) shows one dimensional Poisson equation when charge density is written in terms of charge and particle density.

$$\frac{d^2\phi}{dz^2} = -\frac{\rho}{\epsilon} = -\frac{Z_e n(z)}{\epsilon} \tag{16}$$

Equation (14) and (15) can be rewritten as in (17) and (18) respectively.

$$n(z) Z_e = \frac{j_0}{v_z(z)} \tag{17}$$

$$v_z = \sqrt{-\frac{2Z_e\phi}{m_0}} \tag{18}$$

If v_z in (18) is put in (17), (19) is obtained. Then (20) can be obtained by substituting (19) into (16).

$$n(z)Z_e = \frac{j_0}{\sqrt{-\frac{2Z_e\phi}{m_0}}} \tag{19}$$

$$\frac{d^2\phi}{dz^2} = -\frac{j_0}{\epsilon\sqrt{-\frac{2Z_e\phi}{m_0}}} \tag{20}$$

In order to write (20) more efficiently, dimensionless variables $\zeta=z/d$ and $\Phi=-\phi/V_0$ are introduced and (20) becomes as in (21) with α in (22).

$$\frac{d^2\Phi}{d\zeta^2} = \frac{\alpha}{\sqrt{\Phi}} \tag{21}$$

$$\alpha = \frac{j_0 d^2}{\epsilon V_0\sqrt{\frac{2Z_e V_0}{m_0}}} \tag{22}$$

In order to have unique solution, three boundary conditions are needed. Two boundary conditions are on source anode and cathode potential. Third boundary condition results from space charge limited flow, which allows taking the condition that the electric field at the source equals zero. These three boundary conditions are expressed in (23).

$$\Phi(0) = 0,\ \Phi(1) = 1,\ \frac{d\Phi(0)}{d\zeta} = 0 \tag{23}$$

Equation (21) is multiplied with $2\Phi'$ from both side to solve the equation, with $\Phi'=d\Phi/d\zeta$ and (21) becomes (24).

$$2\Phi'\Phi'' = \frac{2\alpha\Phi'}{\sqrt{\Phi}} \tag{24}$$

$2\Phi'\Phi''$ is differential of $(\Phi')^2$. Integration by part is used to solve the right hand side where $u=\Phi^{-1/2}$ and $dv=\Phi' d\zeta$. When both sides of (24) are integrated from source to position z and boundary condition $\Phi(0) = 0$ is applied, (25) is obtained.

$$\left[\Phi'(\zeta)\right]^2 = 4\alpha\sqrt{\Phi(\zeta)} \tag{25}$$

Then, (25) is rewritten by taking square root of both sides as in (26).

$$\frac{d\Phi}{\Phi^{1/4}} = \sqrt{4\alpha}\,d\zeta \tag{26}$$

When both sides of (26) are integrated, the result is given in (27).

$$\Phi^{3/4} = \frac{3}{4}\sqrt{4\alpha}\zeta \tag{27}$$

The second boundary condition ($\Phi(1)=1$) is applied to (27) and α is calculated as 4/9. Therefore, space charge limited current density can be found by solving (22) with $\alpha=4/9$. Equation (28) gives calculated j_0.

$$j_0 = \frac{4\epsilon}{9}\sqrt{\frac{2Z_e}{m_0}}\frac{V_0^{\frac{3}{2}}}{d^2} \tag{28}$$

Dimensionless variables are changed with $\Phi=\phi/-V_0$ and $\zeta=z/d$ and substitute $\alpha=4/9$ into (27), then electrostatic potential in terms of position for space charge limited flow is obtained in (29). The electric field can be found for space charge limited flow as in (30).

$$\phi(z) = -V_0\left(\frac{z}{d}\right)^{\frac{4}{3}} \tag{29}$$

$$E_z = -\frac{d\phi}{dz} = 4V_0\frac{z^{\frac{1}{3}}}{3d^{\frac{4}{3}}} \tag{30}$$

3.4 Child Law for Spherical Geometry

In practical, spherical geometries are used in particle gun design. In this thesis, simulation and design of spherical gun were carried out also. Therefore, derivation of Child Law for spherical geometry is given in this part. The geometry for spherical

gun is composed of two concentric spheres as shown in Figure 13. The results for geometry in Figure 13 can be used in electron gun design with spherical geometry and spherical flow.

In Figure 13, R_s and R_c represent the source and collector radius respectively. In this derivation, source voltage is taken 0 and cathode voltage is $-V_0$. The Poisson equation for spherical geometry is given in (31).

$$\frac{1}{r^2}\frac{d}{dr}\left(r^2\frac{d\phi}{dr}\right)=-\frac{\rho}{\epsilon_0} \tag{31}$$

The relation between potential energy and velocity of particle was given in (15).

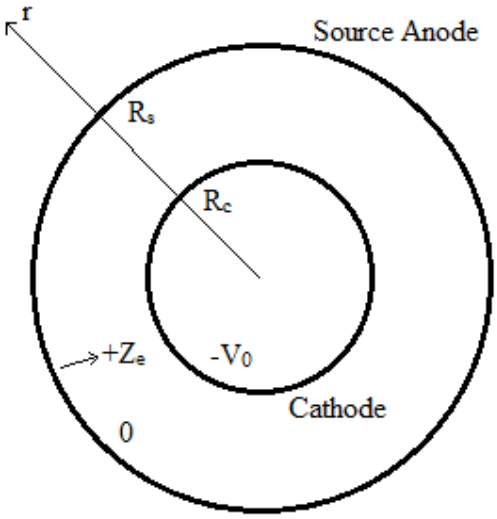

Figure 13 Geometry for the calculation of space charge limited particle flow between spheres

In steady state, current is constant in all radii, thus space charge density ρ is related to velocity as in (32).

$$\rho=\frac{I}{4\pi r^2 v} \tag{32}$$

Equation (33) relates the space charge density and potential energy by substituting (15) into (32). Then (33) is substituted into (31) so (34) is obtained.

$$\rho = \frac{I}{4\pi r^2}\sqrt{\frac{m_0}{-2e\phi}} \tag{33}$$

$$\frac{d}{dr}\left(r^2\frac{d\phi}{dr}\right) = -\frac{I}{4\pi\epsilon_0}\sqrt{\frac{m_0}{-2e\phi}} \tag{34}$$

In order to solve (34) numerically, the potential and radius can be rewritten dimensionless as in derivation of Child law for planar geometry. Dimensionless variables $R=r/R_s$ and $\Phi=-\phi/V_0$ are defined. Equation (34) can be expressed as in (35) with A in (36).

$$\frac{d}{dR}\left(R^2\frac{d\Phi}{dR}\right) = \frac{A}{\sqrt{\Phi}} \tag{35}$$

$$A = \frac{I}{4\pi\epsilon_0 V_0^{\frac{3}{2}}}\sqrt{\frac{m_0}{2e}} \tag{36}$$

As in previous case, three boundary conditions are required to solve (35) and they are given in (37).

$$\Phi(1) = 0, \quad \Phi\left(\frac{R_c}{R_s}\right) = 1, \quad \frac{d\Phi(1)}{dR} = 0 \tag{37}$$

The difference between planar and spherical extractor is that current does not depend the absolute value of source radius, so higher electric field can be achieved with smaller spherical extractor than planar gun.

A numerical solution of (35) is developed by Langmuir and Blodgett **[7]**. They expressed electrostatic potential as (38).

$$\Phi(R)^{3/2} = \frac{9A}{4}\alpha(R)^2 \tag{38}$$

$\alpha(R)$ is called Langmuir function and in APPENDIX-A and APPENDIX-B, the value of α is given for inward and outward flow respectively.

Equation (38) can be rewritten to find total current by substituting A and $\Phi\left(\frac{R_c}{R_s}\right)=1$ into (38) thus (39) and (40) are obtained.

$$\Phi\left(\frac{R_c}{R_s}\right)^{3/2}=\frac{9A}{4}\alpha\left(\frac{R_c}{R_s}\right)^2=1 \tag{39}$$

$$\frac{9I}{4\pi\epsilon_0 V_0^{\frac{3}{2}}}\sqrt{\frac{m}{2e}}\alpha\left(\frac{R_c}{R_s}\right)^2=1 \tag{40}$$

If (40) is rewritten, the space charge limited current can be obtained as in (41).

$$I=\frac{4\epsilon_0}{9}\sqrt{\frac{2e}{m_0}}\frac{\pi V_0^{\frac{3}{2}}}{\alpha\left(\frac{R_c}{R_s}\right)^2} \tag{41}$$

3.5 Pierce Gun Design

In this thesis, only space charge dominated electron gun will be examined. The simulated and designed electron gun is based on Pierce electron gun design procedure. This design procedure provides the shapes of electrodes to obtain laminar beam with uniform current density. The laminarity of a beam shows the quality of the beam. In a laminar beam, all particles have same transverse velocity and the magnitude of the transverse velocity is linearly proportional to the displacement from the axis of beam symmetry [7].

The Pierce gun design method gives electrode shapes geometry for sheet beam, but the procedure can be used for more complex gun.

In this chapter, the design procedure follows the procedure in [7]. In the design procedure, it is assumed that particle motion in the extraction gap is non-relativistic and beam generated magnetic field is negligible. Besides, beam exits the gap through a grid or foil.

The planar electron gun in Pierce design method has sheet beam with $\pm x_o$ and potential difference between source and extractor electrode is V_o. In Figure 14.a, infinite width sheet beam is shown. The source is located at z=0 and extractor is at z=d. In this case, the potential across the gap is varies according to (29) for space charge limited flow. In Figure 14.b, only lower half plane generates electrons. In this situation, geometry should satisfy that there are no electrons for x>0 and the flow on the lower plane must have infinite sheet beam property. One method to satisfy these conditions is to place a large number of electrodes along the x=0 and bias them as the potential varies according to (29). Therefore the electric field in upper plane becomes like infinite sheet beam. Figure 14.c shows the biased electrodes.

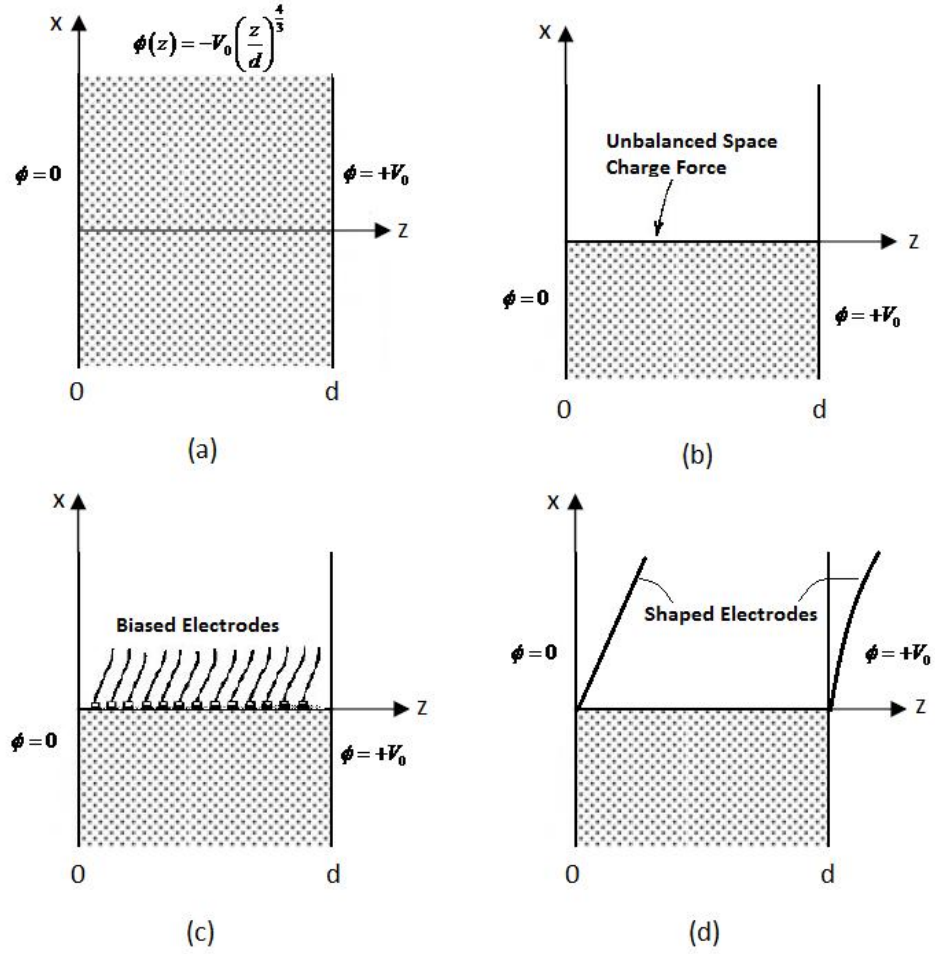

Figure 14 Basis of Pierce gun design procedure, (a) Planar gun with infinite width (b) electron beam with a sharp boundary (electron source only in region x<0) (c) Biased electrode method (d) Shaped electrodes

Other method to create infinite sheet beam condition on the boundary is shaped electrodes. Figure 14.d shows the shaped electrodes. The potential in upper plane should satisfy two conditions at the boundary. First is that potential must follow (29) at x=0. The second condition is that electric field in the x-direction must equal to zero or $\frac{\partial \phi}{\partial x} = 0$, because there are no transverse electric fields in upper half plane.

In order to solve Laplace equation for upper half plane a method using properties of complex function is used [7]. A complex variable u is defined as a linear combination of the real coordinate variables.

$$u = z + jx \tag{42}$$

An analytic function of complex variables, f(u) can be defined and analytic function f satisfy the Laplace equation [7]. In this problem, analytic function is defined as in (43).

$$f(u) = V_o \left(\frac{u}{d} \right)^{4/3} = V_0 \left(\frac{z + jx}{d} \right)^{\frac{4}{3}} \tag{43}$$

Then, electrostatic potential becomes real part of analytic function of f(u) [7].

$$\phi(x, z) = V_o Re \left(\frac{z + jx}{d} \right)^{\frac{4}{3}} \tag{44}$$

In order to obtain real part of the potential, complex function is expressed in polar coordinates.

$$z = \rho cos\theta, \quad x = \rho sin\theta \tag{45}$$

$$e^{j\theta} = cos\theta + jsin\theta \tag{46}$$

When (45) and (46) are substituted into (44), (47) can be obtained.

$$\frac{\phi}{V_o} = Re \left(\frac{\rho}{d} e^{j\theta} \right)^{4/3} = \left(\frac{\rho}{d} \right)^{\frac{4}{3}} Re \left(e^{\frac{j4\theta}{3}} \right) \tag{47}$$

Equation (47) can be used to find shape of the electrodes to satisfy correct fields. The source potential is equal to zero and the real part of the right hand of (47) must be equal to zero as in (48).

$$\cos\left(\frac{4\theta}{3}\right)=0 \tag{48}$$

$$\frac{4\theta}{3}=\frac{\pi}{2}, \qquad \theta=67.5^{o} \tag{49}$$

Equation (48) and (49) represents the straight line oriented with respect to z axis as shown in Figure 15. In order to find the extractor curve real part of right hand side of (47) should be equalized to 1. Equation (50) gives the relation. The extractor curve can be found by solving numerically (50).

$$\left(\frac{\rho}{d}\right)^{4/3}\cos\left(\frac{4\theta}{3}\right)=1 \tag{50}$$

If another boundary is added at $x=-2x_o$, the mirror image of electrode should be used to keep the electric field same as infinite beam. Figure 15 shows the Pierce gun designed according to these design procedure. Slanted electrodes are known as focusing or Pierce electrode, which provides electric force balances the defocusing beam generated force on the edge of beam. It should be noted that electron beam extract the anode via grid or foil as shown in Figure 15, so anode potential are kept same on the anode. However, high power density beams melts conducting mesh or foil. Therefore, most of the application, beam leaves the extraction gap from an aperture. The anode aperture distorts the equipotential line and defocuses electron beam. Moreover, this effect depresses beam current density by reducing electric field at the center of cathode [7]. If the condition that anode aperture is small compared to interaction gap, which is expressed in (51), the change of electric field at the center of cathode is negligible and Pierce gun solution is valid.

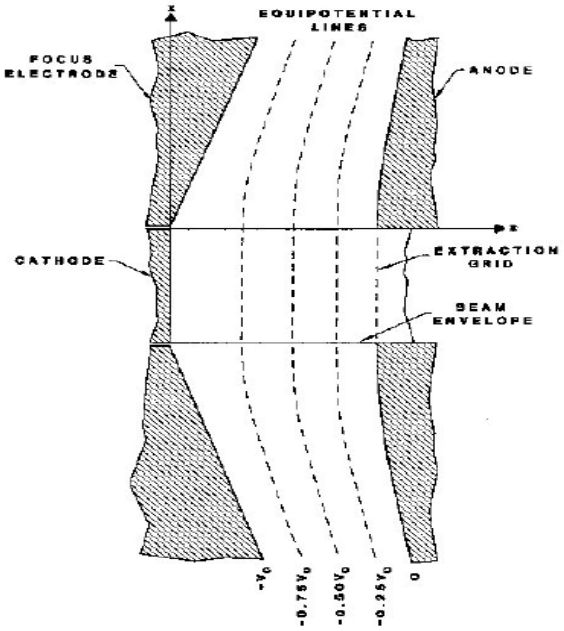

Figure 15 Geometry of planar Pierce gun [7]

$$2r_a << d \tag{51}$$

On the other hand, if the condition in (52) occurs, field perturbation and defocusing is strong, thus the geometry should be modified [7].

$$2r_a \geq d \tag{52}$$

In order to find the limit for valid region of Pierce gun, (28) is multiplied with area and limit current estimated with (53) [7].

$$I = \frac{4\epsilon_o}{9}\sqrt{\frac{2Ze}{m_o}}\frac{\pi r_a^2}{d^2}V_o^{\frac{3}{2}} \tag{53}$$

If the current is divided by quantity, $V_o^{\frac{3}{2}}$, obtained quantity is called gun perveance which depends on geometry and type of particle. Perveance can be calculated with (54). The condition $2r_a=d$ is substituted into (54), the limit for electron gun for valid Pierce gun design procedure becomes as in (55).

$$P = \frac{I}{V_o^{3/2}} = \frac{4\epsilon_o}{9}\sqrt{\frac{2Ze}{m_o}}\frac{\pi r_a^2}{d^2} \tag{54}$$

$$P << \frac{\pi\epsilon_o}{9}\sqrt{\frac{2e}{m_e}} = 0.6\times10^{-6} \tag{55}$$

Equation (55) states that planar Pierce gun derivation is valid for apertured cylindrical guns with perveance less than 1 μperv. Cylindrical gun with $P \leq 1\mu perv$ is called medium perveance gun and the design procedure is modified for these guns [7]. Moderate perveance guns generally have converging geometry. The converging gun geometry with moderate perveance is given in Figure 16. The beam density is smaller near the cathode for converging gun, thus space charge limited current for a given aperture is higher. Also, the aperture diameter can be small, because the beam diameter is the smallest at the anode. Moreover, converging electrons counter the negative lens effects, so parallel beam can be achieved.

The converging gun can be considered as section of spherical electrodes mentioned in Section 3.4. The perveance for full sphere can be calculated from (41) by putting radii of curvature ρ_a and ρ_c as shown in (56).

$$\frac{I}{V_o^{3/2}} = \frac{4\epsilon_o}{9}\sqrt{\frac{2e}{m_e}}\frac{4\pi}{\alpha\left(\frac{\rho_a}{\rho_c}\right)^2} \tag{56}$$

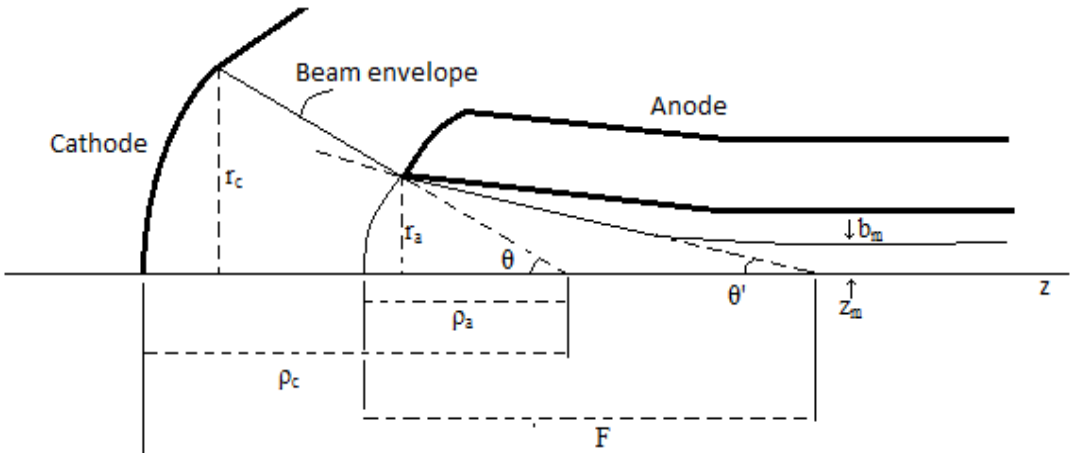

Figure 16 Converging gun geometry with moderate perveance

The converging gun perveance can be calculated by multiplying the ratio of cathode area to full sphere area. Area of cathode can be calculated as integrating the differential surface element in (57).

$$A_c = 4\pi\rho_c^2 \frac{(1-cos\theta)}{2} = 4\pi\rho_c^2 sin^2\left(\frac{\theta}{2}\right) \tag{57}$$

With (56) and (57), gun perveance for converging gun can be calculated and shown in (58).

$$\frac{I}{V_o^{\frac{3}{2}}} = \frac{4\epsilon_o}{9}\sqrt{\frac{2e}{m_e}} \frac{sin^2\left(\frac{\theta}{2}\right)}{\alpha\left(\frac{\rho_a}{\rho_c}\right)^2} \tag{58}$$

The focal length due to negative lens effect of anode aperture can be estimated as in (59) [7]. In (59), E_a is the axial electric field near the anode.

$$F \cong -\frac{4V_o}{E_a} \tag{59}$$

If E_a is taken as electric field without the beam and aperture, focal length becomes approximately as in (60).

$$F \cong -4\frac{\frac{\rho_c}{\rho_a}}{\rho_c - \rho_a} \tag{60}$$

Due to negative lens effect, the beam envelope convergence angle changes from θ to θ' and converging point becomes ρ'. θ' and ρ' are obtained by solving (61) and (62) respectively.

$$\theta' = \theta - \frac{r_a}{f} = \theta\left[1 - \frac{\rho_c}{4(\rho_c - \rho_a)}\right] \tag{61}$$

$$\rho' = \frac{\rho_a}{\left[1 - \frac{\rho_c}{4(\rho_c - \rho_a)}\right]} \tag{62}$$

High perveance gun, whose extraction aperture and perturbation of field are large, should be modified by numerical methods [7]. Figure 17 illustrates different perveance gun and modification on the geometry according to perveance.

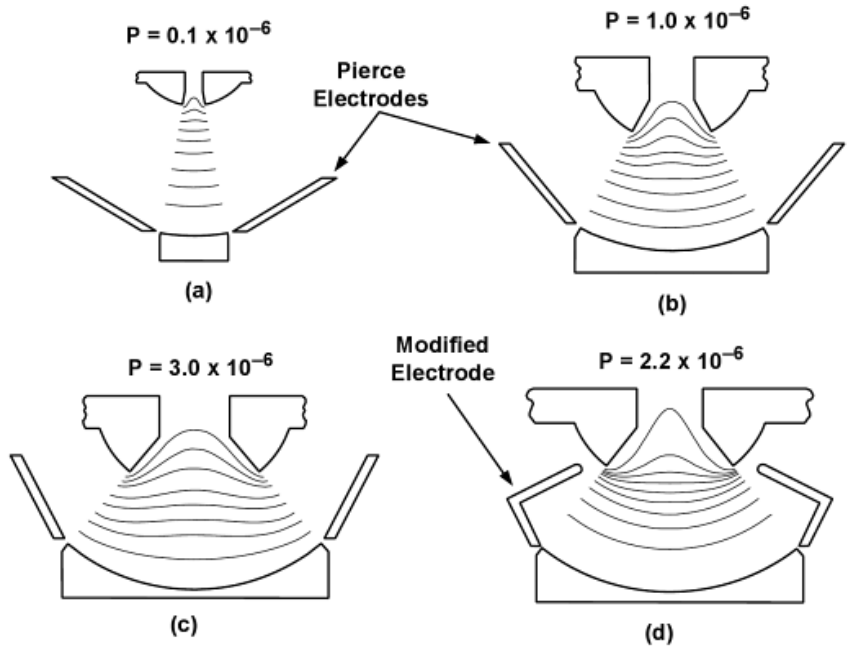

Figure 17 Guns with different perveance [6] (a) Low perveance gun, (b) Moderate perveance converging gun, (c) High perveance gun, (d) Modified high perveance gun

3.6 Beam Focusing

Electrons tend to diverge after passing through the anode extraction gap because their beam generated forces. External axial magnetic field is applied to electron beam to maintain focused beam envelope. For example, in TWTA, electron beam travels in long transition region while interfering with RF field and without axial magnetic field electron beam cannot propagate long distance.

If electron beam has ignorable transverse velocity component, laminar electron beam is obtained. However, in transport region, when space charge force starts to dominate, electron beam diverges. If axial magnetic field is exerted on the electron beam, the magnetic force on electron is in φ direction due to transverse component. Then electron beam is refocused with rotational motion by magnetic force. After refocusing, electric force became more effective and divergence occurs again. This procedure repeats itself along the transport region. Generally, electron trajectory under uniform magnetic field has shape as in Figure 18. In Figure 18, r_{max} and r_{min} depend on electrical force due to electron beam and applied axial magnetic field.

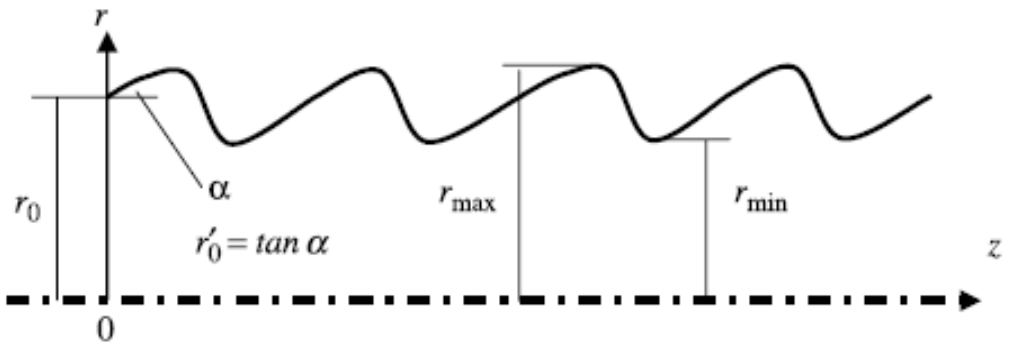

Figure 18 Electron trajectory in uniform magnetic field [5]

It is important to obtain electron beam without ripple for laminar beam transportation. The minimum magnetic field required to obtain laminar flow known as the Brillouin field.

In order to exert magnetic field on the electron beam, generally, two types of magnet system are used. First method is electromagnetic solenoid whose magnetic field is uniform through solenoid. In Figure 20, geometry of solenoid is shown. In this geometry there are helical winding of wire in many turns which creates azimuthally current sheet. Then azimuthally current sheet produces uniform B field in z direction inside the windings according to (63).

$$B = \mu NI \tag{63}$$

Second way is periodic permanent magnet (PPM) shown in Figure 19. In PPM system, field is not uniform and it requires complex design to prevent instabilities in

electron beam. One of the advantages of PPM over the solenoid is that PPM does not need power supply.

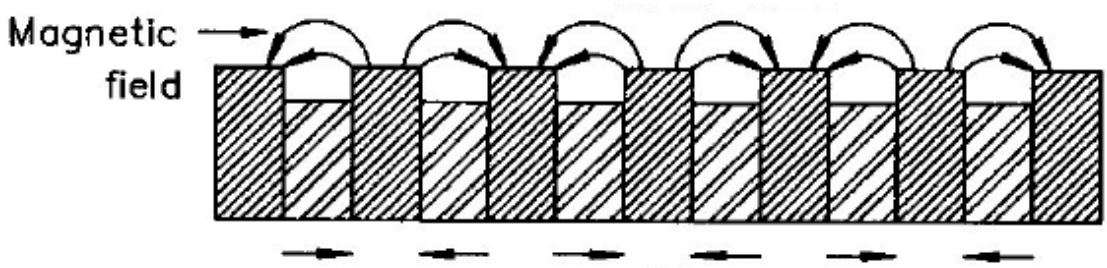

Figure 19 Periodic permanent magnet array [7]

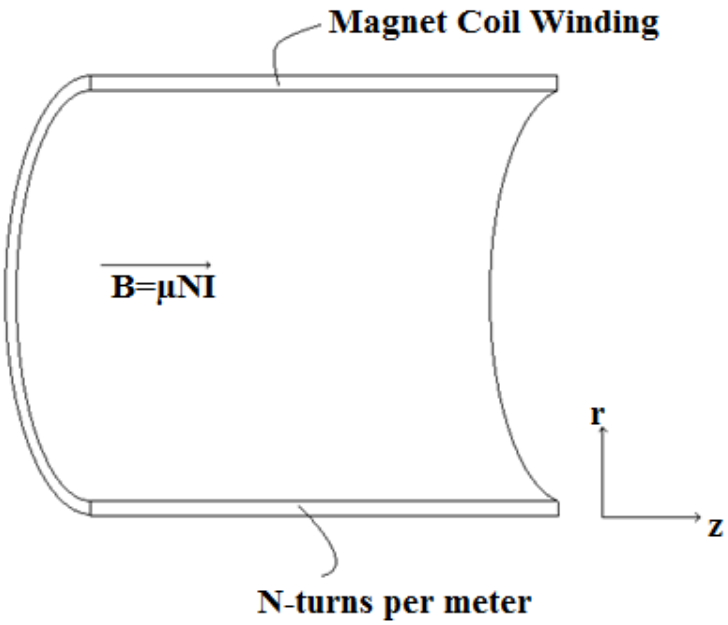

Figure 20 Geometry of solenoid

In this thesis study, our main concern is design of electron gun; however beam focusing can be required for some application. Therefore effects of solenoid and uniform magnetic field on the electron beam will be investigated in proceeding parts for some cases.

CHAPTER 4

SIMULATION OF ELECTRON GUN AND PARAMETRICAL ANALYSIS

4.1 Particle in Cell Method

Particle in Cell (PIC) is commonly used computer simulation code which simulates the motion of charged particles. In1950s, first PIC simulation was conducted by Buneman and Dawson and they simulated motion of 100-1000 particles and their interaction [21**]**. Today, PIC codes can simulate in the order of 10^{10} particles. Many simulation tools have been developed by PIC code, such as EGUN, KARAT, TRAK, MAGIC and CST PS.

SLAC Electron Trajectory Program known as EGUN development was started by Bill Herrmannsfeldt at Stanford Linear Accelerator Center (SLAC) in 1962 to compute charged particles trajectories under electromagnetic fields [8], [22]. EGUN is the first program developed by SLAC program. Then EGUN family became wider. POLYGON and INTMAG was developed to set up boundaries and to calculate magnetic fields without saturation. Lastly, IGUN was introduced to simulate plasma sheath for the extraction of positive ions [23**]**.

KARAT is another PIC code to be developed to solve electrodynamics problems with relativistic electrons and nonrelativistic ions by V.P. Taranakov in Russia [24**]**. KARAT is appropriate to simulate high current devices like vircators, free electron lasers. In [24**]** and [25**]**, vacuum tube geometries with relativistic electron beam were simulated by using KARAT.

MAGIC Tool Suite is a commercial PIC code of ATK - Mission Systems Group, USA. It is electromagnetic PIC code based on time domain finite difference (EM PIC

FDTD), which provides reliable solution to interaction between charged particles and electromagnetic fields problems [26]. MAGIC code has powerful algorithms to represent structural geometries, material properties, incoming and outgoing waves, particle emission processes, and ionization of background gaseous media thus it has very widespread usage in plasma physics [26]. Moreover, ATK has published many researches to measure performance of MAGIC as in [27], [28] and [29].

Simulation of coaxial cylindrical vircator was performed using MAGIC code in METU and represented SAVTEK Conferences in 2012 [30]. In this study, vircator geometry in Figure 21, was simulated and effect of anode cathode gap on resonance frequency was investigated. MAGIC2D simulator was used since the geometry is symmetrical around z-axis.

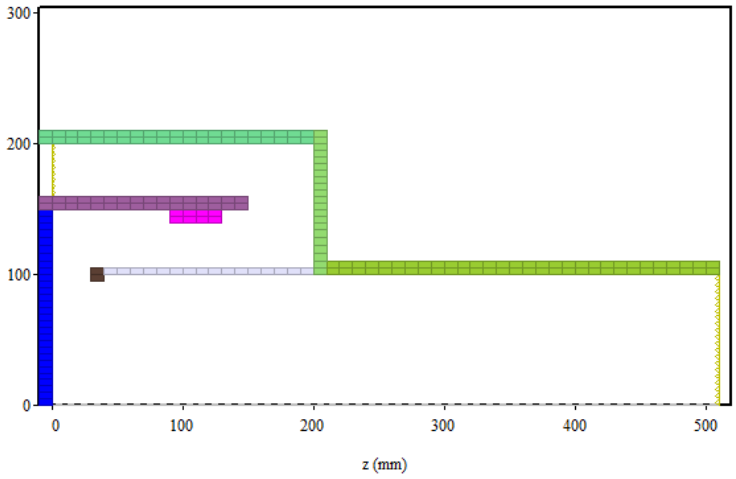

Figure 21 Cross section of coaxial cylindrical vircator [30]

Anode cathode gap was chosen according to efficiency and frequency dispersion. Example of simulation outputs such as power density spectrum and output power is illustrated in Figure 22 and Figure 23 respectively.

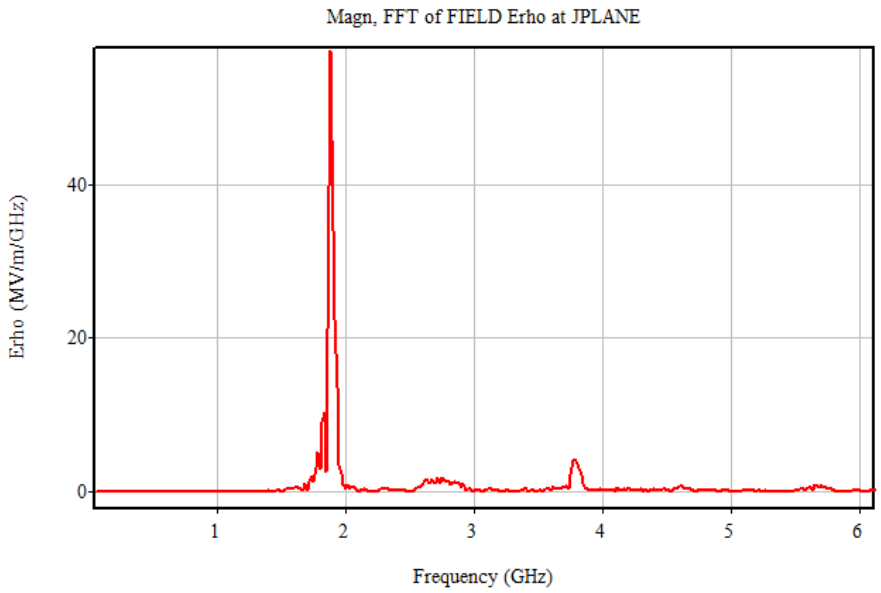

Figure 22 Radial E field power density spectrum [30]

CST Particle Studio is developed by Computer Simulation Technologies lately to simulate charged particle dynamics under electric and magnetic fields. In this thesis, CST PS was used since access of CST PS is easer and user interface is more convenient. CST PS has some special tool to simulate different type of problems namely, Tracking, PIC and Wakefield Solver. In [31**]**, single and multibeam electron gun is simulated by Tracking Solver. In addition to that, collector design is performed more effectively since secondary emission can be included as in [32**]**. When RF excitation and time domain simulation are required, PIC Solver must be used. With PIC solver, magnetron, TWT or BWO can be simulated. In [33**]**, 140 GHz spatial harmonic magnetron was designed and simulated by CST PS PIC Solver.

All over the world, researchers are studying on development of their own PIC codes in order to use their specific vacuum electronic device studies. For example, VORPAL has been built by Center of Integrated Plasma Studies and Department of Physics to simulate laser plasma interaction problems [34**]**. Furthermore, Draco ES-PIC Code was introduced by Lubas Briedo to use in simulations of ion beam neutralization [35**]**. The other specific code is UNIPIC software was constructed to analyze power terahertz vacuum electronic devices [36**]**.

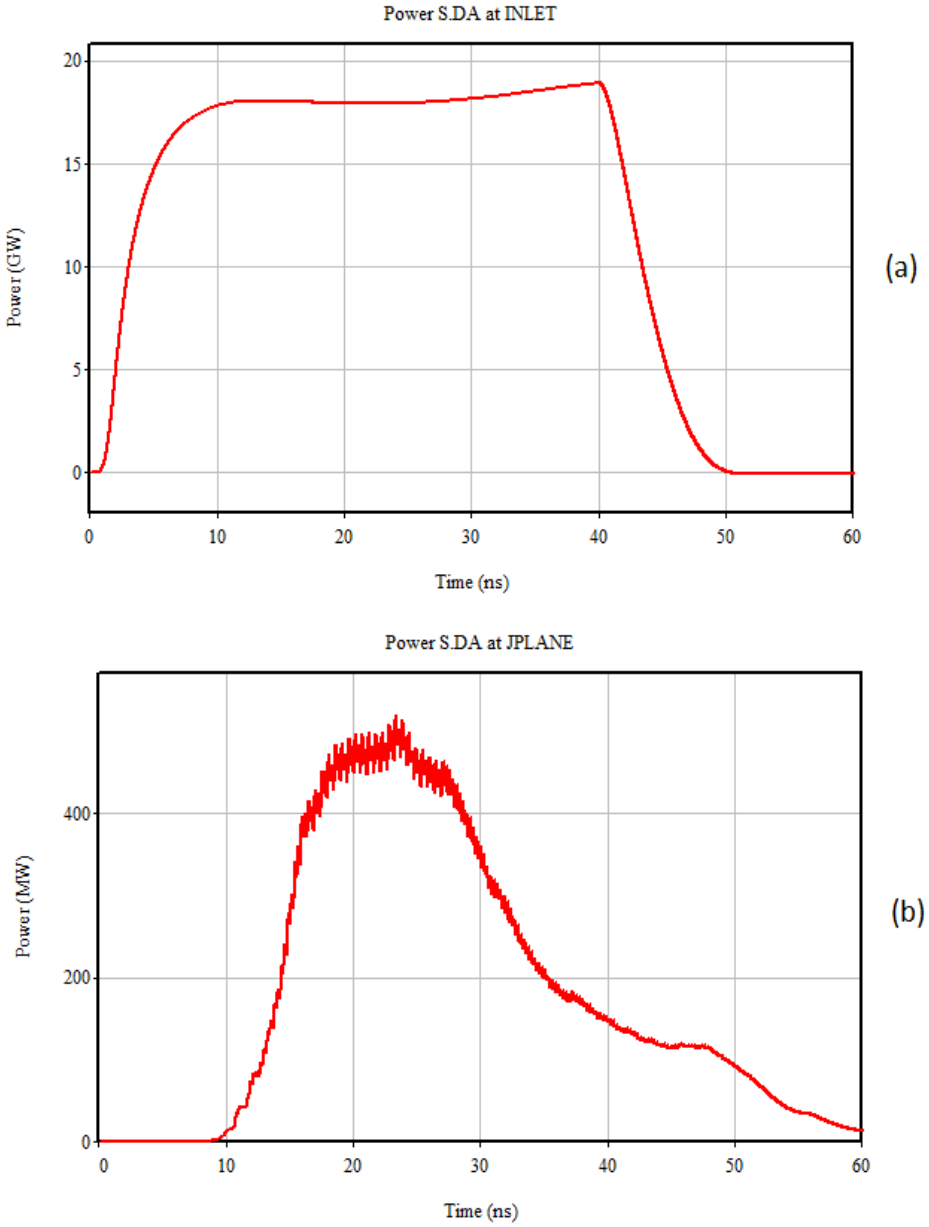

Figure 23 Microwave powers [30], (a) Input power, (b) Output power

Charged particle motion simulation is very complicated problem which can include external and self induced electromagnetic fields, motion of particles, particle interactions and their interaction with solid objects. However, PIC simulation method reduced computational procedures with its algorithms. In PIC method, simulation region is divided in cells and discrete charge and current density arrays are defined in each cell [7]. The charge density in a cell at time *t* is calculated by multiplying

number of computational particles in the cell with the charge per computational particle divided by the cell volume. On the other hand, current density is product of average vector velocity of computational particles and their charge divided by the cell area [7**]**. In order to generate electromagnetic field, finite difference solution of Maxwell's equation and space charge and current density equation are solved together.

The most common and simple method to simulate particle motion is leapfrog. In Figure 24, leapfrog algorithm is illustrated.

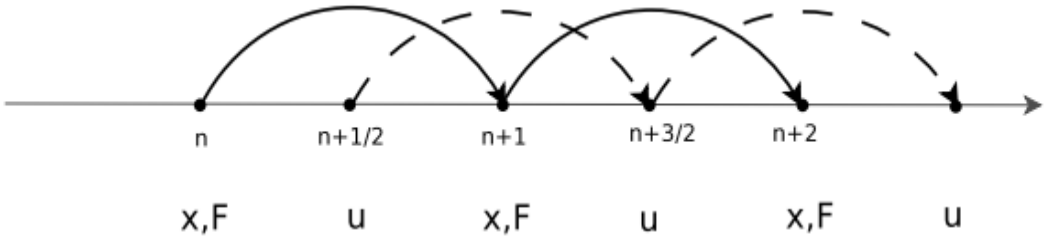

Figure 24 Leapfrog algorithm representation [37]

In Figure 24, progress in position from time level n to n+1, uses the velocity at midpoint $v^{n+1/2}$, while progress of velocity from time level n-1/2 to n+1/2 uses position at midpoint $\vec{r}^{\,n}$. For particle motion simulation, velocity and position are updated according to (64) and (65) [38**]**. That means that ν(t+Δt) is calculated from ν(t) and electromagnetic field at t+Δt/2 in (64) and position r(t+3Δt/2) is calculated from r(t+Δt/2), previous time step for position, and ν(t+Δt) in (65). Then at the next time step field values are calculated from that position.

$$\frac{d}{dt}(m\vec{v}) = q(\vec{E} + \vec{v} \times \vec{B}) \Rightarrow m^{n+1}v^{n+1} = m^n v^n + q\Delta t(\vec{E}^{n+1/2} + \vec{v}^{n+1} \times \vec{B}^{n+1/2}) \quad (64)$$

$$\frac{dr}{dt} = v \Rightarrow \vec{r}^{\,n+3/2} = \vec{r}^{\,n+1/2} + \Delta t\vec{v}^{n+1} \quad (65)$$

Stability is important concern in PIC simulation. Time step and cell size should be properly chosen to have stable simulation. Time step limitation is given in (66) and (67). These equations states that time step should satisfy both light wave and Langmuir wave propagations [37**]**.

$$c\Delta t < \Delta x \tag{66}$$

$$\omega_{pe}\Delta t < 2 \tag{67}$$

In addition to that, cell size should satisfy condition in (68), where ς is constant of order of 1.

$$\Delta x < \varsigma\lambda_{De} \tag{68}$$

4.2 CST Particle Studio Simulation Tool

In this thesis, simulation studies were carried on by Computer Simulation Technologies (CST) Particle Studio (PS) software. CST PS is a simulator to analyze charged particle dynamics in 3D electromagnetic fields fast and accurately [10]. It is very powerful tool in simulation vacuum device like magnetron, travelling wave tube and electron gun. In Particle Studio, there are three different solvers namely Particle Tracking, Particle-in-Cell and Wakefield Particle solver. These three solvers focus different type of particle problems, thus they provides more accurate and efficient solution. Besides these three solvers, Particle Studio tool is integrated with CST 3D Electromagnetic Studio electro-magnetostatic solver and CST Microwave Studio [10]. CST PS is based on the algorithms used in the MAFIA-4 simulation package. MAFIA-4 is a general purpose electro-magnetic simulation software package whose solution method is Finite Integration. MAFIA-4 includes module for simulation of transient magnetoquasistatic fields including effects of nonlinear material and eddy currents induced by moving conductors [39].

Particle Tracking Solver track particles in pre-calculated electromagnetic fields by using Lorenz force equations. Gun iterations option provides to taking into account space charge effects on electromagnetic fields [10]. Particle Tracking Solver is suitable for the problem types such as electron gun, collector, magnets and cavities, which do not include time variation and RF field. In this thesis, Particle Tracking solver is used in electron gun and coil simulations, therefore in the next section Particle Tracking Solver and its capabilities will be investigated in detail.

Particle-in-Cell is the most sophisticated module which takes into account particle and time-varying electromagnetic fields. In PIC mode, the particles can interact with a combination of electrostatic, magnetostatic, eigenmode, transient electromagnetic and user defined fields [10]. Simulation of microwave vacuum device such as travelling wave tube, klystrons and backward wave oscillators should be performed in this solver because of RF excitation.

Wakefield solver is used to calculate the electric and magnetic field when longitudinally Gaussian shaped charge distribution, representing the beam is imposed to the geometry. This solver provides beam frequency, wakepotential, impedance and loss factors [10]. The simulation of cavities, collimator and beam position monitors are typical applications of Wakefield solver.

4.2.1 CST PS Particle Tracking Solver Capabilities for Gun Design

The tracking algorithm of CST PS use leapfrog algorithm which is mentioned before. In addition to that, in the gun simulation, gun iteration should be used to take into account space charge effects. Gun iteration procedure follows the algorithm in Figure 25. Until space charge converged to user defined value, the process in Figure 25 continues.

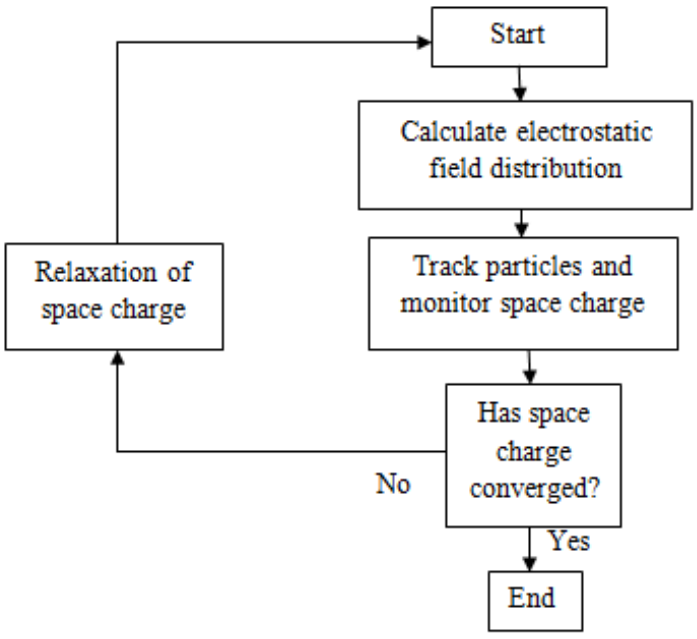

Figure 25 CST PS Tracking Solver gun iteration algorithm

In Figure 26, simulations of particle gun without and with gun iteration algorithm is seen respectively. In Figure 26.a the space charge effects are ignored, which is not realistic particle gun simulation.

In the gun simulation, the most important component is particle source. The emitted particle can be electron, proton or helium ion. Moreover, the particle type can be defined with its charge and mass. It is possible to define more than one particle sources with different particle type on different faces; however from one face only one particle type can be emitted.

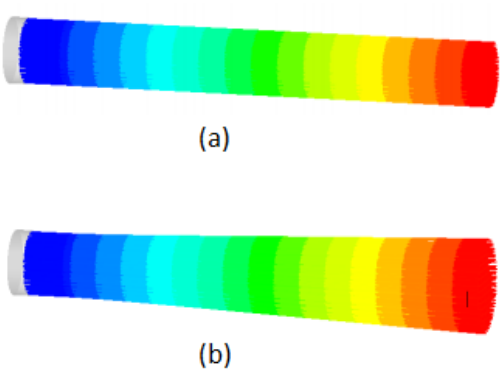

Figure 26 Particle gun examples, (a) Without gun iteration, (b) With gun iteration [40]

There are four types of emission models namely fixed, thermionic, field induced and space charge. In fixed emission, charge and kinetic energy is defined and unlimited number of particles is emitted from particle source [41]. Space charge emission model is based on Child-Langmuir model and particles are emitted according to Child law in (28). In Figure 27 Child-Langmuir model is shown. In this model, $V_0^{3/2}$ in (28) is taken as $(\Phi(d)-\Phi(0))^{3/2}$, thus unlimited particle is extracted depending on this field value [41].

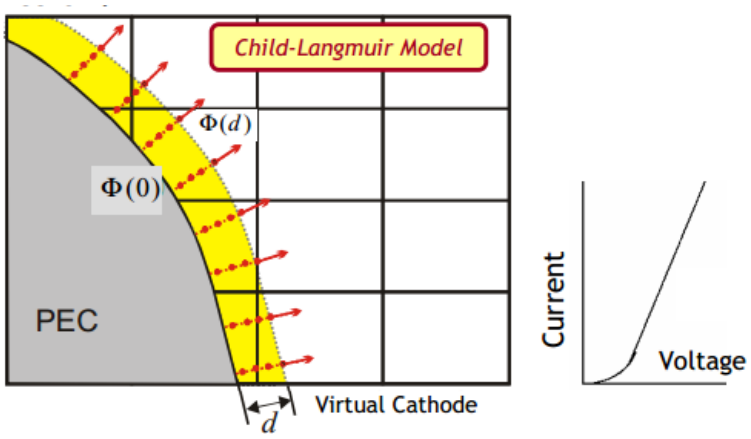

Figure 27 Space charge limited emission model in CST PS [41]

In this thesis, electron gun simulation was performed in space charge emission model, because simulated guns are assumed to have space charge limited electron flow. In simulation, the distance d between PEC and virtual cathode in Figure 27, should be minimized to obtain reliable results. The distance can be lowered by dense meshing the region around the cathode. In Figure 28, the red face is defined particle source while blue face is virtual cathode. The virtual cathode is too much far away from defined surface for the particle source in Figure 28.a. The distance is reduced by increasing mesh; however number of mesh raises simulation time, therefore mesh size can be reduced locally. In Figure 28.b it can be seen acceptable virtual cathode distance.

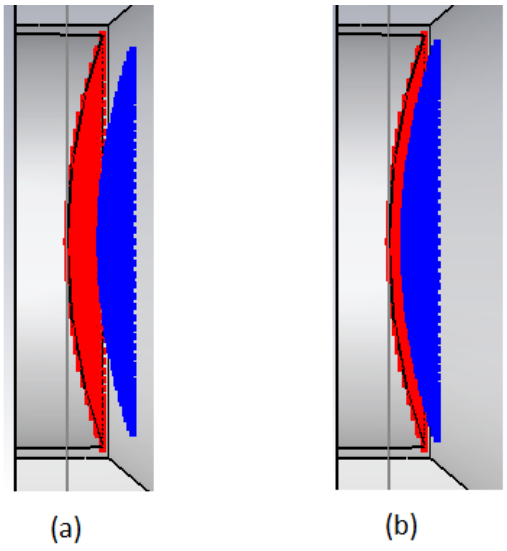

Figure 28 Virtual cathode examples in space charge emission model,
(a) Improper virtual cathode distance, (b) Acceptable virtual cathode distance

Thermionic emission model is based on Richardson-Dushman equation given in (69). In this model, limited particles are emitted according temperature. Particle extraction is depending on field close to emitting surface until all particles are emitted. Space charge limited and temperature limited current voltage relation is illustrated in Figure 29.

$$J_s = AT^2 e^{-\frac{e\Phi}{kT}} \tag{69}$$

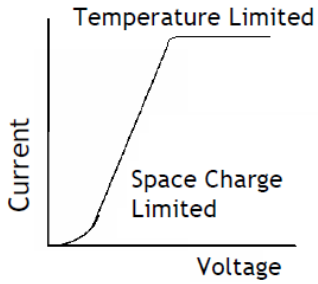

Figure 29 Temperature and space charge limited current voltage relation

The last emission model is field induced emission in which particle extraction occurs due to high electric field. Fowler-Nordheim equation in (70) governs the field induced emission. Field and current relationship is shown in Figure 30.

$$J_s = AE^2 e^{-B/E} \tag{70}$$

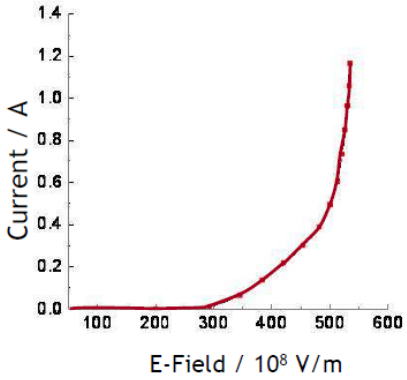

Figure 30 Current vs. electric field in field induced emission

Furthermore CST PS can handle secondary emission caused by particle hitting a metal surface. This effect is important in collector design.

Since there are magnetostatic solver and electrostatic solver inside CST PS, it is possible to create magnetic field with periodic permanent magnet and coils and to observe its effects on particle beam.

The outputs related to particle beam of the CST PS are 3D trajectory, beam current, energy and etc. E and H field can be computed and illustrated in 3D. Moreover with particle monitors it is possible to take particle parameters such as kinetic energy, current, velocity on 2D plane.

4.3 Simulation of Planar and Cylindrical Pierce Gun

In Chapter 3, analysis of Pierce gun design was described. In this part of the thesis, results of simulation of planar and cylindrical gun will be discussed. For planar pierce gun simulation, geometry in Figure 15 was taken. In the simulation, planar gun is constructed in y-z plane, so in x dimension is large compared to the extraction gap. Furthermore, anode was formed with extraction grid to keep the potential same on the anode. The geometry of planar gun in simulation is given in Figure 31. The cathode and focus electrode potential is -50kV and anode potential is 0V. Also, anode cathode gap is taken as 4cm.

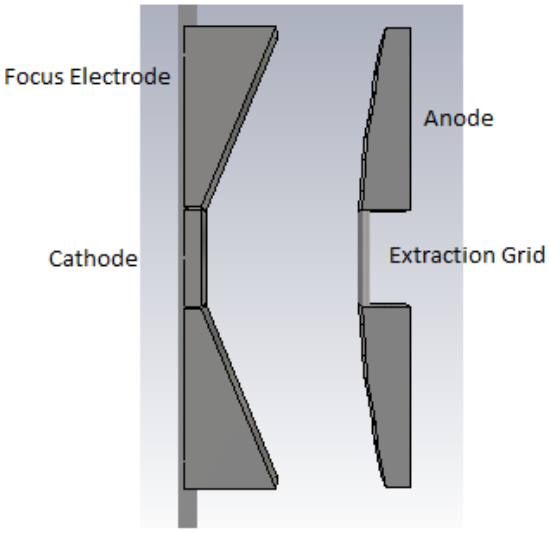

Figure 31 Geometry of Pierce gun in CST Particle Studio

In Chapter 3, it is mentioned that if there is infinite width sheet beam electron gun as in Figure 14.a, (29) is valid. However, when bounded width sheet beam electron gun,

to satisfy (29), focus electrode and modified anode are needed. In CST PS, electron gun geometry in Figure 14.a with bounded electron beam and Pierce electron gun are simulated to compare results and effects of focus electrode and modified anode. In Figure 32, potential line and beam trajectories are shown for both configurations.

In Figure 32.a, equipotential line near cathode region cannot follow (29), therefore electron beam diverges as in Figure 32.c. However, in Pierce planar gun geometry in Figure 32.b and Figure 32.d, equipotential lines is same as in Figure 15 and satisfy (29) and electron beam travels through extraction gap without diverging.

In general, cylindrical electron beam is required in application. The design of electron gun is the same as planar Pierce gun. This time, potential line should follow (71) along a beam boundary at r_o.

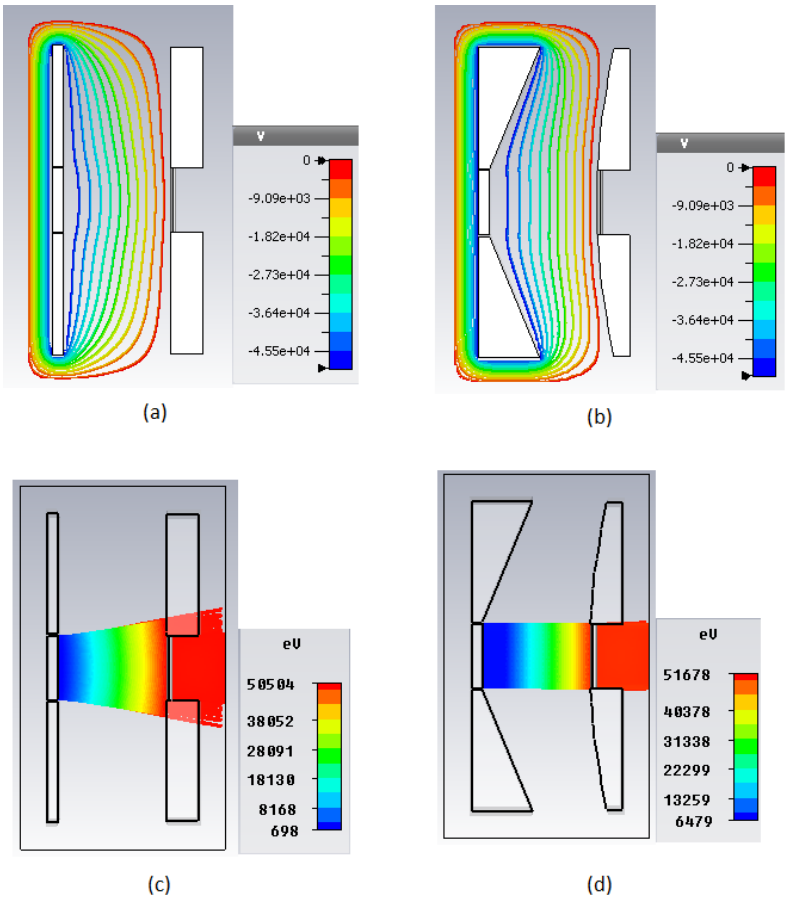

Figure 32 Comparison of planar gun and Pierce planar gun (a) Potential line of planar gun, (b) Potential line of Pierce planar gun, (c) Electron beam of planar gun, (d) Electron beam of Pierce planar gun

$$\phi(r_o, z) = V_o(\frac{z}{d})^{\frac{4}{3}} \tag{71}$$

Cylindrical Pierce gun simulation performed by CST PS and the results are compared with cylindrical Pierce gun simulation in [7], which is shown in Figure 33.

In Trak simulation, V_o is taken 50kV and current is found as 79.83A, while calculated current according to planar Child law in (28) is 81.84A.

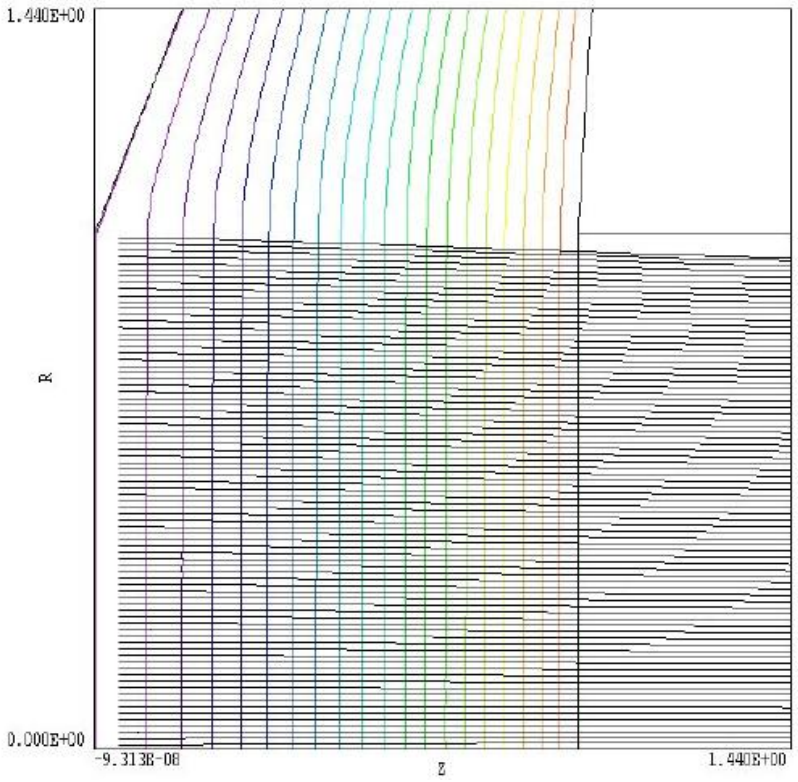

Figure 33 Cylindrical Pierce gun simulations by Trak code in [7]

In CST PS simulation of cylindrical Pierce gun equipotential line and electron beam are given in Figure 34. In this geometry, V_o=50 kV, anode cathode gap d=8.55mm and cathode radius r_c=9.2mm are taken. When Child law equation in (28) is solved for these dimensions, beam current is calculated as 94.755A. In CST PS simulation, current is found 91.18 A, which is slightly lower than calculated current as in the case of Trak simulation.

From Figure 34, it can be concluded that simulation of cylindrical Pierce gun with CST PS is totally consistent with analytical solution and simulation done by Trak in [7].

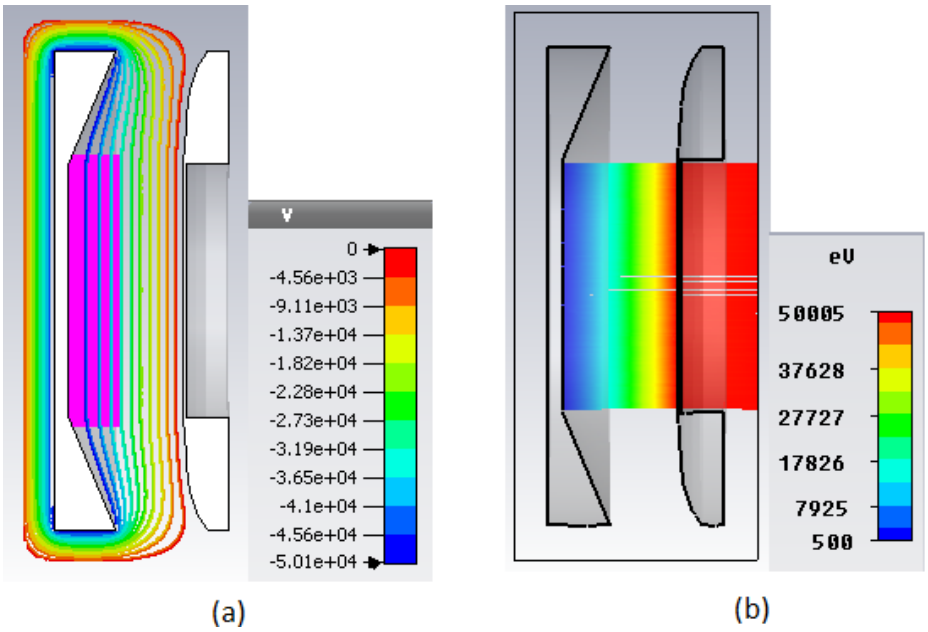

Figure 34 Simulation of cylindrical Pierce gun by CST PS (a) Potential lines, (b) Electron beam

4.4 Simulation of Medium and High Perveance Gun

In Section 3.5, the perveance value is described and the formula for the perveance is given in (54). Medium perveance gun, whose perveance near 1 μperv, is generally cylindrical gun with modified geometry. The design procedure also was given in Section 3.5.

In this part, two medium perveance converging gun geometries (Figure 7.7.a and 7.7.b in [7]) taken from [7] were simulated and results will be discussed. Electrical and geometrical parameters of the converging gun and calculated current and perveance values according to (58) are given in Table 1. The geometrical parameters are consistent with the Figure 16.

Table 1 Simulation parameters of medium perveance converging gun

r_c	r_a	θ	V_o	I	P
20.8mm	9.6mm	37^o	20kV	0.686A	0.2425μP

In the first geometry, the focus electrode is inclined 22.5^{o} according to vertical axis as in Pierce gun geometry. The potential line and electron beam trajectory is given in Figure 35.

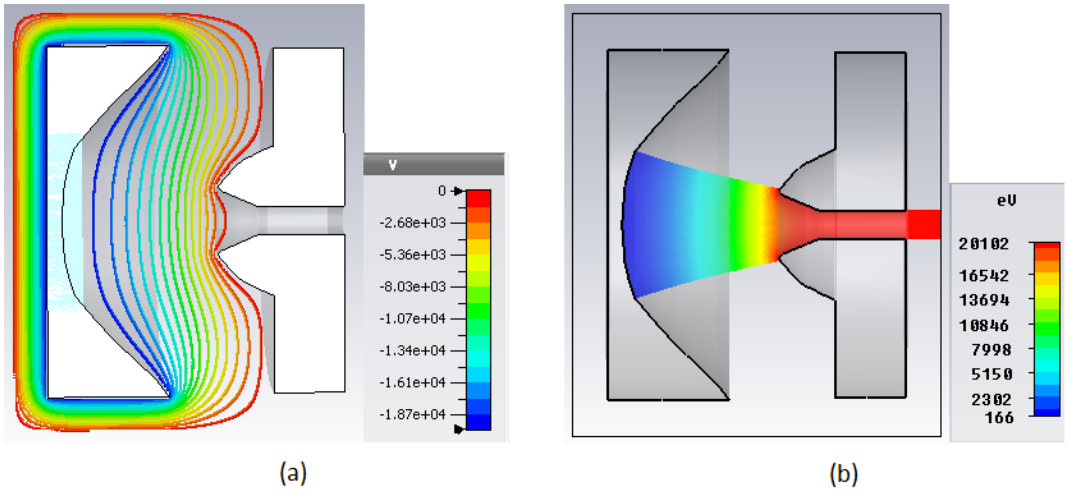

Figure 35 Simulation results of medium perveance converging gun with 22.5^{o} focus electrode (a) Potential lines, (b) Electron beam trajectory

The current and perveance values taken from simulation are 1.681A and 0.6µP respectively, that is far away from calculated values in Table 1. From Figure 35.b, it can be seen that focus electrode cannot be sufficient and beam intercepts with the anode. For the second geometry, the focus electrode is inclined 37.5^{o} wrt. cathode edge while keeping other parameters same. Then, equipotential line and beam trajectory become as in Figure 36 for modified converging gun.

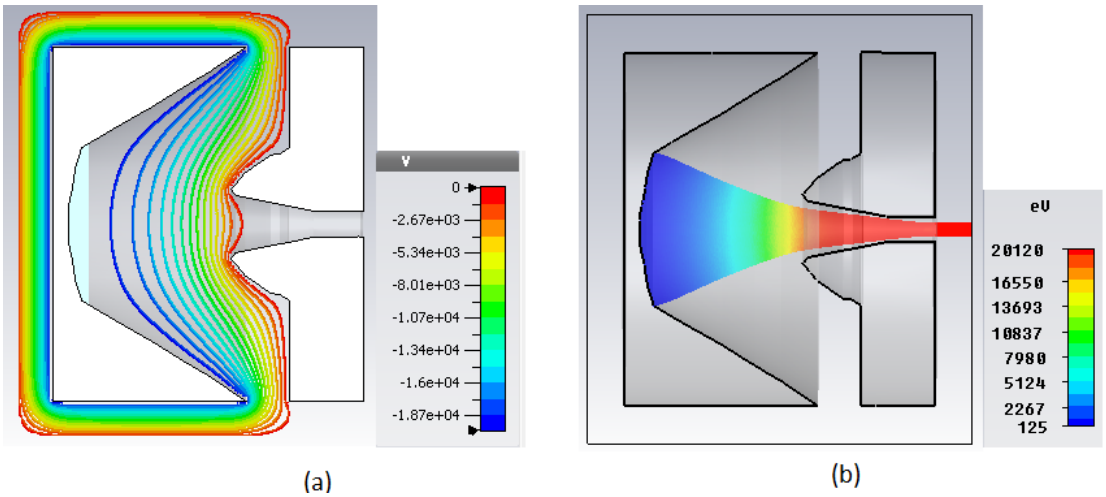

Figure 36 Simulation results of medium perveance converging gun with 37.5^{o} focus electrode (a) Potential lines, (b) Electron beam trajectory

In Figure 36, it is seen that all electrons can passing through into anode aperture. Also, the current and perveance are found as 0.733A and 0.26µP respectively, which are in good agreement with calculated values. Moreover, from Figure 35.a and Figure 36.a, perturbation of potential line at anode aperture can be observed.

For the case of high perveance gun, perturbation is very strong at anode and cathode electric fields. The Pierce gun theory is not valid for high perveance guns. Modification on the focusing electrode can compensate large anode aperture effects. Since theory is not valid, simulation tool should be used to optimize high perveance gun design. A high perveance gun with modified focus electrode is taken from [7] and simulated in CST PS. The equipotential lines and electron beam trajectory of high perveance gun is shown in Figure 37. In this geometry anode and cathode radius are 3.65mm and 4.22mm respectively, while V_o is 50kV.

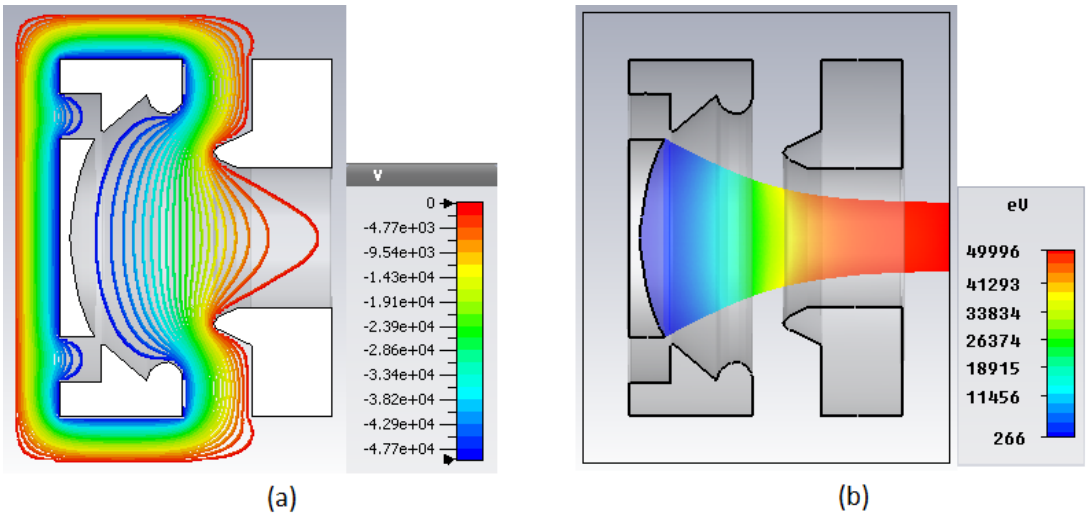

Figure 37 Simulation results of high perveance gun (a) Potential lines, (b) Electron beam trajectory

The total current and perveance were found in the simulation as 1.224A and 1.1μP respectively. In Figure 37.b, electron beam travels in extraction gap without diverging with the help of modification of focus electrode, although anode aperture distorts the electric field at extraction gap as seen in Figure 35.a.

4.5 Parametric Analysis of Converging Pierce Gun

In this part of the thesis, parametrical analysis of medium perveance converging gun is conducted in CST PS. Six geometrical parameters and two electrical parameters are investigated to understand their effects on the beam quality. Electrical parameters are cathode voltage (V_o) and focus electrode voltage (V_{foc}) whose initial values are 20kV. The geometrical parameters are shown on the gun geometry in Figure 38. Initial values of the geometrical parameters are listed in Table 2. In Table 2, some parameters have offset values like h1_offset, this offset values are added to initial values which are also shown in Table 2 in parenthesis.

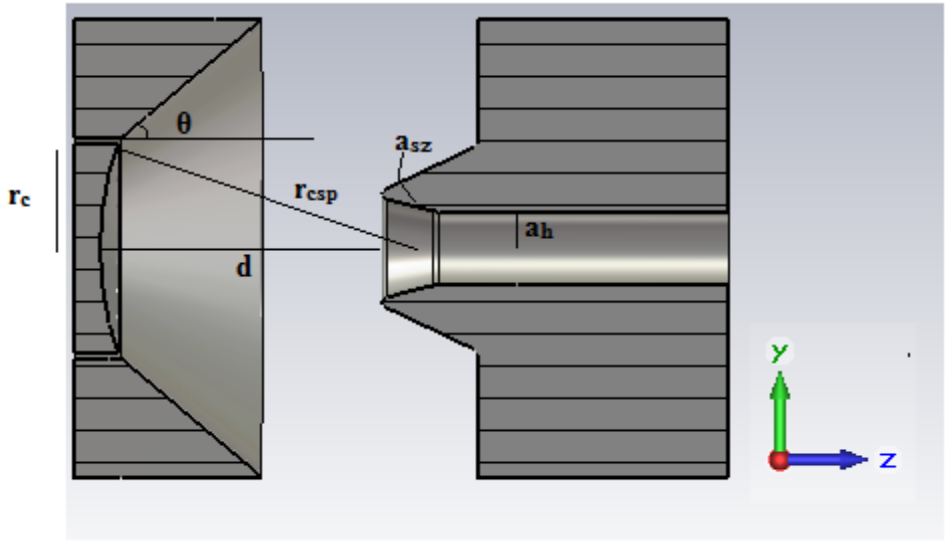

Figure 38 Geometrical parameters on the Pierce gun geometry

Table 2 Pierce gun simulation geometrical parameters in Figure 38

Parameter	Symbol	Controlling parameter in CST PS	Initial value
Focus electrode angle	θ	teta_d	40^o
Anode cathode gap	d	cat_anode_gap	5.2 mm
Anode height	a_h	h1_offset	0mm (0.7mm)
Anode slope in z	a_{sz}	anode_sl_b_z	1.20mm
Cathode radius	r_c	cat_rad_offset	0mm (2mm)
Cathode spherical radius	r_{csp}	cat_sp_offset	0mm (6mm)

In the simulation of Pierce gun, four beam parameters were taken into account, namely current, perveance, beam waist radius and beam waist position. The beam current and perveance is related each other by cathode voltage. Beam waist radius is the measure of the how much the beam confines, that is the minimum beam radius.

On the other hand, beam waist position defines that where the minimum beam radius is achieved. After that point, the beam starts to diverge. Therefore, these two properties are important. For example, if the beam waist radius is too small and beam waist position is too close to cathode, repelling force between the electrons is too strong and electron beam diverges and strike the anode. So, in order to obtain higher beam quality, to keep the beam envelope constant is more desirable.

Table 3 Swept parameters values

Controlling parameter in CST PS						
teta_d(^{o})	10	24	38	52	66	80
cat_anode_gap(mm)	2.5	3.6	4.7	5.8	6.9	8
h1_offset(mm)	-0.4	-0.2	0	0.2	0.4	
anode_sl_b_z(mm)	0.3	0.84	1.38	1.92	2.46	3
cat_rad_offset(mm)	-0.5	-0.25	0	0.25	0.5	
cat_sp_offset(mm)	-0.5	-0.25	0	0.25	0.5	
V_o(kV)	-10	-15	-20	-25	-30	
V_{foc}(kV)	-22.5	-22	-21.6	-20.8	-20	

In this part, current, perveance, beam waist radius and beam waist position are obtained for the parameters values in Table 3. This parametric simulation allows knowing that how each geometrical parameter should be modified to obtain desired beam property. For the initial value of the design parameters in Table 2, beam trajectory and beam property is given in Figure 39.

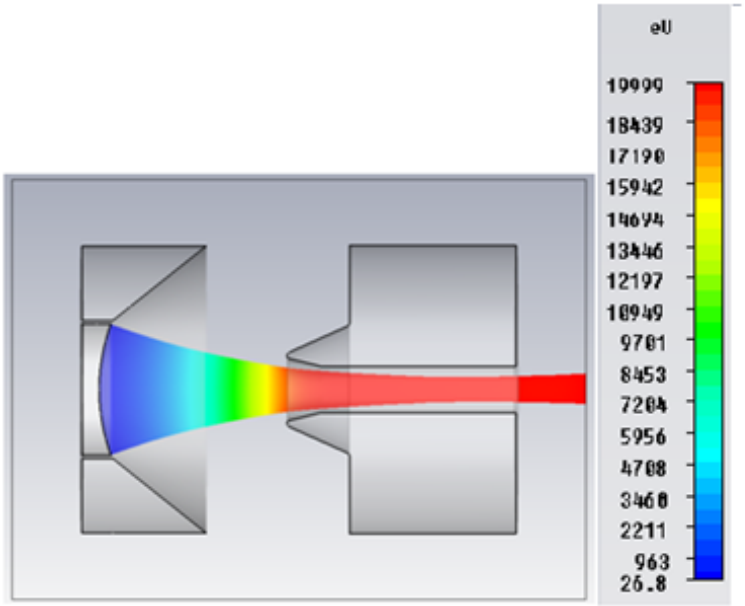

(a)

Initial Parameter Result	
Current (A)	0.75
Perveance (uP)	0.27
Beam waist radius (mm)	0.38
Beam waist position (mm)	10.25

(b)

Figure 39 Result of Pierce gun with initial parameters, (a) Beam trajectory, (b) Beam properties

4.5.1 Focus Electrode Angle

The effect of the focus electrode angle is mentioned in previous sections briefly (see Figure 35 and Figure 36). It is expected that while the focus angle decreases according to definition in Figure 38, beam waist radius decreases and beam waist position gets close to the cathode. In this part, Pierce gun was simulated for teta_d values in Table 3. The results of the simulation for beam parameters are listed in Table 4.

Table 4 Simulation result for swept focus angle

Focus Angle (teta_d(^{o}))	**10.00**	**24.00**	**38.00**	**52.00**	**66.00**	**80.00**
Current(A)	0.150	0.300	0.700	1.200	1.900	2.750
Perveance (µP)	0.053	0.106	0.247	0.424	0.672	0.972
Beam waist radius(mm)	0.13	0.170	0.34	-	-	-
Beam waist position(mm)	4.670	6.74	10.2	-	-	-

In order to observe the trend of the beam current, the graphic of the current vs. focus angle is illustrated in Figure 40. Moreover, in Figure 41, the beam trajectories for all angle values are shown.

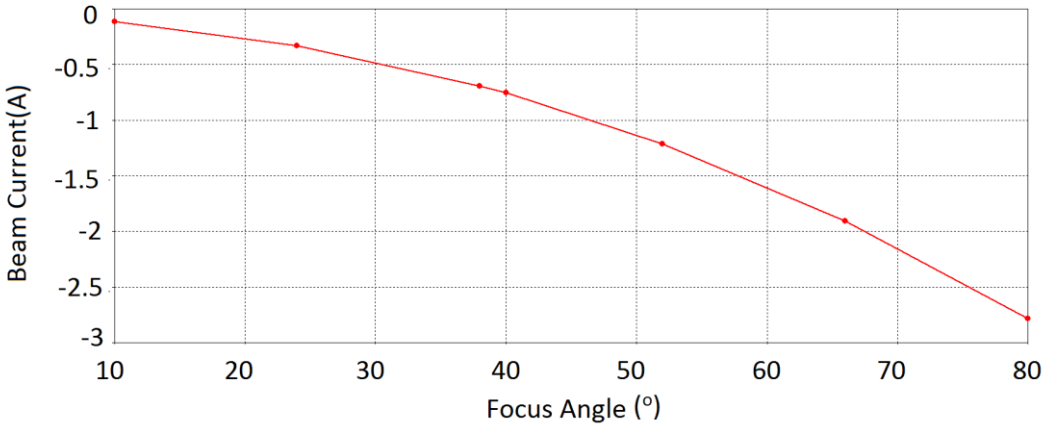

Figure 40 Focus angle vs. beam current graph

From Table 4 and Figure 41, the beam current and perveance accordingly increases with rise of focus angle from 0.15A to 2.75A. However, only 38° focus angle which is very close to initial value gives logical results. Because while first two angle values, the beam converges too early and diverges after that position, thus electrons collides the anode in extraction region. On the other hand, for last three focus angle, the beam could not confine sufficiently before entering anode and electrons strike the entrance of the anode. For 38° focus angle, the electron beam converges properly and electron could pass through into anode without diverging.

4.5.2 Anode Cathode Gap

Another important parameter in gun design is anode cathode gap. In (58), θ angle decreases with increasing the anode cathode gap according to Figure 16. Thus, from (58), the beam current is expected to decrease. Moreover, if the planar Pierce gun is considered basically, from (53), the current decreases with anode cathode gap. In this part, Pierce gun was simulated for cat_anode_gap values in Table 3. The results of the simulation for beam parameters are listed in Table 5.

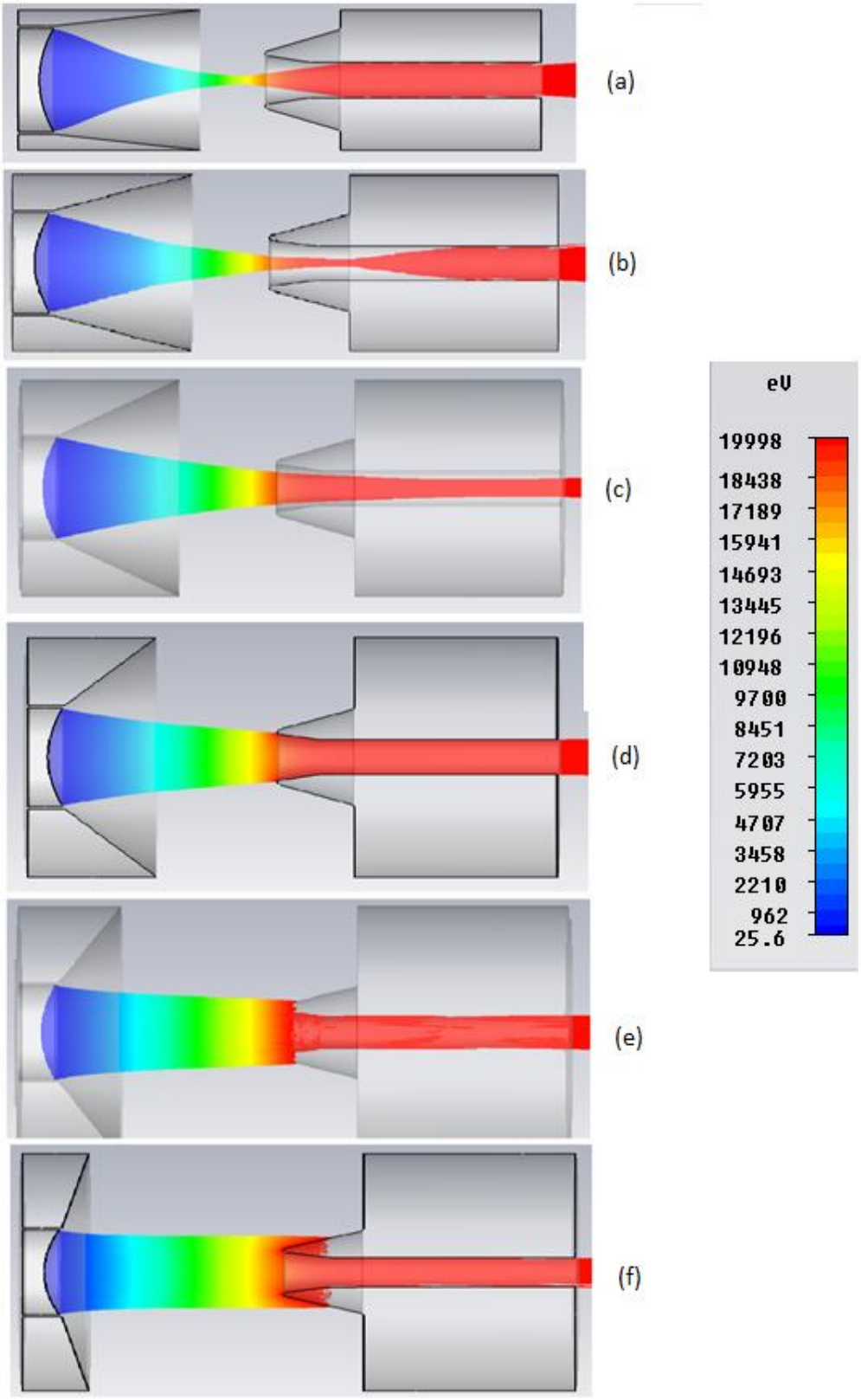

Figure 41 Beam trajectories at different focus angle (a) 10^{o}, (b) 24^{o}, (c) 38^{o}, (d) 52^{o}, (e) 66^{o}, (f) 80^{o}

Table 5 Simulation result for swept anode cathode gap

Anode Cathode Gap (cat_anode_gap (mm))	2.500	3.600	4.700	5.800	6.900	8.000
Current(A)	3.750	1.500	0.850	0.650	0.550	0.520
Perveance(µP)	1.325	0.530	0.300	0.230	0.194	0.184
Beam waist radius(mm)	-	-	0.386	0.395	0.430	0.516
Beam waist position(mm)	-	-	9.570	10.17	11.020	11.540

The current vs. anode cathode gap is given in Figure 42. It can be seen that from Figure 42, the current descends as anode cathode gap rises as expected. The beam trajectories for swept anode cathode gap value are given in Figure 43.

From Table 5 and Figure 43, it is concluded that expect for first two guns while increasing anode cathode gap, beam waist position moves away from cathode and beam waist radius becomes wider. However, for first two electron beam, due to insufficient focusing, electrons strike to anode entrance and definition of beam waist radius and position is meaningless.

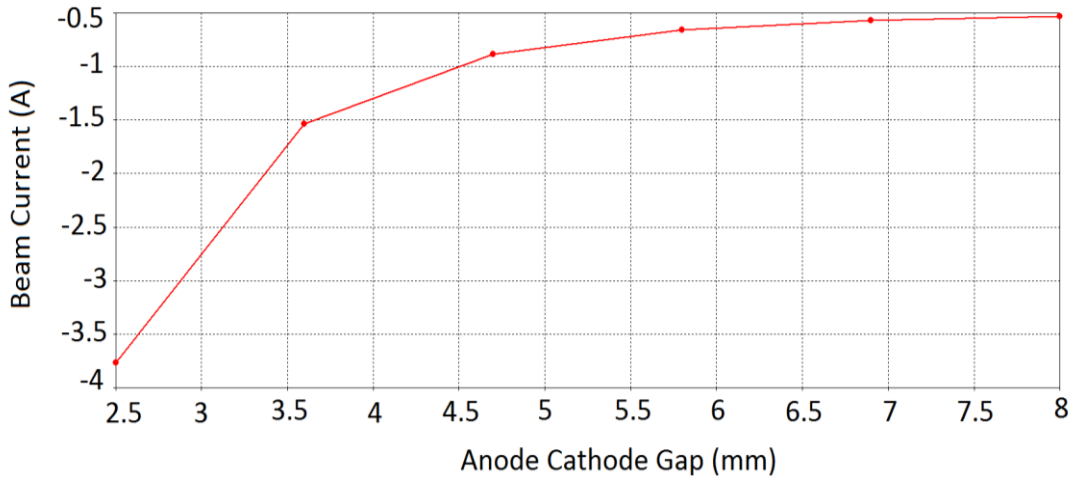

Figure 42 Anode cathode gap vs. beam current graph

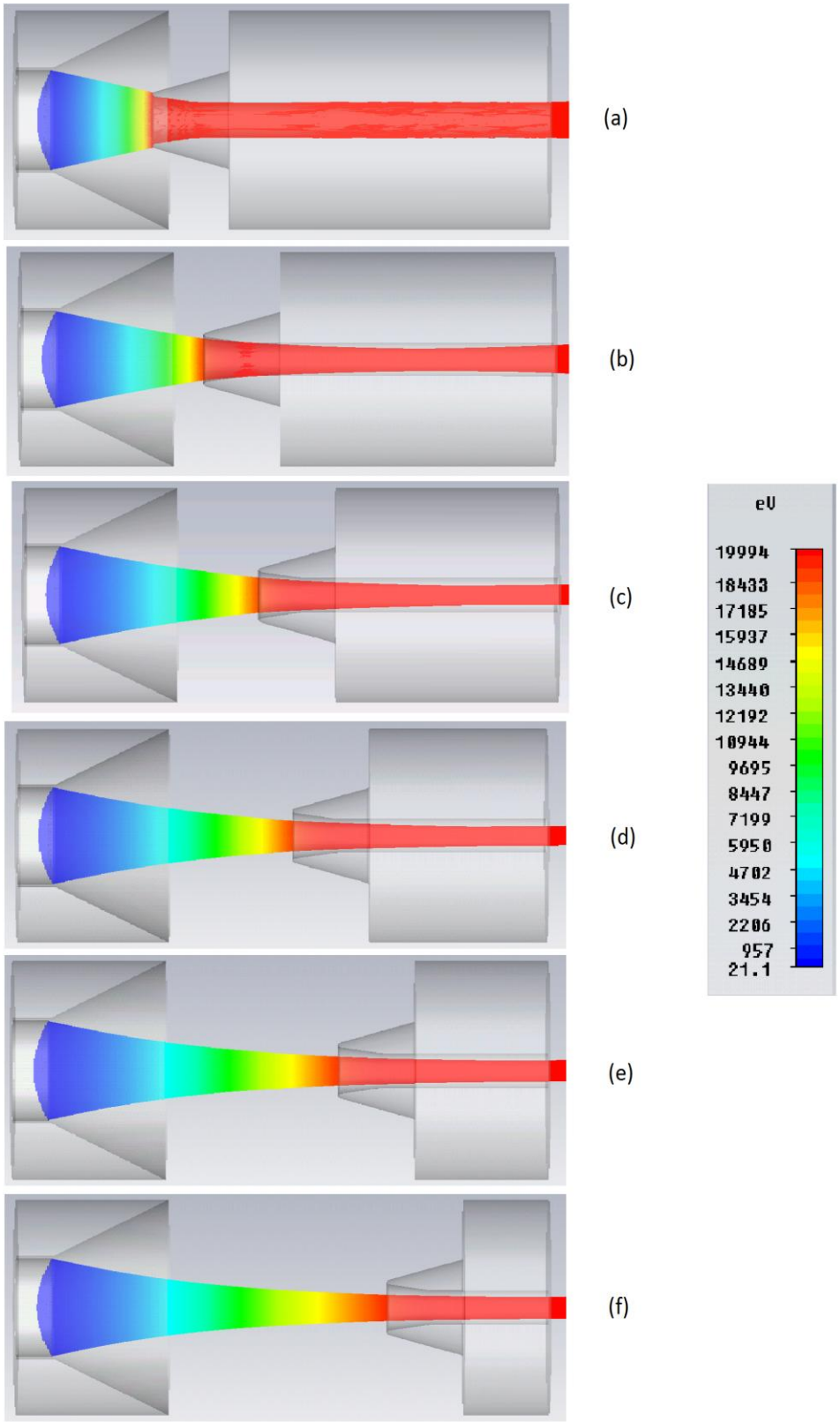

Figure 43 Beam trajectories at different anode cathode gap (a) 2.5mm, (b)3.6mm, (c) 4.7mm, (d)5.8mm, (e)6.9mm, (f) 8mm

4.5.3 Anode Height

Anode height parameter is controlled by h1_offset parameter in CST PS simulation. The initial value of a_h in Figure 38 is 0.7mm. According to (58), θ angle decrease and $\alpha\left(\frac{\rho_a}{\rho_c}\right)^2$ value decreases with increasing anode radius, thus the change in the beam current could increase or decrease according to θ angle and α^2 . The results of the simulation for anode height parameters are given in Table 6.

Table 6 Simulation result for swept anode height

Anode Height (h1_offset(mm))	**-0.40**	**-0.20**	**0,00**	**0,20**	**0,40**
Current(A)	0.735	0.745	0.755	0.755	0.760
Perveance(μP)	0.260	0.263	0.267	0.267	0.269
Beam waist radius(mm)	-	-	0.380	0.384	0.425
Beam waist position(mm)	-	-	10.250	10.1	10.000

The beam current vs. anode height graph is shown in Figure 44. The current value increases 0.735 to 0.760 from Figure 44 and Table 6, however the change is not dramatic as in anode cathode gap and focus angle simulations, because the effects of θ angle and α^2 are close to each other. For first two guns, focusing is not enough for small anode radius, so electrons collide to anode.

In previous two parts, beam waist radius and beam waist position increases together, but for this case, while beam waist position move close to cathode, beam waist radius gets wider. This situation may results from that change in anode height is more effective on beam waist radius than beam waist position. In Figure 45, the beam trajectory for the different value of anode height is illustrated.

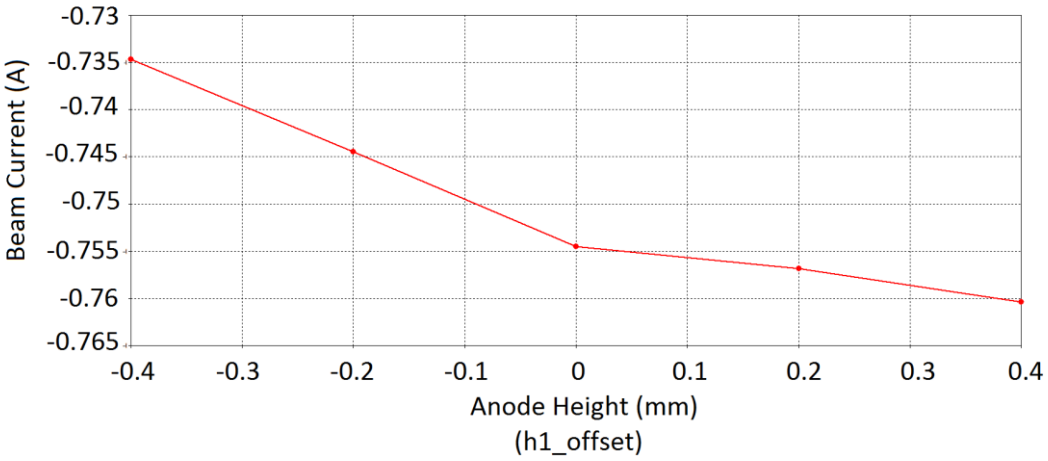

Figure 44 Anode height vs. beam current graph

4.5.4 Anode Slope

Anode slope parameter defines quantity of slope at the entrance of anode in z-direction. In some cases, as in Figure 43.c, electrons strike the anode at the entrance of anode and anode slope can be important for these cases. Therefore in this part, different anode slope values are simulated and the beam parameter results are given in Table 7.

Table 7 Simulation result for swept anode slope in z

Anode Slope in z (anode_sl_b_z (mm))	**0.30**	**0.84**	**1.38**	**1.92**	**2.40**	**3.00**
Current (A)	0.7710	0.7590	0.7510	0.7475	0.7450	0.7435
Perveance(µP)	0.2725	0.2683	0.2655	0.2643	0.2630	0.2628
Beam waist radius(mm)	0.3720	0.3950	0.3820	0.4000	0.3800	0.4000
Beam waist position(m)	10.7600	10.8900	10.6800	10.1900	10.1200	10.3200

The current graph for anode slope is given in Figure 46. As seen in Figure 46 the current decreases while anode slope rises, however the change is minimal as in anode height.

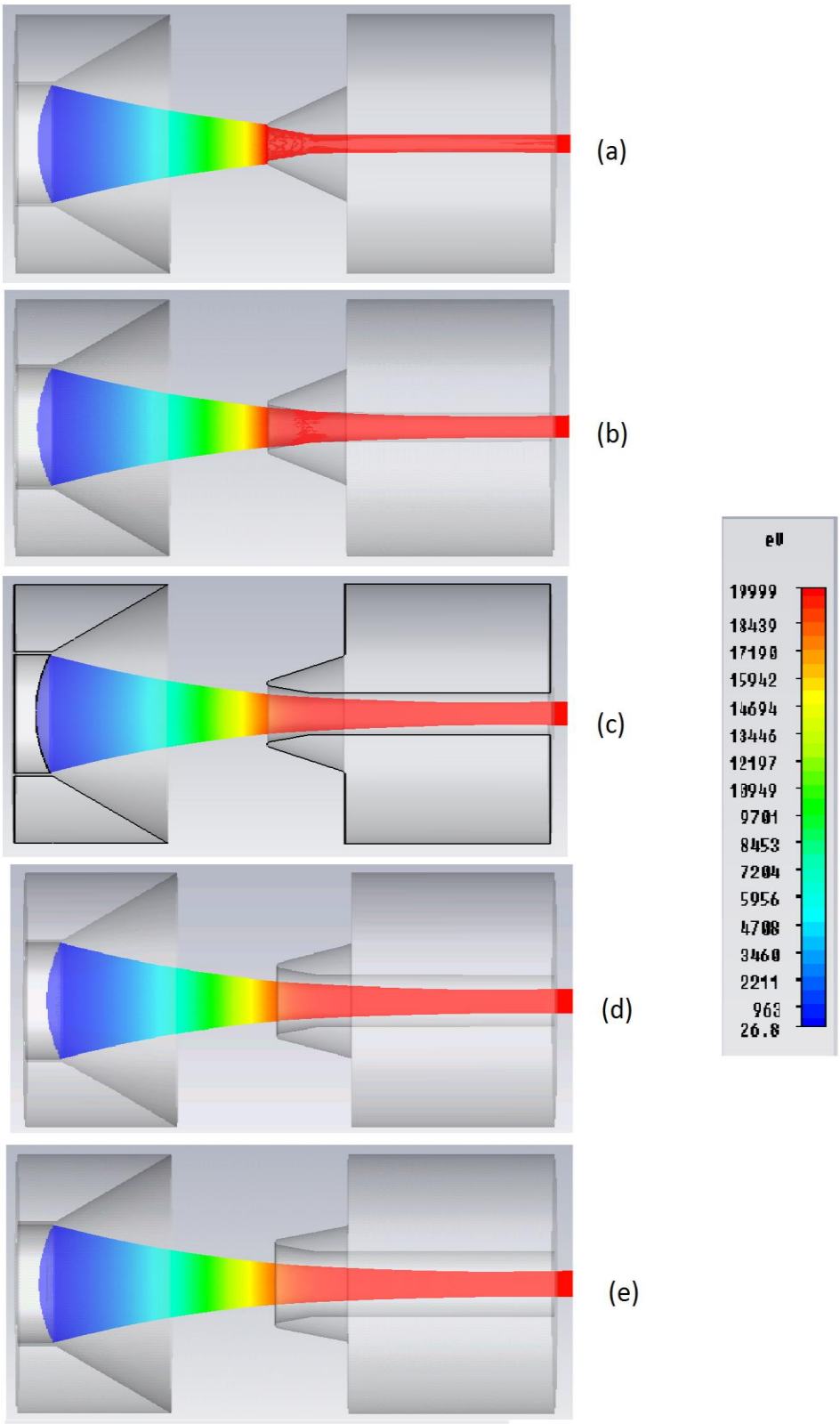

Figure 45 Beam trajectories at different anode height offset (a)-0.4mm, (b)-0.2mm, (c) 0mm, (d) 0.2mm, (e) 0.4mm

Moreover, the correlation between of anode slope and beam waist radius and beam waist position could not be observed.

The beam trajectory according to anode slope is shown in Figure 47. From Figure 47, it is concluded that anode slope change beam trajectory inconsiderable.

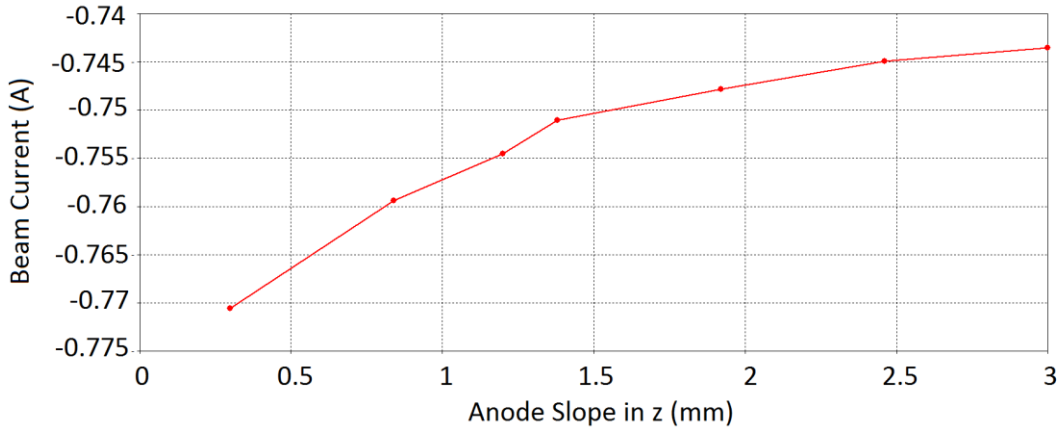

Figure 46 Anode slope vs. beam current graph

4.5.5 Cathode Radius

Cathode radius which is defined on Figure 38 is one of the most important parameters on beam current. In simulation cathode radius is controlled by cat_rad_offset parameter and initial value of cathode radius is taken 2 mm.

Cathode area is directly related to current according to (53). However for converging gun geometry equation in (58), θ angle gets large while $\alpha\left(\frac{\rho_a}{\rho_c}\right)^2$ increases, so the dominated parameter will decide the current trend. From Table 8 and Figure 48, it can be understood that beam current increases from 0.42A to 1.25A and the determining parameter is θ angle.

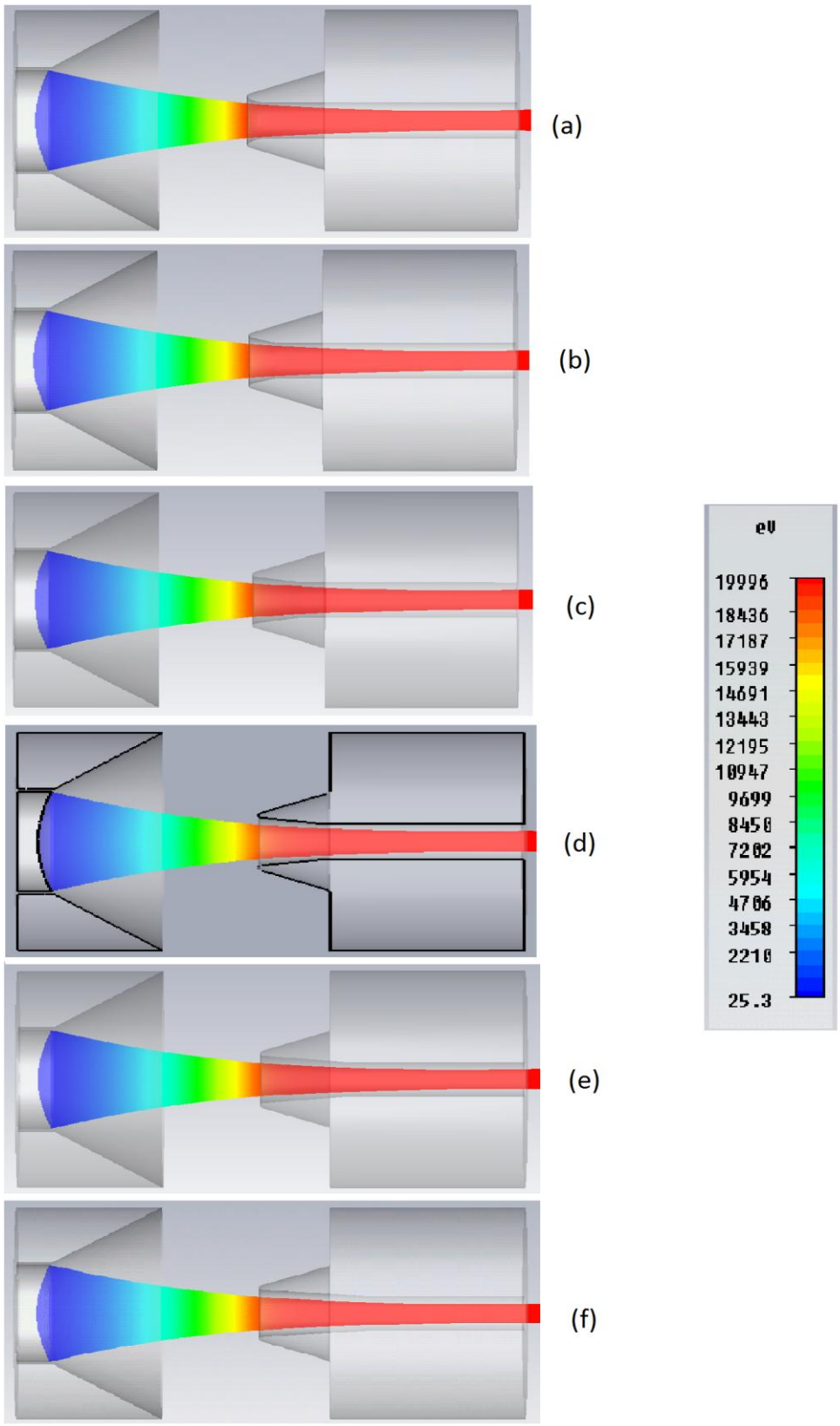

Figure 47 Beam trajectories at different anode slope in z (a) 0.3mm, (b) 0.84mm, (c) 1.38mm, (d) 1.92mm, (e) 2.4mm, (f) 3mm

Table 8 Simulation result for swept cathode radius

Cathode Radius (cat_rad_offset(mm))	-0.50	-0.25	0.00	0.25	0.50
Current (A)	0.425	0.575	0.750	1.000	1.250
Perveance(µP)	0.150	0.203	0.265	0.353	0.442
Beam waist radius(mm)	0.2760	0.3530	0.380	-	-
Beam waist position(mm)	10.2100	10.6600	10.250	-	-

For last two electron guns in Figure 49, electrons strike the anode, because the anode gap is not wide enough or focusing is insufficient. Beam waist radius is growing for the first three values of cathode radius; however the effect of cathode radius on beam waist position could not be understood.

Beam waist position value for cat_rad_offset=-0.25, is expected between 10.21 and 10.25 according to beam waist radius trend, it can be resulted from simulation and measurement accuracy. Figure 48 and Figure 49 show the beam current and beam trajectories according to cathode radius respectively.

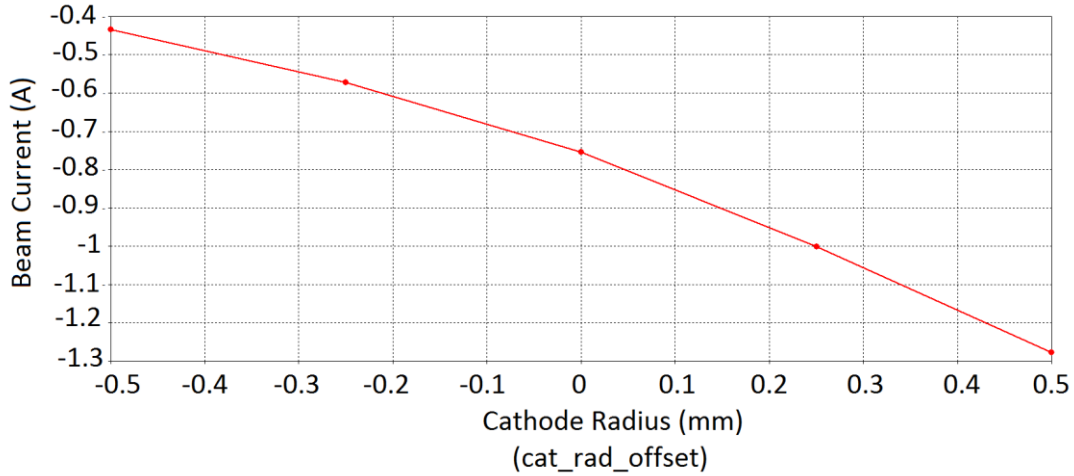

Figure 48 Cathode radius vs. beam current graph

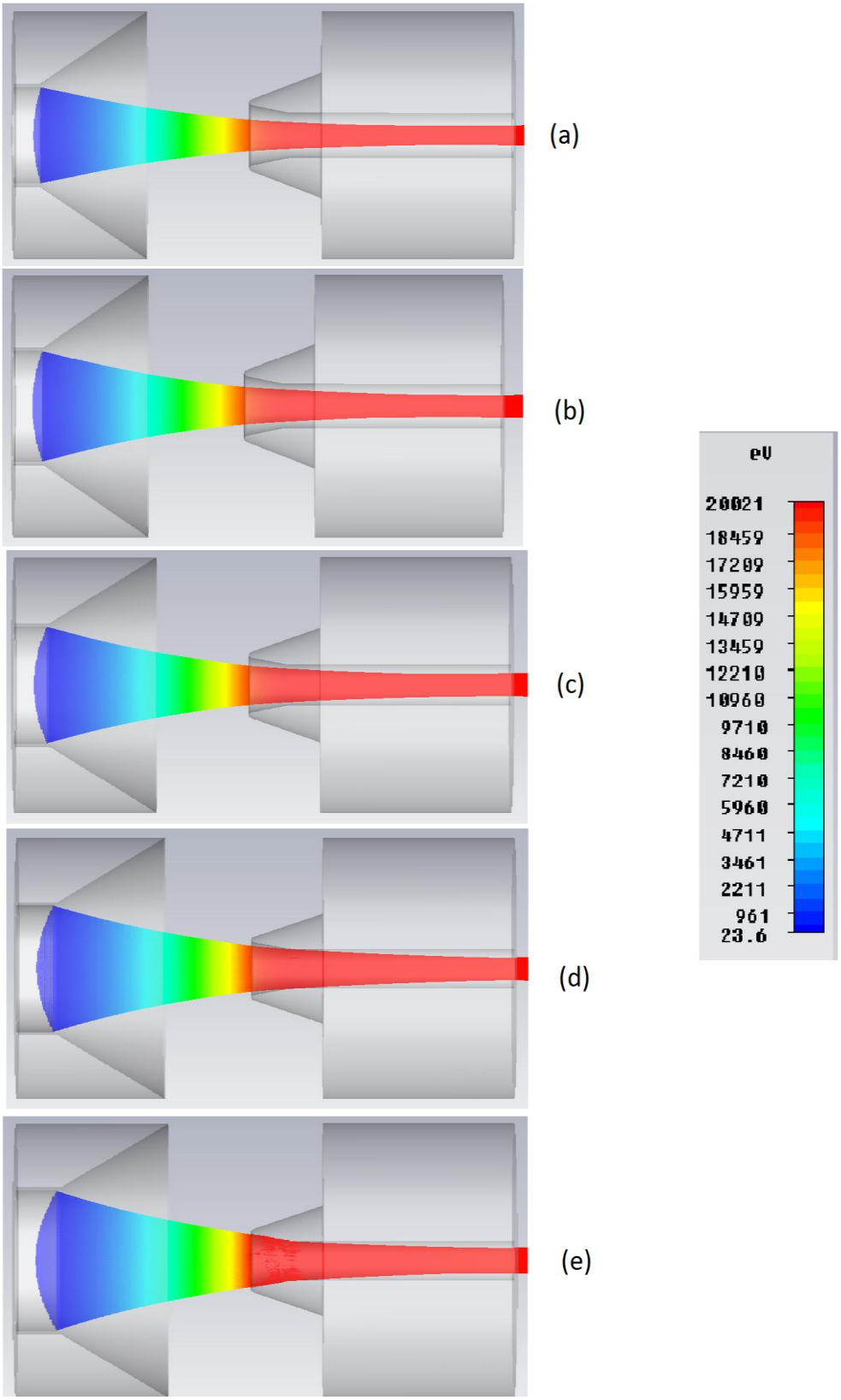

Figure 49 Beam trajectories at different cathode radius offset (a) -0.5mm, (b) -0.25mm, (c) 0mm, (d) 0.25mm, (e) 0.5mm

4.5.6 Cathode Spherical Radius

Cathode spherical radius is the measure of curvature inside the cathode, such that curvature increases while cathode spherical radius increases. The initial value of cathode spherical radius is 6 mm. It is expected that this quantity is effective on beam current because the emitting area gets larger. The results for the cathode spherical radius are listed in Table 9. The beam current graph is given in Figure 50.

Table 9 Simulation result for swept cathode spherical radius

Cathode Spherical Radius (cat_sp_offset(mm))	-0.50	-0.25	0.00	0.25	0.50
Current (A)	0.6600	0.7125	0.7500	0.8200	0.8800
Perveance(µP)	0.2330	0.2520	0.2650	0.2890	0.3110
Beam waist radius(mm)	0.30	0.34	0.380	-	-
Beam waist position(mm)	9.43	10.10	10.250	-	-

From Table 9, it is seen that beam waist position move away from cathode whereupon beam waist radius gets wider. The curvature of cathode acts like focusing electrode and the effects on the current is also same as focusing electrode, which is seen from beam trajectories in Figure 51.

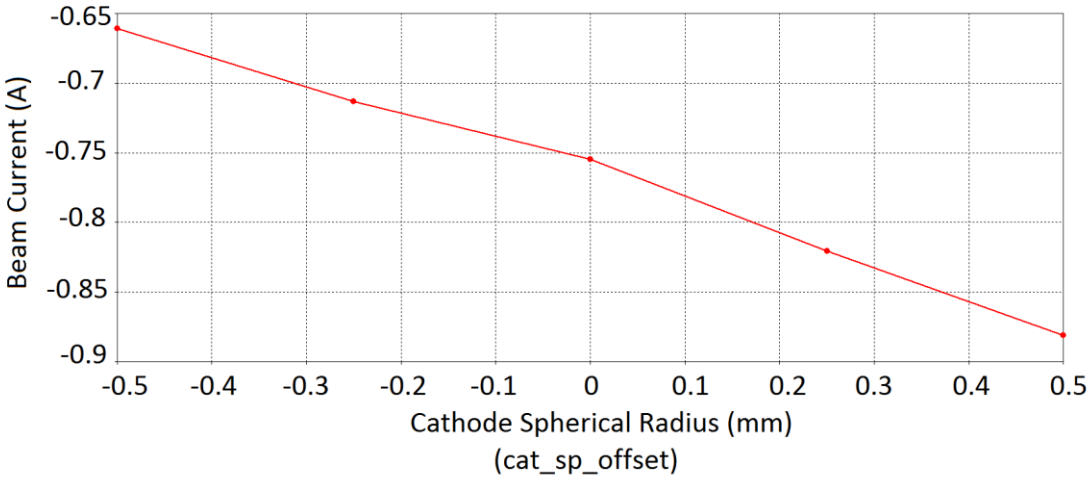

Figure 50 Cathode spherical radius vs. beam current graph

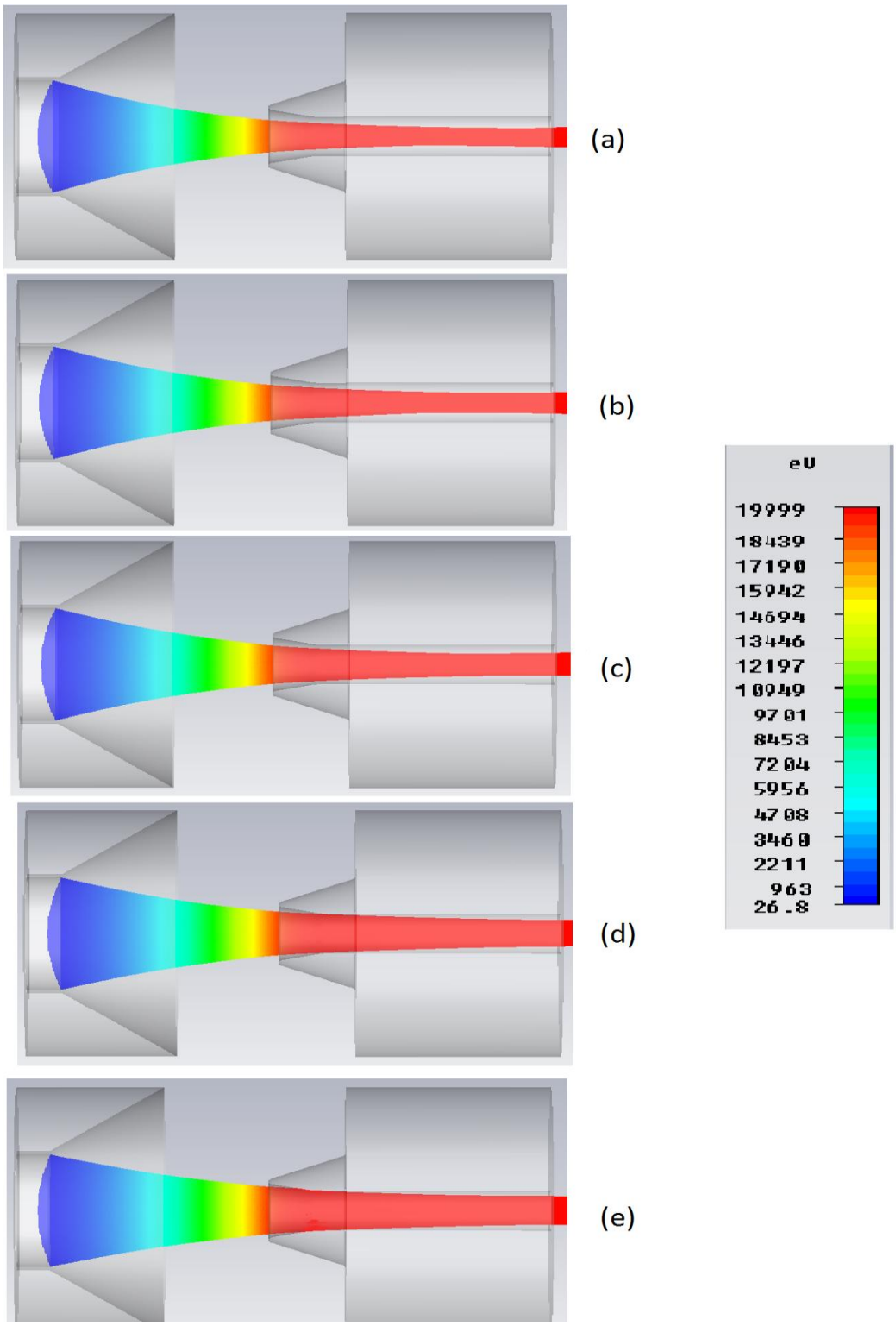

Figure 51 Beam trajectories at different cathode spherical radius offset (a)-0.5mm, (b) -0.25mm, (c) 0mm, (d) 0.25mm, (e) 0.5mm

4.5.7 Cathode Voltage

The voltage potential between the cathode and anode is produced by inserting negative voltage value to cathode body. In this simulation, focus electrode voltage is kept same with the cathode voltage. The cathode voltage is directly related to beam current with power of (3/2). However the perveance is equal to $I/V^{3/2}$ and only depends on the geometry of the electron gun. Thus, it is expected that current rises with cathode voltage but the perveance remains same. In Table 10, the simulation result for cathode voltage is given. Figure 52 and Figure 53 illustrates beam current and perveance respectively.

Table 10 Simulation result for swept cathode voltage

Cathode Voltage (kV)	-30.00	-25.00	-20.00	-15.00	-10.00
Current (A)	1.3800	1.0500	0.7500	0.5000	0.2500
Perveance(µP)	0.2656	0.2656	0.2667	0.2668	0.2669
Beam waist radius(mm)	0.3830	0.3800	0.380	0.3830	0.3830
Beam waist position(mm)	10.3200	10.3600	10.250	10.5000	10.3500

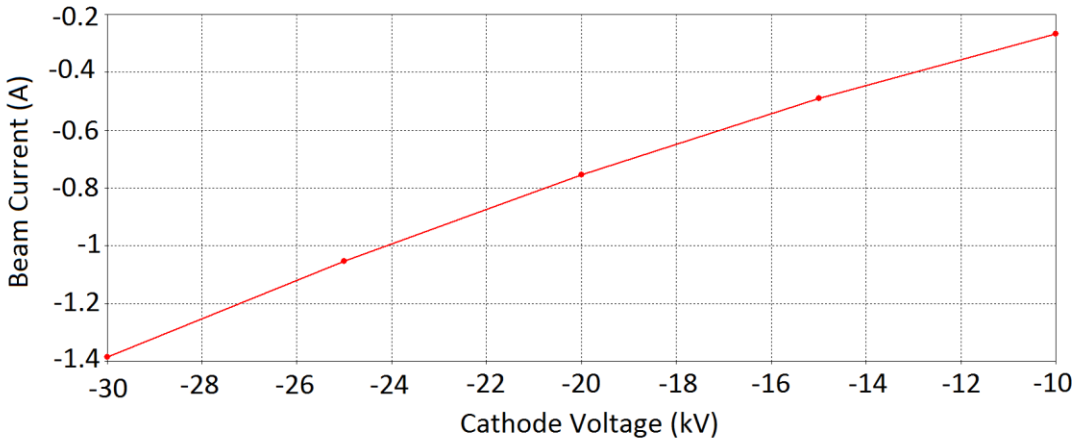

Figure 52 Cathode voltage vs. beam current graph

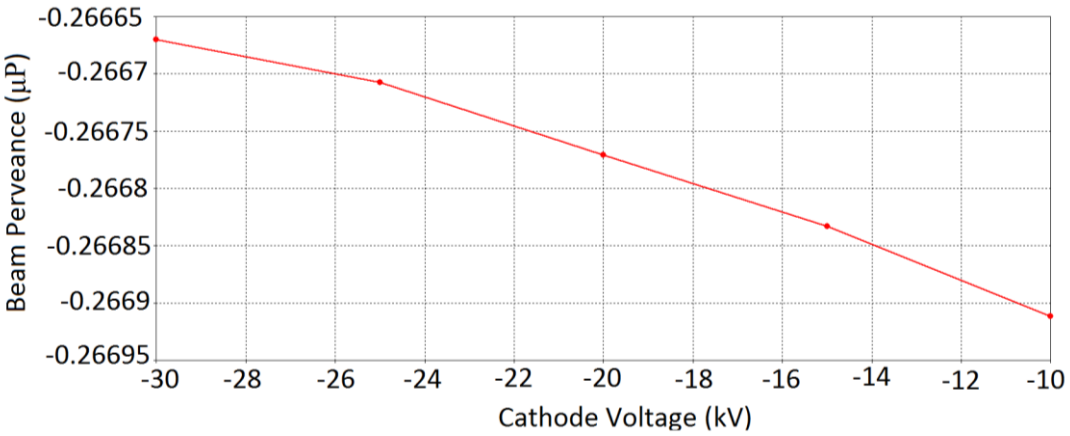

Figure 53 Cathode voltage vs. perveance graph

It can be seen that from Figure 52 and Figure 53, current reduces with cathode voltage and change in perveance is negligible as expected. Figure 54 shows the beam trajectories for cathode voltages. The beam trajectories are also the same because the geometry and perveance of the gun does not change.

4.5.8 Focus Electrode Voltage

The focus electrode voltage usually kept same with the cathode voltage. However in some application, beam can be modulated by focus electrode as seen in Figure 5.c. The modulation is done by biasing negatively the focus electrode according to cathode [4]. In the simulation focus electrode voltage is changing from -22kV to 20kV while cathode potential is kept 20kV.

Table 11 Simulation result for swept focus electrode voltage

Focus Electrode Voltage(kV)	-22.50	-22.00	-21.60	-20.80	-20.00
Current (A)	0.0200	0.0700	0.1100	0.3000	0.7500
Perveance (µP)	0.0070	0.0247	0.0389	0.1060	0.2667

The simulation result is given in Table 121. The beam waist radius and beam waist position results are not given here, because they are irrelevant for this case. The beam current is reduced to 20mV from 0.75V, if the focus electrode has -2500V potential with respect to cathode. Therefore beam can be modulated by switching voltage difference only 10% of cathode voltage.

The beam current is increasing exponentially as potential difference between cathode and focus electrode voltage decreases in Figure 55.

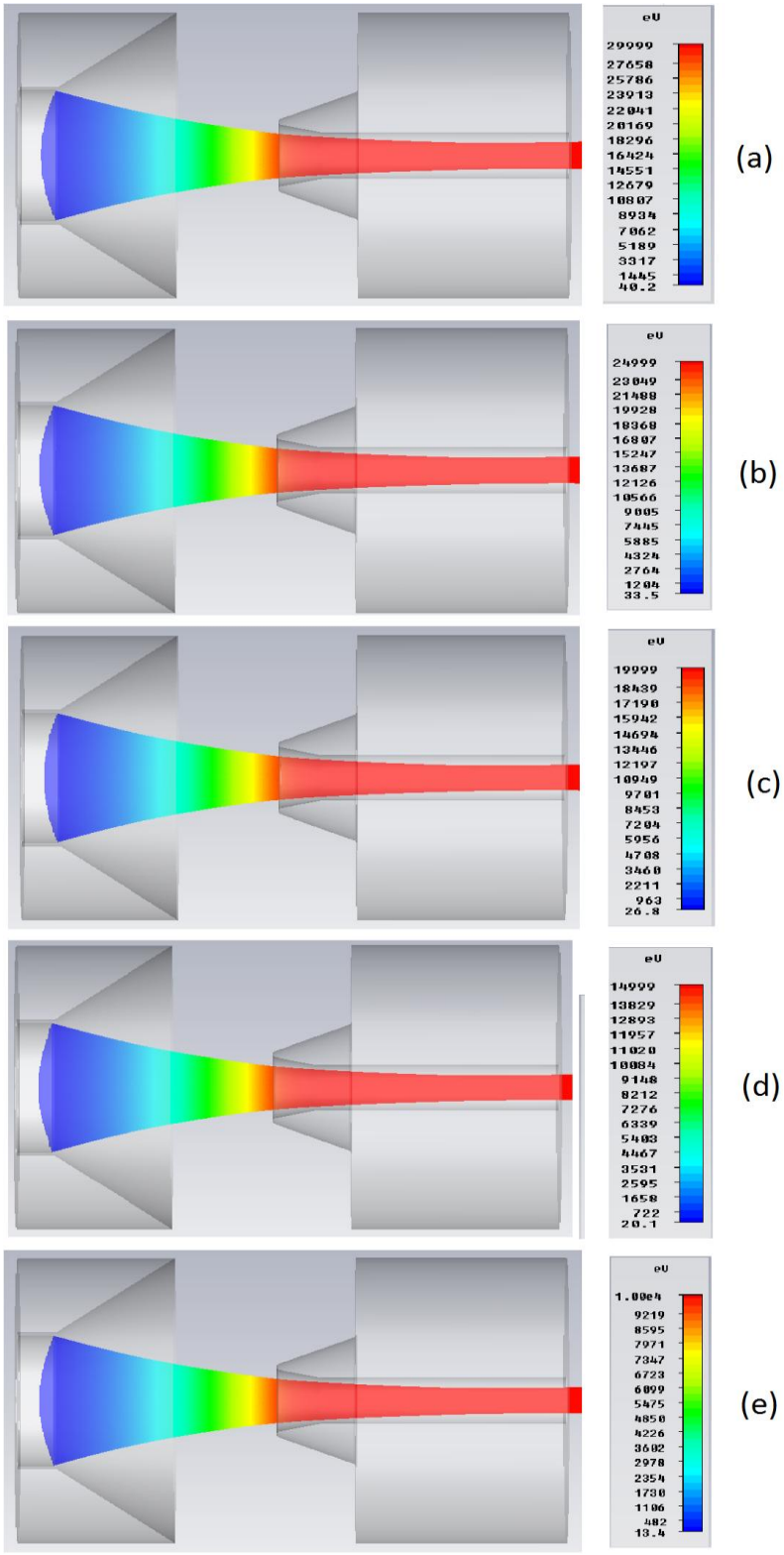

Figure 54 Beam trajectories at different cathode voltage (a) -30kV, (b) -25kV, (c) -20kV, (d) -15kVmm, (e) -10kV

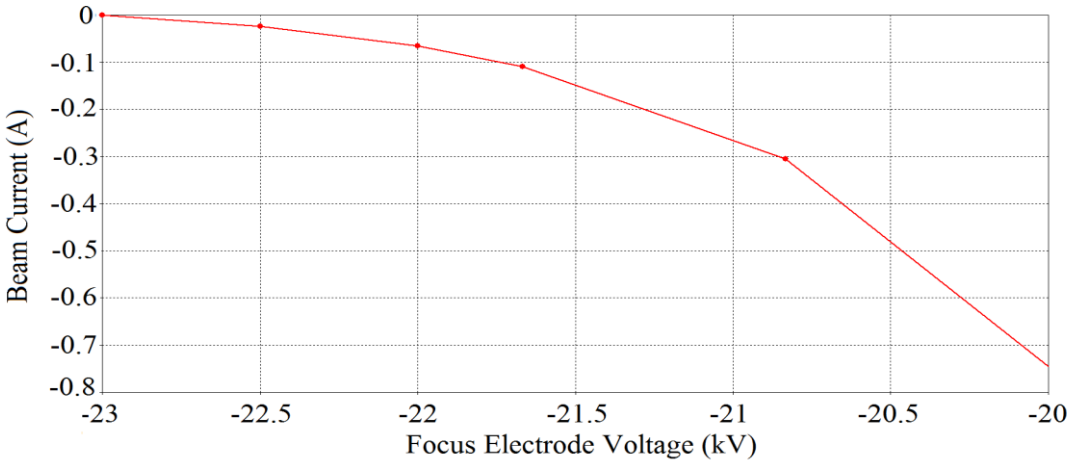

Figure 55 Focus electrode voltage vs. beam current graph

The beam trajectory is given for the last four voltage value in Figure 56. Since beam current is too low for -22.5kV focus electrode value, the beam trajectory could not be obtained in simulation.

4.5.9 Summary of Parametrical Analysis of Pierce Gun

From the Pierce gun parametrical analysis in pervious sections, it can be concluded that the beam parameters can be optimized with adjusting of geometrical and electrical parameters of electron gun. The most crucial part of the gun design is to obtain specified beam parameters with well focused beam which means that electrons can travel anode extraction gap without collision as in Figure 39.

The perveance and beam shape value is directly related to gun geometry as seen in (58). In the gun design, if required perveance is obtained, the beam current can be adjusted with changing cathode potential as in Figure 52 and Figure 53. However, if the cathode voltage is fixed in the design, the geometrical parameters should be optimized to obtain desired electron beam current. These situations are valid for nonrelativistic case. If cathode voltage is in relativistic region, beam mechanism is different and optimization of gun geometry is required to have laminar beam.

From the simulation results, it is seen that the while beam current is increasing, beam focusing becomes harder. However if the electron beam is too much focused, because of beam generated force, it tends to diverge and electrons collides to anode as in Figure 41.

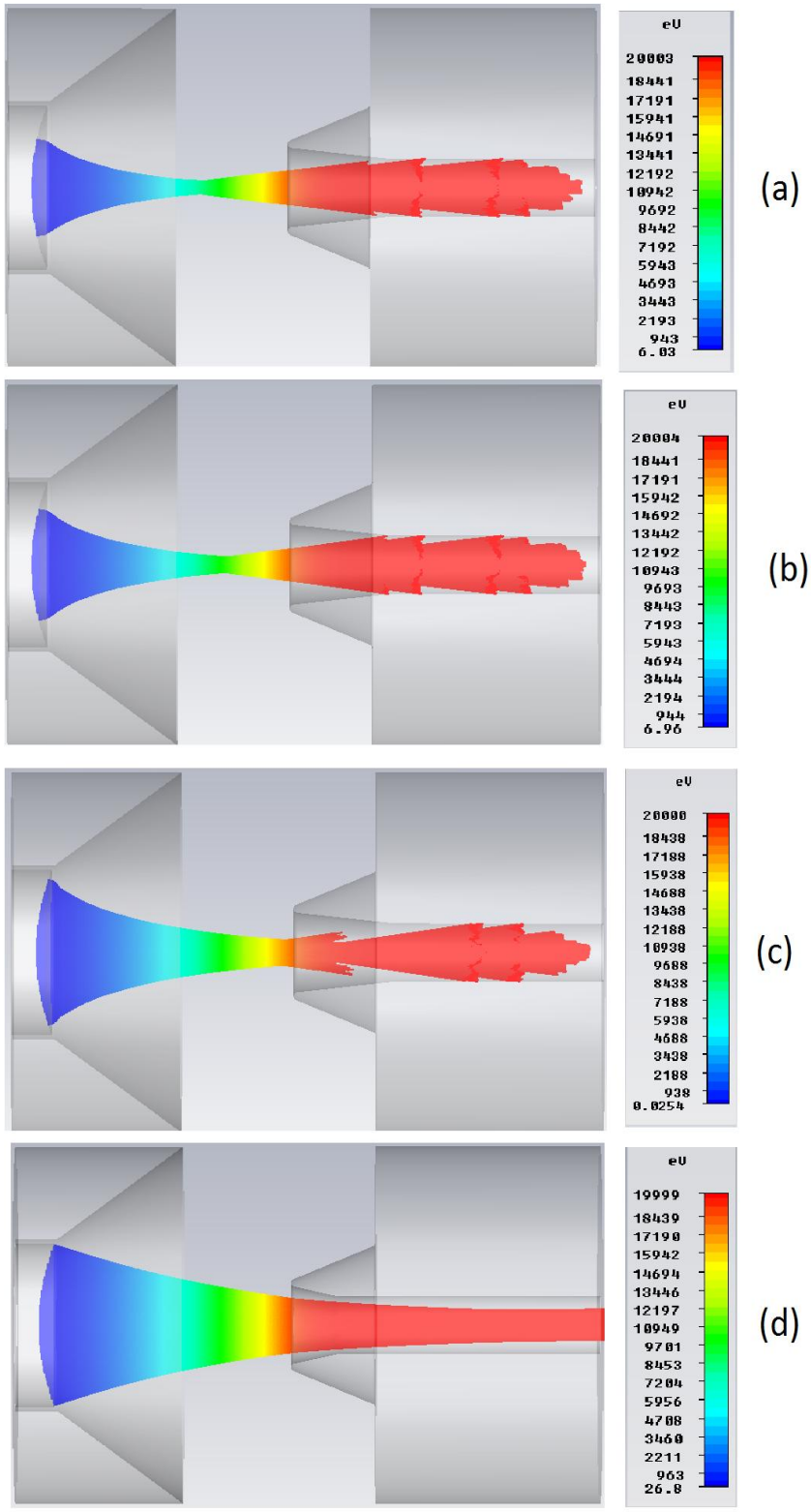

Figure 56 Beam trajectories at different focus electrode voltage (a) -22kV, (b) -21.6V, (c) -20.8kV, (d) -20kV

The anode parameters (anode height and anode slope in z) are not effective as much as cathode parameters (cathode radius and cathode spherical radius). Because the cathode area is directly related the beam current. The beam current can be increased with increasing cathode radius and cathode spherical radius as seen in Figure 48 and Figure 50. However, if beam current increases too much, focusing can be insufficient and focus electrode angle modification is needed. Focus electrode angle is important both on focusing and beam current, but as expected too much focusing is not desirable. Another effective parameter on beam current is anode cathode gap. Anode cathode gap decreases beam current exponentially, thus effect on beam current decreases as anode moves away from cathode. The anode cathode gap can be changed in small range to optimize beam parameters. Focus electrode potential is not related to beam quality. It can be used to modulate beam current instead of modulating cathode voltage.

In conclusion, a Pierce gun designer should begin initial gun geometry obtained according to (58). Then the results are compared with the desired beam parameters and optimization process should be performed with above considerations. This parametrical analysis of Pierce gun is useful not only Pierce gun design, but also gives insight for other geometries. Because anode, cathode and focus electrode components are common for all gun geometry although they are modified. In addition, the relations with beam parameters and geometrical dimension are similar to relations obtained by Pierce gun analysis.

4.6 Simulation of Solenoid in CST

In CST PS Tool, solenoid can be constructed and simulated by magnetostatic solver. A solenoid is defined with its radius and thickness. The magnetic field is directly related to number of windings and current inside the windings with (63). In the gun simulation, axial magnetic field is important. Therefore in simulation, the axial magnetic field is measured and illustrated.

The basic geometry of the solenoid is given in Figure 57. Axial magnetic field is calculated along the blue line in Figure 57 and plotted in Figure 58.

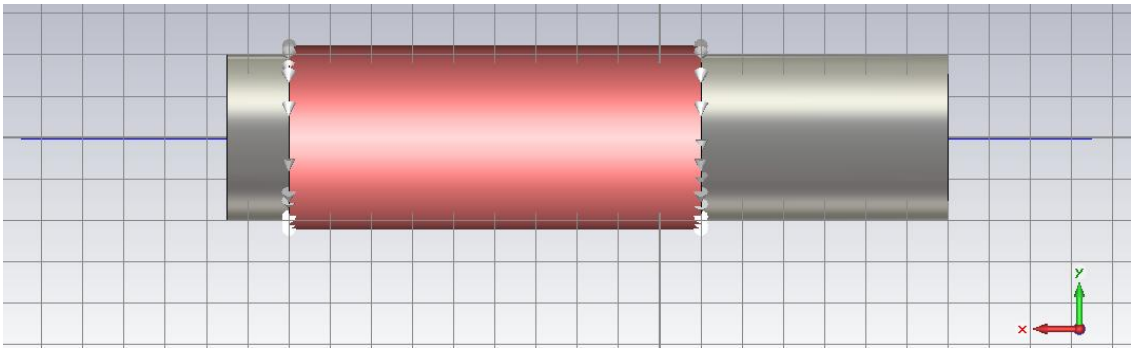

Figure 57 Solenoid geometry in CST

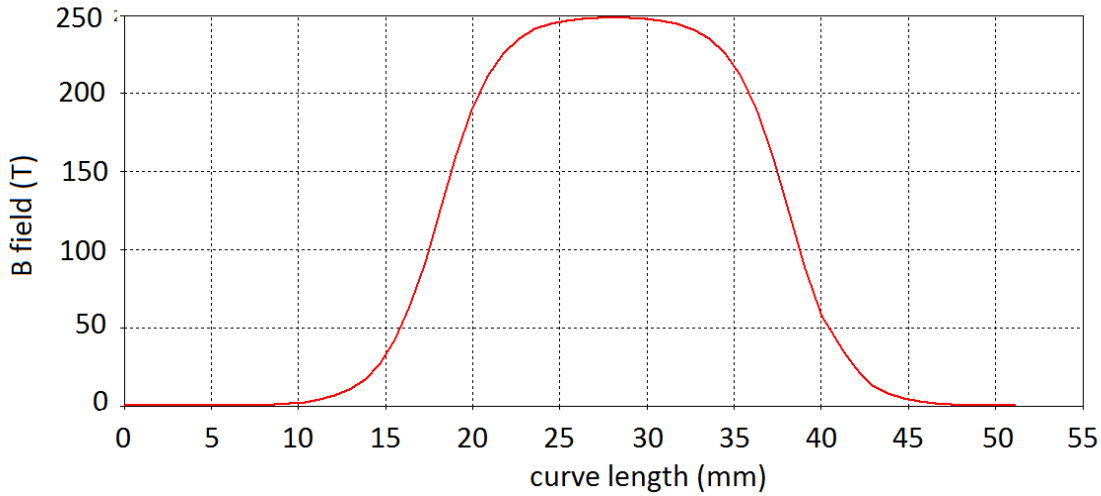

Figure 58 B field along the blue line in Figure 57

The magnetic field of multiple solenoids can be superposed directly. Thus, by multiple solenoids, desired axial magnetic field can be obtained by adjusting geometry and the current.

In Figure 59, there are two cocentric solenoids which have different lengths. Their individual magnetic fields are calculated and plotted in Figure 60 with red and green lines. In this situation, outer coil current is 250A and inner coil current is 1000A and outer coil windings are opposite of inner windings. When both solenoids are active,

their magnetic field is added and total magnetic field is obtained. In Figure 60, individual and total magnetic field along the blue curve are shown.

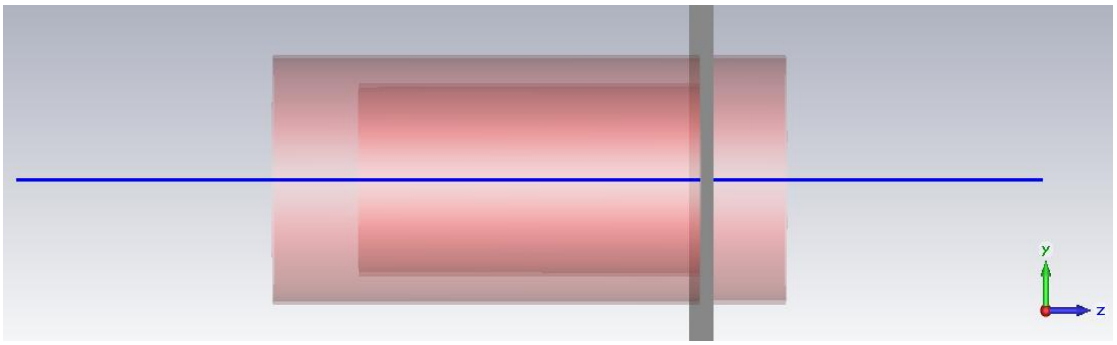

Figure 59 Multilayer solenoid

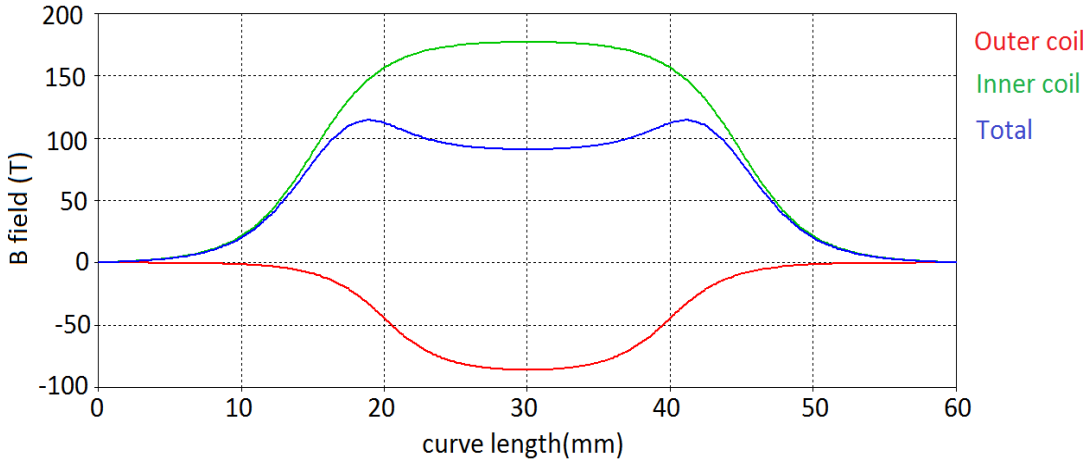

Figure 60 B field along blue line in Figure 59

Sinusoidal B field along in axial dimension can be produced periodic placement of the solenoid as in Figure 61 and B field of these coils are shown in Figure 62.

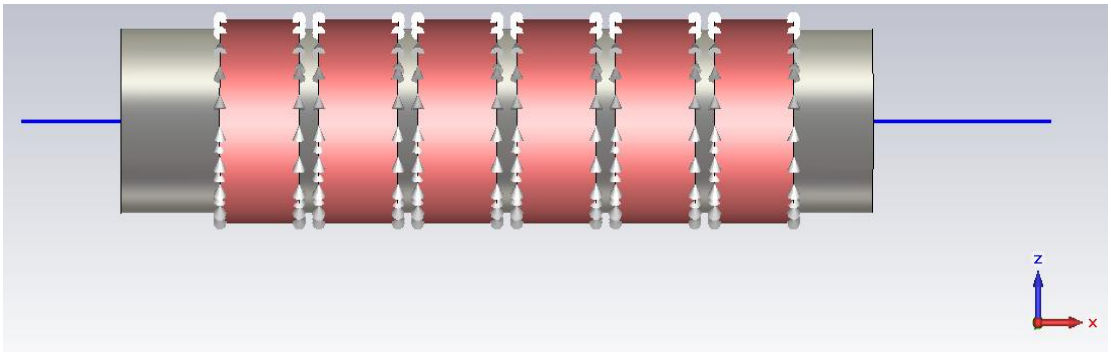

Figure 61 Periodic solenoids

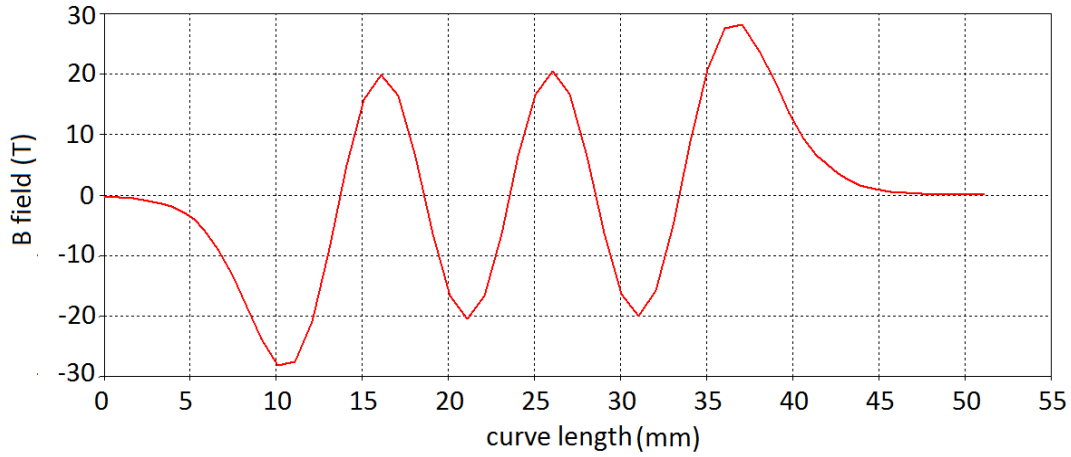

Figure 62 B field along blue line in Figure 61

4.6.1 Pierce Gun Simulation with Solenoid

Pierce gun simulation is performed with solenoid in this section. The Pierce gun geometry is the same as in Section 4.4, only the extraction region is lengthened to observe defocusing of electron beam. Electron trajectory in Pierce gun with long extraction gap without solenoid is given in Figure 63. While electron beam travels along extraction region, electron beam diverges and strikes the anode because of beam generated field. In the Pierce gun geometry, the solenoid is placed the region between beam waist position and end of the anode. Solenoid was driven with two different current values, 10A and 20A with number of turn 1000. Axial B field along the Pierce gun geometry is given in Figure 64.

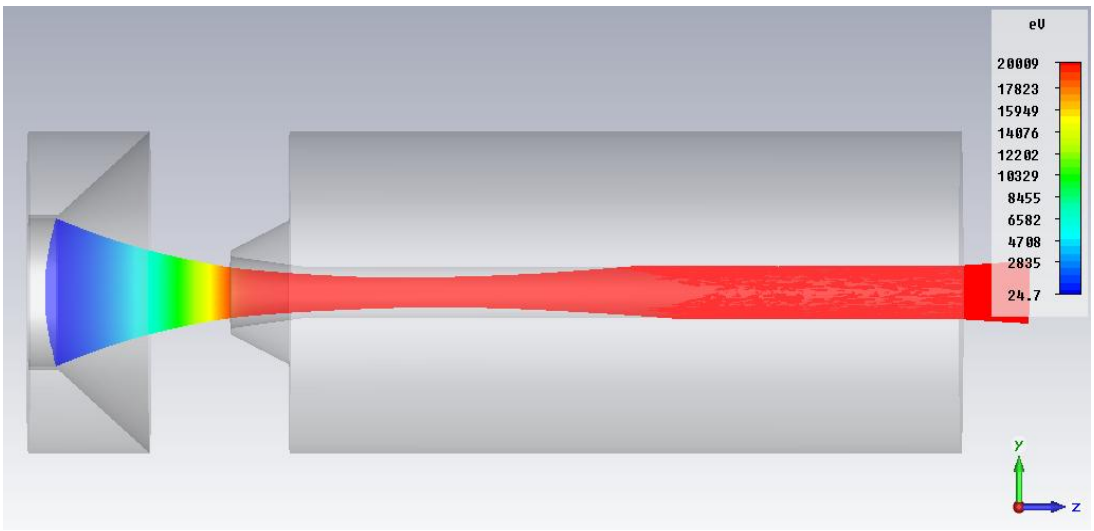

Figure 63 Electron beam trajectory in Pierce gun without solenoid

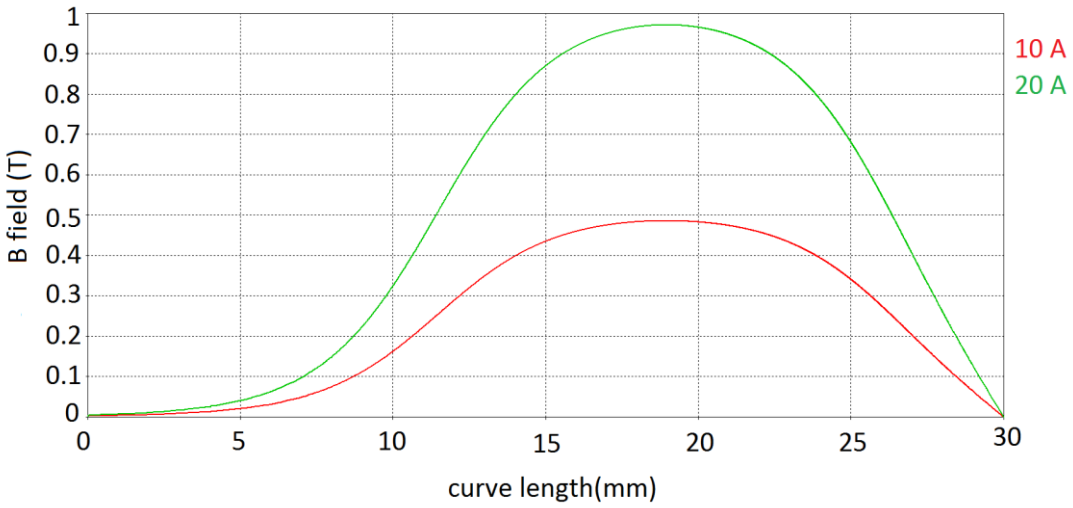

Figure 64 B field along the Pierce gun geometry in z direction

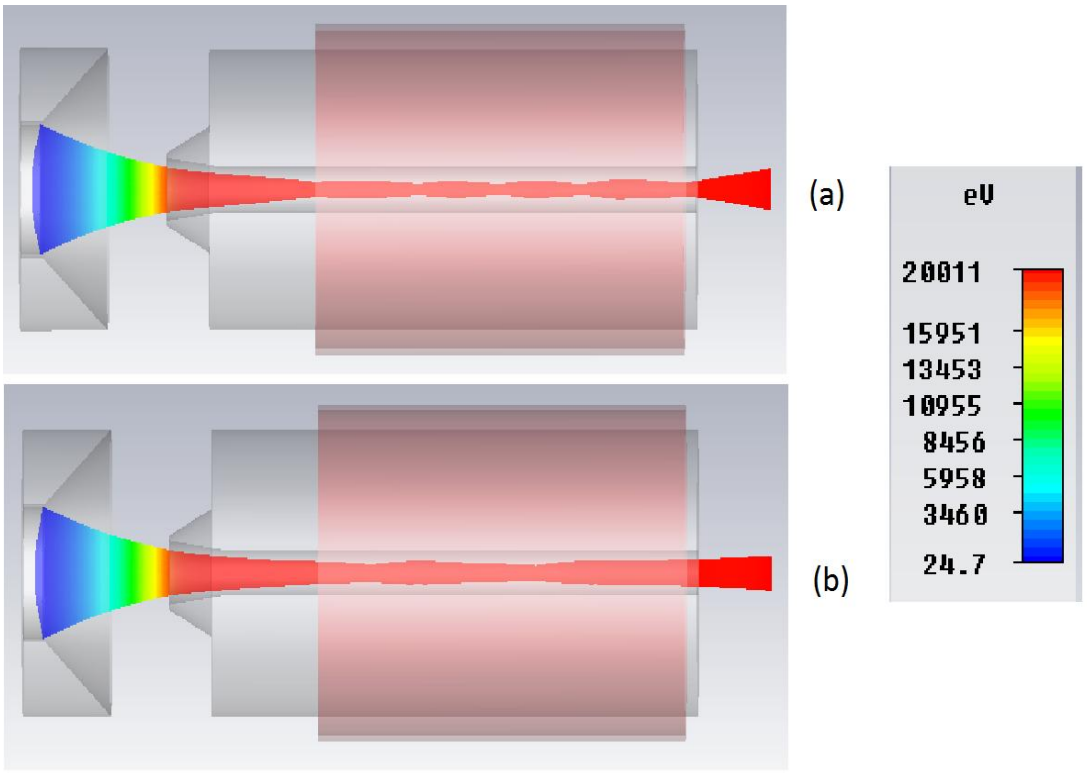

Figure 65 Electron beam trajectories in Pierce gun with solenoid (a) Solenoid current 20A, (b) Solenoid current 10A

Beam trajectories for 10A and 20A solenoid current values are given in Figure 65. Ripple on the beam in Figure 65.a is greater than ripple in Figure 65.b. The calculated beam current values are 0.724A for Pierce gun geometry with solenoid. The beam current is lower than Pierce gun without solenoid, because due to solenoid, some of the axial energy is consumed by rotation thus beam velocity and beam current decreases.

CHAPTER 5

ELECTRON GUN DESIGN FOR TWTA

5.1 Simulation of Pinto-Xavier-Motta Electron Gun

In this section, electron gun designed by César C. Xavier, C. Motta and Marcelo N. Pinto in [4**]**, is simulated and compared with their studies. Moreover, gridded version of this electron gun in [11**]** is analyzed. This electron gun is called as Pinto-Xavier-Motta electron gun inside the thesis.

Pinto-Xavier-Motta electron gun in [4**]** is designed for C-band TWT with 9kV cathode voltages. Simulation geometry of Pinto-Xavier-Motta electron gun in CST PS is illustrated in Figure 66. Focusing electrode and anode structure is different from Pierce gun. Electron beam properties like beam current and beam trajectory are observed according to cathode-anode distance, anode height and focusing electrode angle. Starting geometrical dimensions are 9.78mm, 5.1mm and 44.6^{o} for cathode-anode distance, anode height and focus electrode angle respectively.

Table 12 Simulation parameter values for Pinto-Xavier-Motta electron gun

Parameter	**Swept Values**				
Cathode-anode distance(mm)	9.78	10.342	10.905	11.467	12.03
Anode height(mm)	3.88	4.442	5	5.57	6.13
Focus electrode angle(^{o})	19	34.5	50	65.5	81

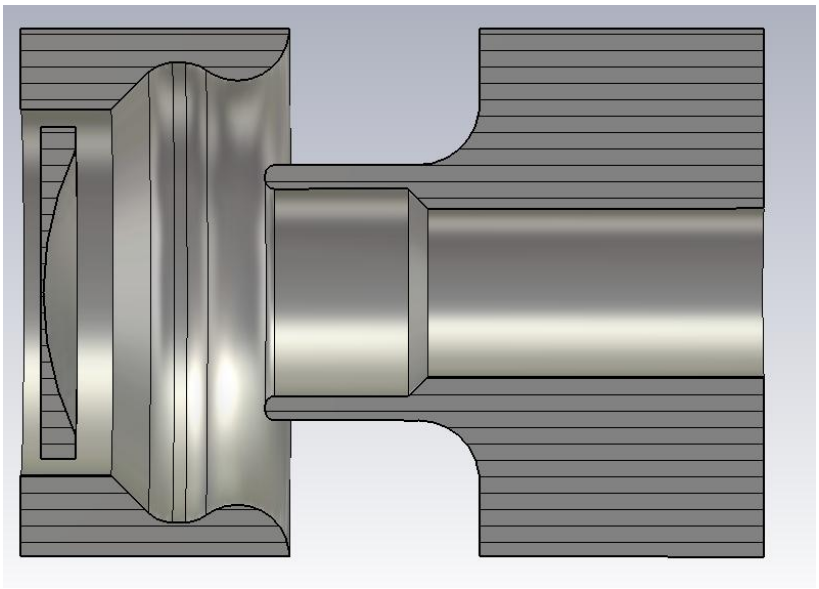

Figure 66 Pinto-Xavier-Motta Electron Gun Geometry

The swept values for cathode-anode distance, anode height and focusing electrode angle is listed in Table 12. For the initial beam geometry, electron beam current is found as 0.825A in CST PS simulation and electron beam trajectory is given in Figure 67.

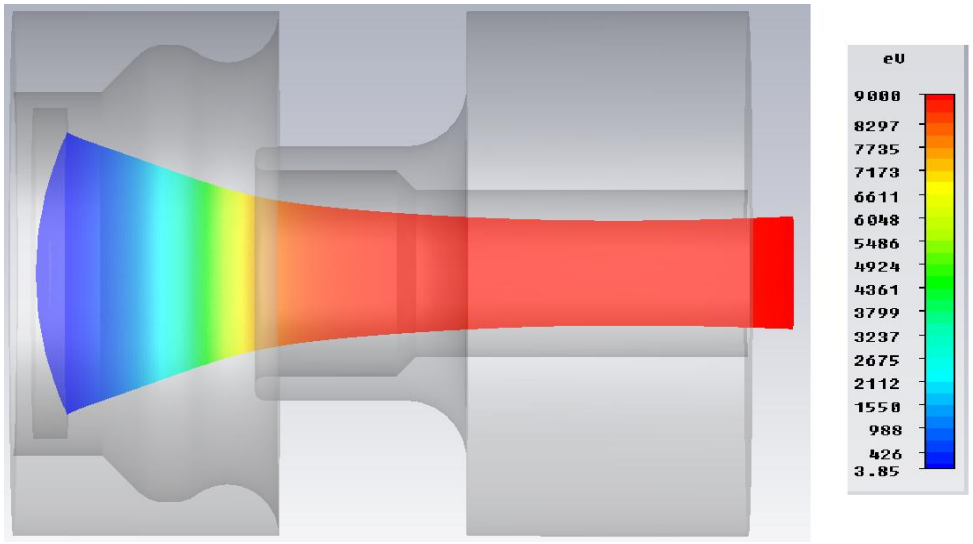

Figure 67 Beam trajectory with initial geometrical parameters in Pinto-Xavier-Motta electron gun

Electron beam current graph for cathode-anode distance values given in Table 12 is shown in Figure 68. Beam current value increases with cathode-anode distance, which is consistent with the result of cathode anode gap simulation of Pierce gun parametrical analysis shown in Figure 42.

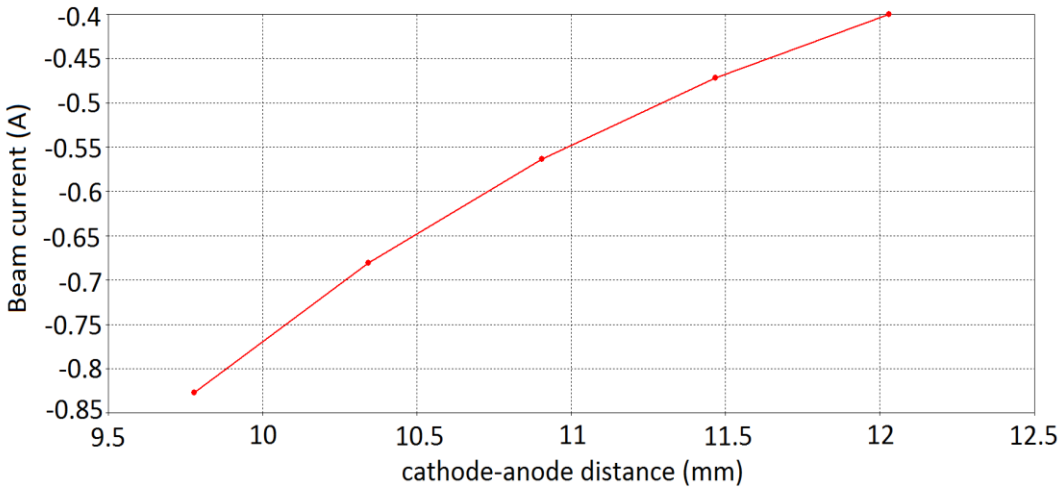

Figure 68 Cathode anode distance vs. beam current graph for Pinto-Xavier-Motta electron gun

The beam trajectories for cathode-anode distance value of 9.78, 10.90 and 12.03mm are given in Figure 69. In this figure, it is observed that beam is getting more focused and electron beam quality decreases due to too much focusing with increase of cathode-anode distance as in Pierce gun.

The second parameter of Pinto-Xavier-Motta electron gun simulation is anode height. Beam current graph according to anode heights is given in Figure 70. Beam current is increased with anode height, which is also same as in Pierce gun. The effect of anode height is not dramatic as anode cathode gap. Beam trajectory for three anode height values are given in Figure 71.

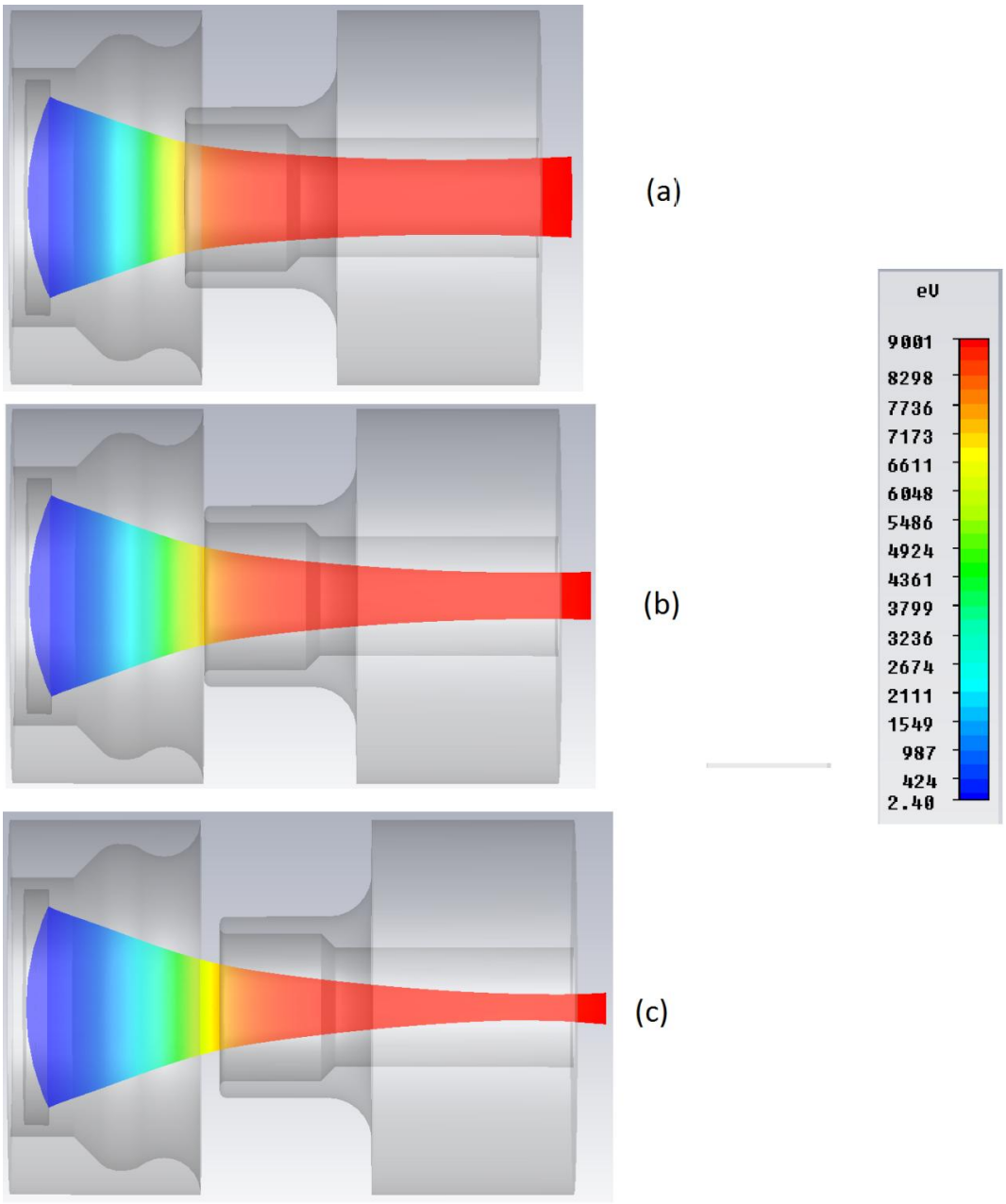

Figure 69 Beam trajectories for swept cathode-anode distance for Pinto-Xavier-Motta electron gun (a) 9.78mm, (b) 10.90mm, (c) 12.03 mm

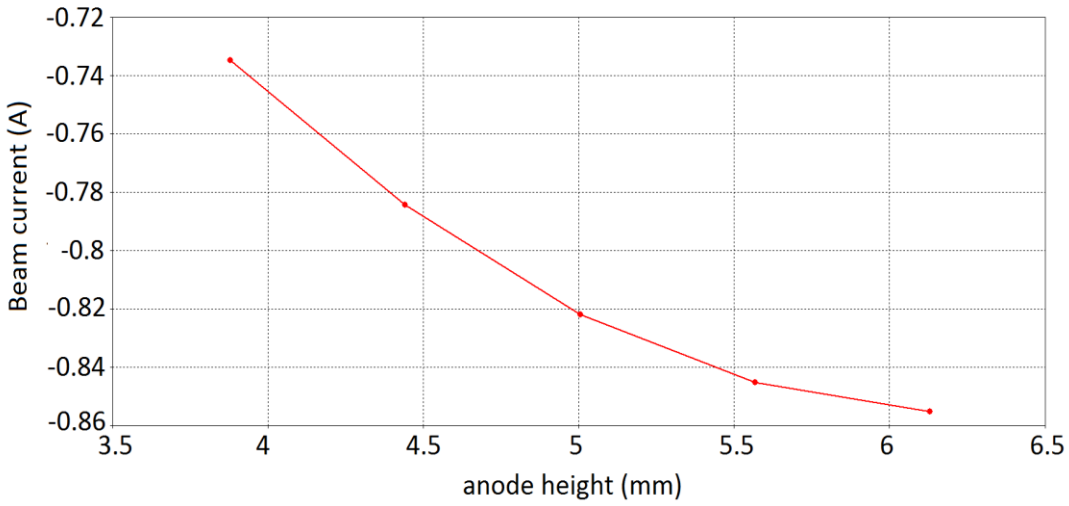

Figure 70 Anode height vs. beam current graph for Pinto-Xavier-Motta electron gun

Focusing electrode angle provide beam focusing, thus it is expected to obtain more focused beam and lower beam current if the focusing beam angle decreases, which occurred in Pierce gun. From Figure 73, it is understood that beam current increases as focusing electrode angle increases. For the focusing electrode angle values 19^{o}, 50^{o} and 81^{o}, beam trajectories are illustrated in Figure 72. In Figure 72.a, electron beam is too focused, so beam quality and beam current reduced. On the other hand, for the electron gun in Figure 72.c, beam focusing is not sufficient.

For the Pinto-Xavier-Motta electron gun, parameter analysis gives same relations between parameters and beam current with Pierce electron gun, although the focus and anode electrode geometries are different than Pierce gun.

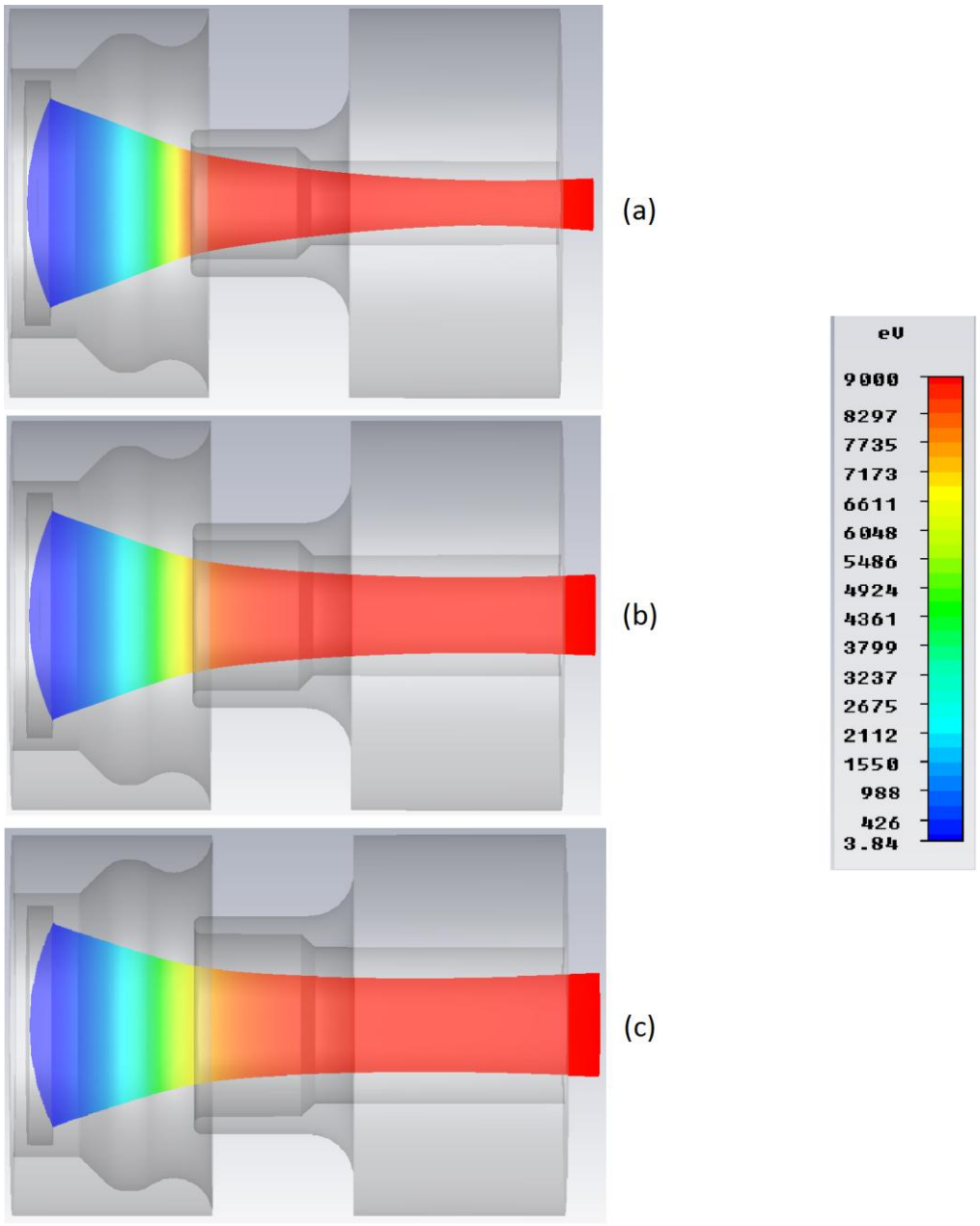

Figure 71 Beam trajectories for swept anode height for Pinto-Xavier-Motta electron gun (a) 3.88mm, (b) 5mm, (c) 6.13mm

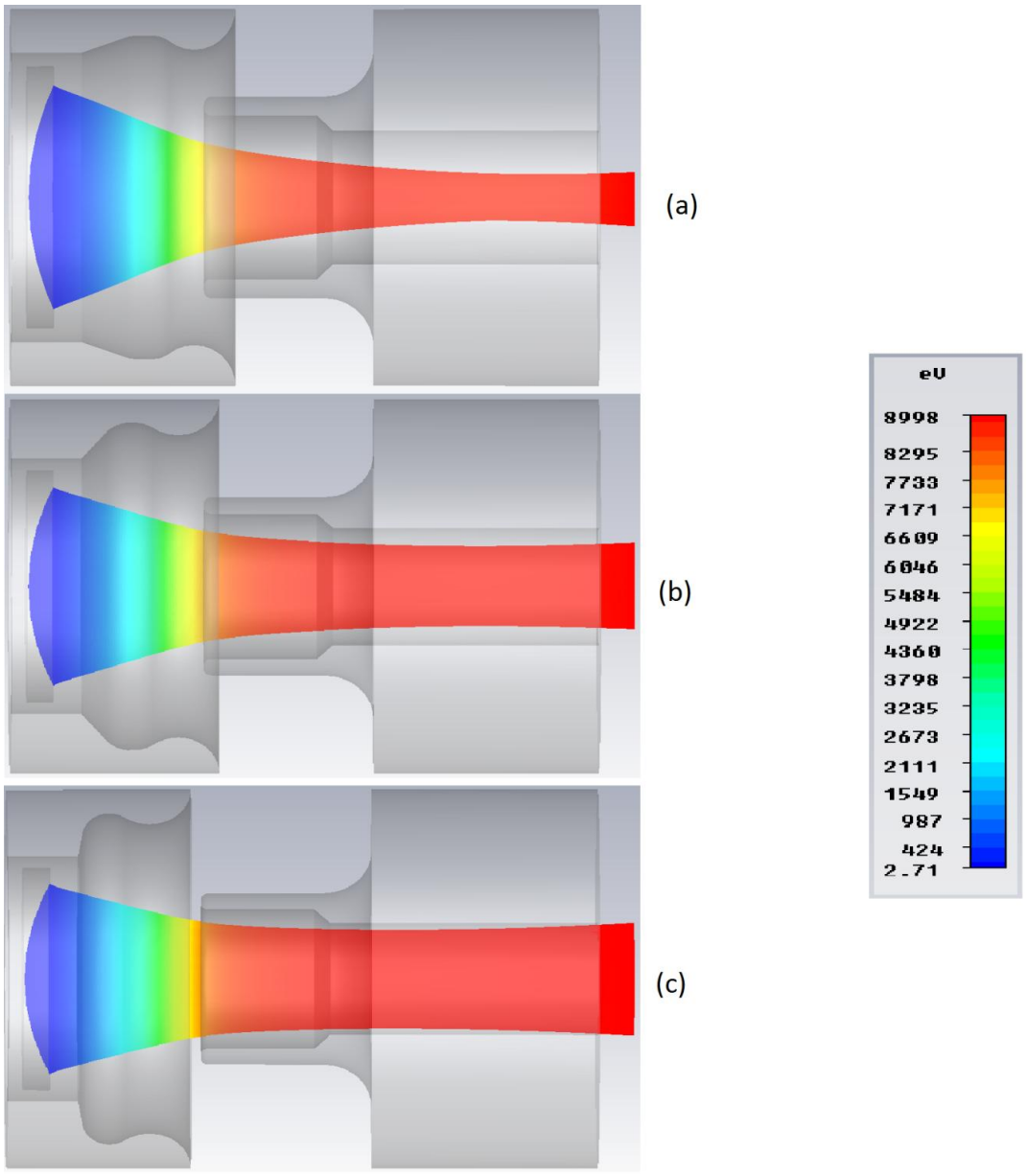

Figure 72 Beam trajectories for swept focusing electrode angle for Pinto-Xavier-Motta electron gun (a) 19^{o}, (b) 50^{o}, (c) 81^{o}

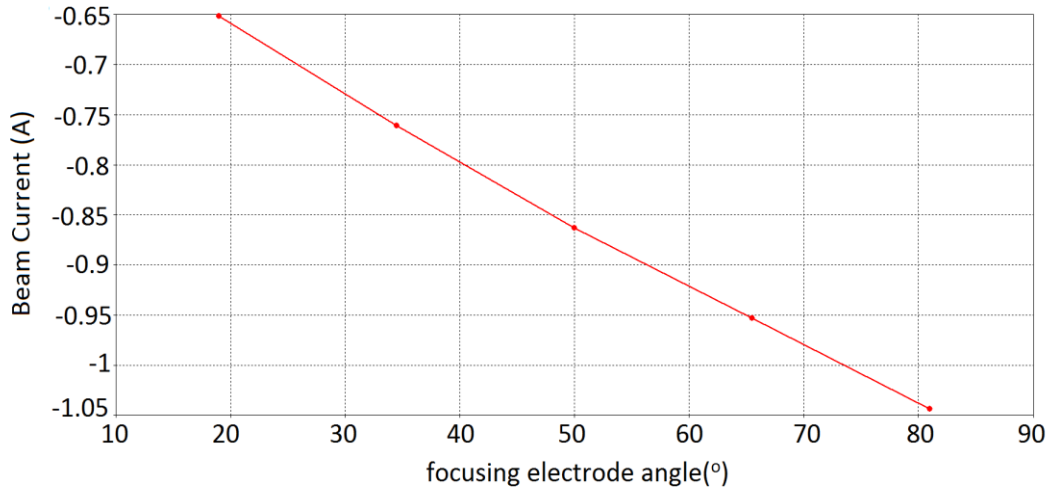

Figure 73 Focusing electrode angle vs. beam current graph for Pinto-Xavier-Motta electron gun

5.1.1 Simulation of Gridded Pinto-Xavier-Motta Electron Gun

In [11**]**, the gridded version of Pinto-Xavier-Motta electron gun is analyzed according to grid voltage. Their aim is to obtain 30kV and 3.5A (0.7μP) electron gun with grid. Grid control is one of the beam control method. That means that electron beam can be pulsed by changing grid potential with respect to cathode as shown in Figure 5. The gridded Pinto-Xavier-Motta electron gun geometry in [11] is given in Figure 6. In CST PS simulation grid structure was constructed by CST Macros utility. In order to obtain 0.7μP, geometrical dimensions which gives that perveance value are chosen from Pinto-Xavier-Motta parametrical analysis in previous section,. Initial Pinto-Xavier-Motta electron gun geometry was taken and cathode anode distance is changed to 10.75mm from Figure 68. The distance between cathode and grid is 0.9mm as in [11**]**.

In the CST PS simulation, grid voltage is swept between 0-600V with respect to cathode voltage and beam current and beam trajectory are observed. The beam current increases drastically with increasing grid voltage wrt. cathode, which is shown in Figure 74.

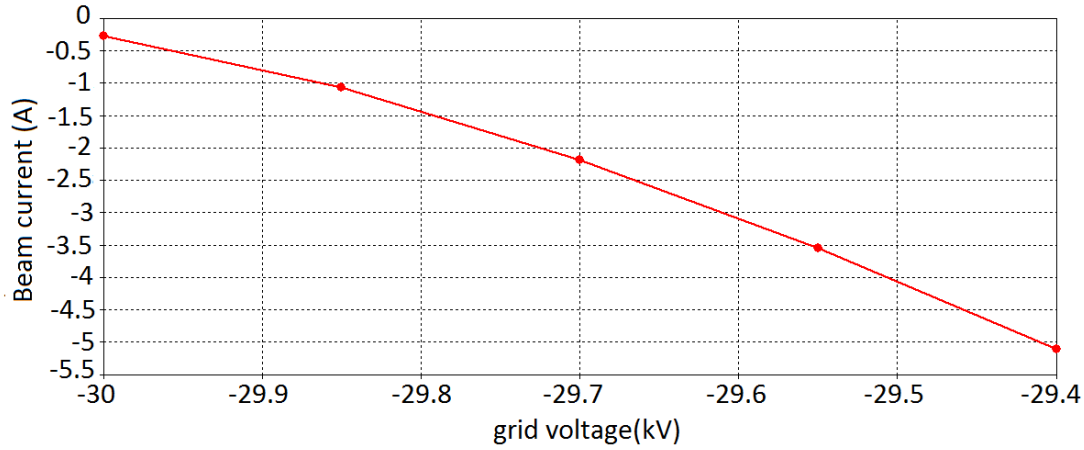

Figure 74 Grid voltage vs. beam current graph for gridded Pinto-Xavier-Motta electron gun

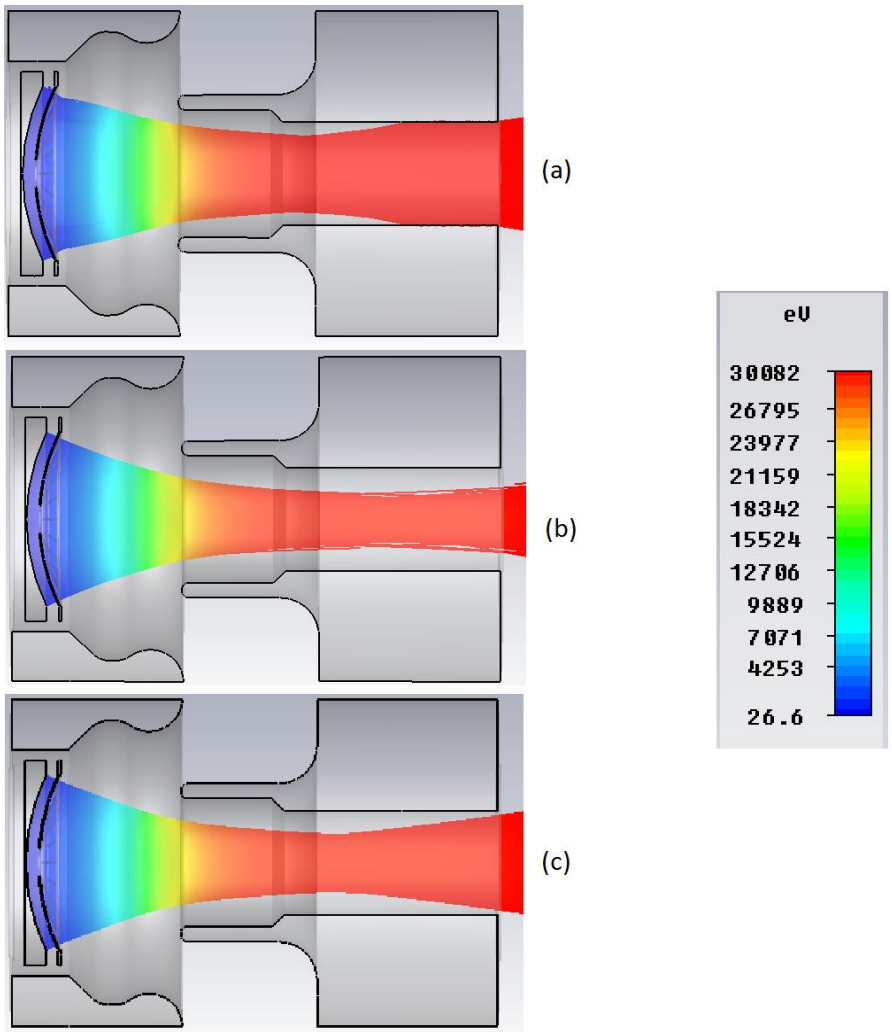

Figure 75 Beam trajectories for swept grid voltage for gridded Pinto-Xavier-Motta electron gun (a) -30kV, (b) -29.55kV, (c) -29.4 kV

When the grid voltage is adjusted to -29.55kV, desired 3.5A beam current can be achieved. Therefore if potential difference between grid and cathode is switched between 0 and 450V, electron beam can be modulated. The beam trajectories are illustrated in Figure 75. For Figure 75.a, beam current is very low, 0.25A, thus trajectory cannot be considered meaningful.

5.2 Simulation of Dual Anode Electron Gun

Dual anode electron gun design was conducted based on study in [16**]** which consists the design of 0.14µP dual anode electron gun for Ka band helix TWTA. For TWT used in space applications, long life and high reliability are required, thus dual anode is designed to satisfy these requirements [16**]**.

In dual anode geometry given in Figure 76, there are control anode (A_c) and ion barrier anode (A_i) in addition to ground anode (A_g). Control anode help prolong the electron gun life by regulating beam current during the life of tube. When the electron emission from cathode starts to decays, beam perveance can be kept constant by changing control anode potential [16**]**. Ion barrier anode also provides longer gun life. This anode potential is adjusted +100-150V wrt. to ground anode and prevent the cathode from ions generated in interaction region.

Geometrical dimension is taken from [16] such that cathode diameter and cathode spherical diameter are chosen 3.1mm and 5.5mm respectively. The distances between electrodes are optimized in CST PS to obtain 75mA beam current. Figure 76 also shows voltages of the electrodes. In CST PS simulation, A_i is assigned as 0V and ground anode 100V negatively biased according to A_i. Control anode potential is adjusted -5.3kV while cathode and focusing electrode potentials are adjusted -6.9kV. For optimized dual anode electron gun, geometrical dimension and distance between electrodes are given in Table 13.

Table 13 Geometrical dimensions for optimized dual anode electron gun

Parameters	Values(mm)
Cathode radius	1.55
Cathode spherical radius	2.75
Cathode-Ac gap	3.05
Ac-Ai gap	3.12
Ai-Ag gap	1.1
Ac aperture radius	1.485
Ai aperture radius	1.01
Ag aperture radius	0.74
Ag extraction gap radius	0.55

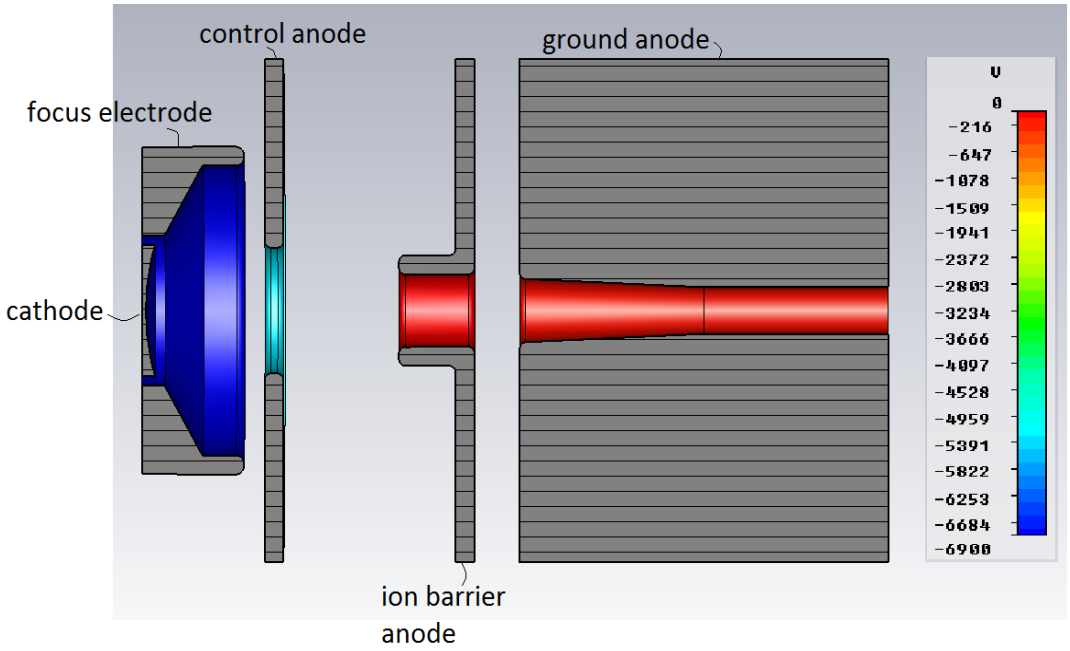

Figure 76 Dual anode geometry and electrode voltage configuration

Table 13, beam current and perveance are obtained as 75.5mA and 0.134µP respectively. These current and perveance values are very close to desired values. The beam trajectory of the dual anode geometry is given in Figure 77. Beam waist

radius is measured as 0.38mm while beam waist position from cathode is calculated 12.1mm..

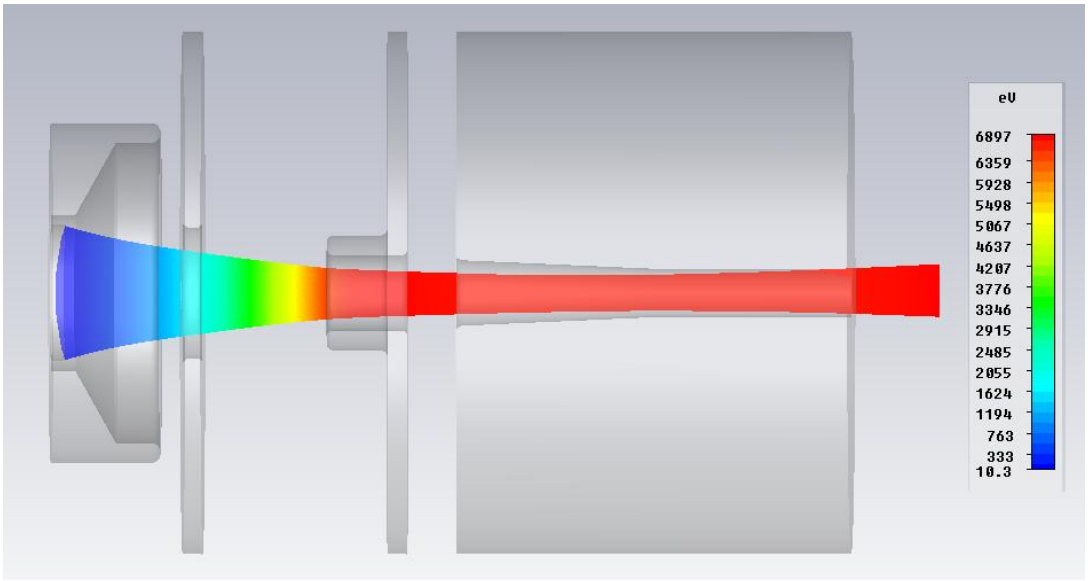

Figure 77 Beam trajectory for dual anode electron gun

In [16**]**, PPM is designed to confine beam along the interaction region. In order to represent beam focusing effect, single permanent magnet is placed in CST PS simulation. In simulation tool, permanent magnet gives desired magnetic field within magnet geometry in specified direction like solenoid. In Figure 78, B field along the electron gun geometry shown in Figure 79 is plotted.

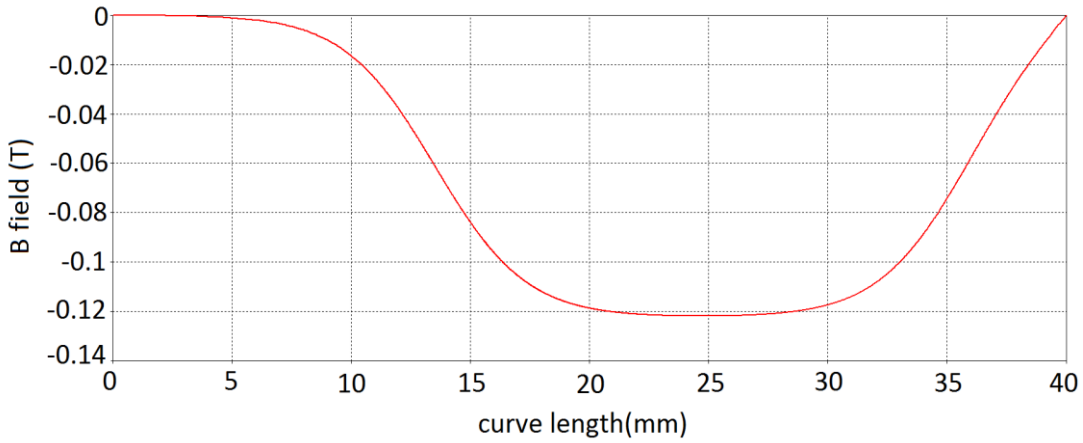

Figure 78 B field along the geometry of dual anode geometry in z direction

Beam current value becomes to 75.4mA with permanent magnet, slightly lower than previous geometry due to rotational motion as mentioned previously. From Figure

79, it is concluded that electron beam focusing along the interaction region is achieved by permanent magnet having axial B field in Figure 78.

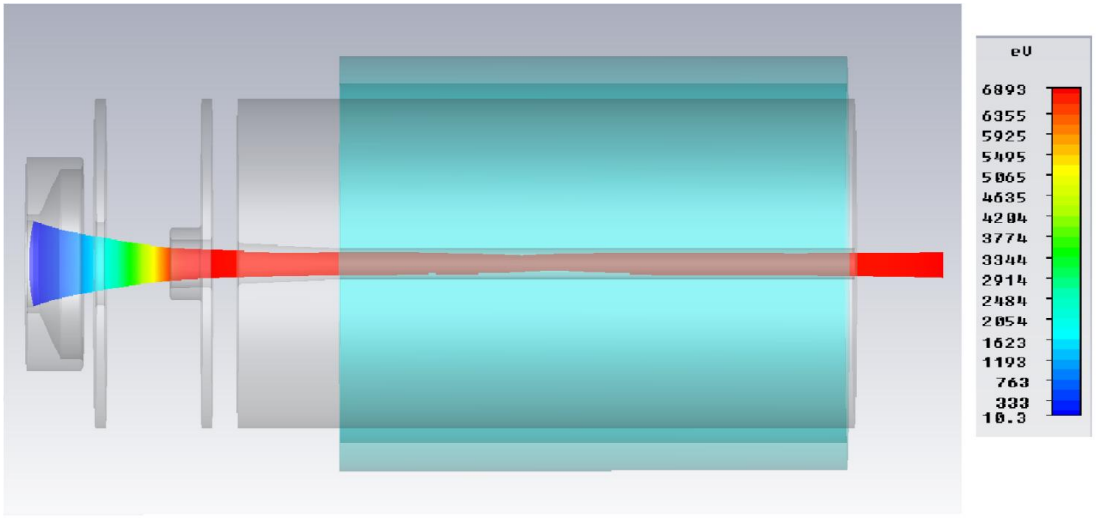

Figure 79 Beam trajectory for dual anode electron gun with solenoid

5.3 Simulation of Annular Beam Electron Gun

Annular beam electron gun simulation whose geometry is given in Figure 7 was performed in CST PS in the light of [13]. Annular beam electron gun has usage of HPM systems like relativistic magnetron, relativistic klystron and relativistic BWO. Electron gun of HPM systems should provide high current electron beam of the order of kV. Annular beam has more electron beam current than solid beam, if their anode extraction gaps have same dimension. The disadvantage of annular beam is that focusing of annular electron gun is harder than that of solid beam.

The geometry of annular beam electron gun is given in Figure 80. The blue dotted annular area is assigned as electron emission area. The electrode in the middle of electron emission area helps focusing electron beam. Other electrode which consists of electron emission area also functions as focusing electrode. The anode geometry is almost same as Pierce gun anode.

In Figure 80, the width of blue dotted region is 32mm. In addition, anode extraction gap is 57mm and anode cathode gap is 152mm, while total gun length is 910mm. 1MV is applied to cathode and focusing electrode.

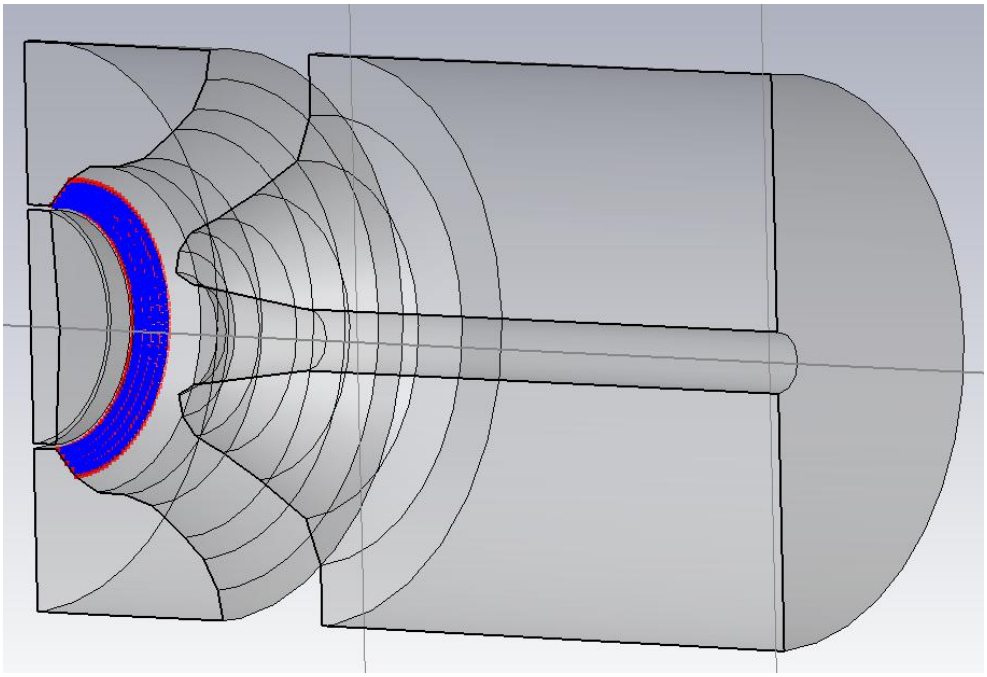

Figure 80 Electron emission face in annular beam electron gun in CST PS

First, simulation is held without solenoid and beam trajectory is obtained as in Figure 81. As mentioned before, focusing of annular beam is challenging, thus magnetic field is needed to focus annular beam. In Figure 81, annular beam cannot be seen because of CST 3D drawing, thus in order to illustrate more clearly, particle monitors are placed at various z positions. These particle monitors shown on the Figure 81 as PM1-PM3.

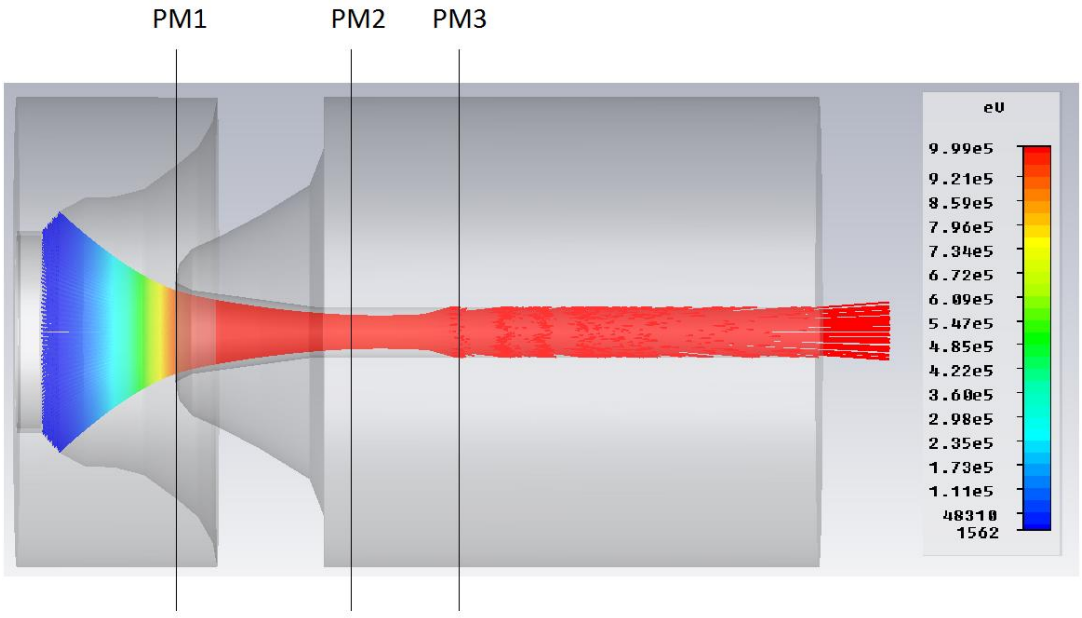

Figure 81 Beam trajectory for annular beam electron gun

In Figure 82, phase space plot representing x-y position of electrons are shown corresponding to particle monitors PM1, PM2 and PM3 respectively. Particle monitors distance to beginning of electron gun is also given in Figure 82.

In Figure 82, x-y position of electrons is plotted for three particle monitors. From Figure 82.a, it is understood that before beam enters the anode region, electron beam preserves its annular shape. After entering anode, beam starts to diverge and losses its annular shape, thus beam cross section is no longer annular as seen in Figure 82.b and Figure 82.c.

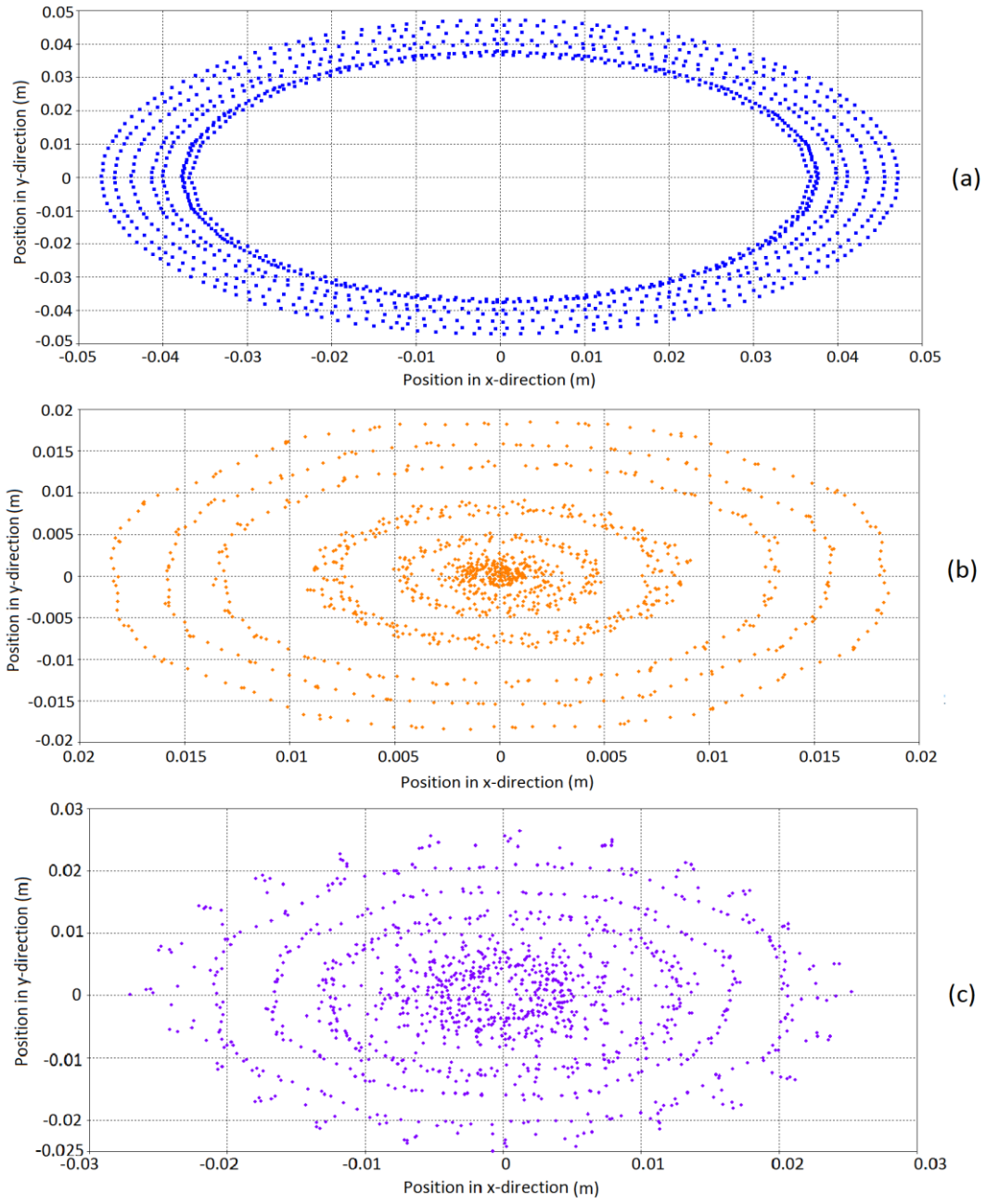

Figure 82 Phase space of planes in z direction for annular beam electron gun in Figure 81, (a) PM1, distance to origin=178mm, (b) PM2, distance origin 380mm, (c) PM3, distance to origin=487mm

In order to focus the electron beam, B field, which has 0.19T peak value, in Figure 83, is applied by permanent magnet along z direction of annular beam electron gun geometry. Beam trajectory in Figure 84, is obtained when magnetic field is applied. It is seen that proper focusing can be achieved and ripple on electron beam is acceptable.

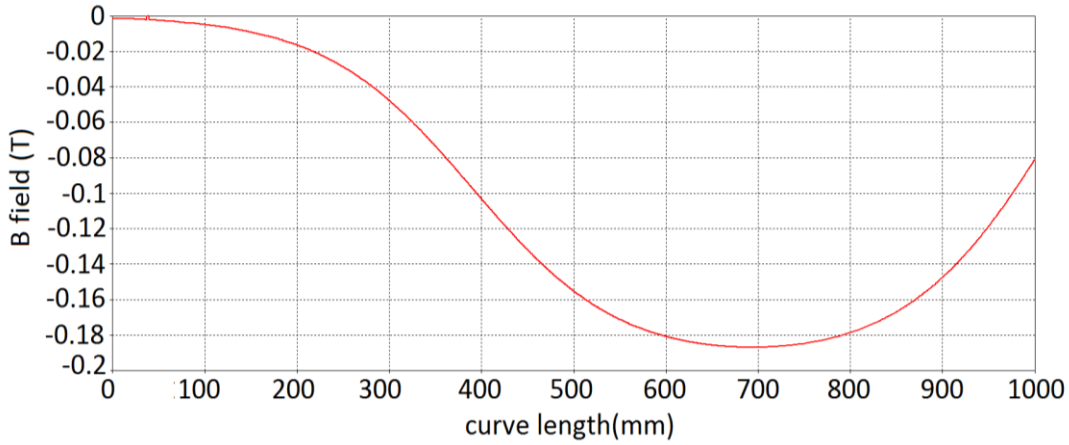

Figure 83 B field along geometry of annular beam electron gun geometry in z direction in Figure 84

Electron beam in Figure 84 carries 477A current. In order to compare beam current with solid beam, Pierce gun having same extraction gap value with annular beam electron gun, 57mm, is simulated. Electron beam geometry and beam trajectory of solid beam gun is shown in Figure 85, and beam current value is calculated as 284A. Therefore, annular beam electron gun gives almost double of beam current of solid beam electron gun.

On the other hand, four particle monitors are placed annular beam electron gun geometry with permanent magnet as in previous case. These particle monitors position are shown on Figure 84. In Figure 86, phase space plots are shown corresponding to particle monitors. Figure 86.a shows beam cross section before entering the anode. After beam enters the anode region and magnetic field, it continues to travel in annular shape. Moreover, from Figure 86.a to Figure 86.d, rotational motion of electron beam due to magnetic field can be observed.

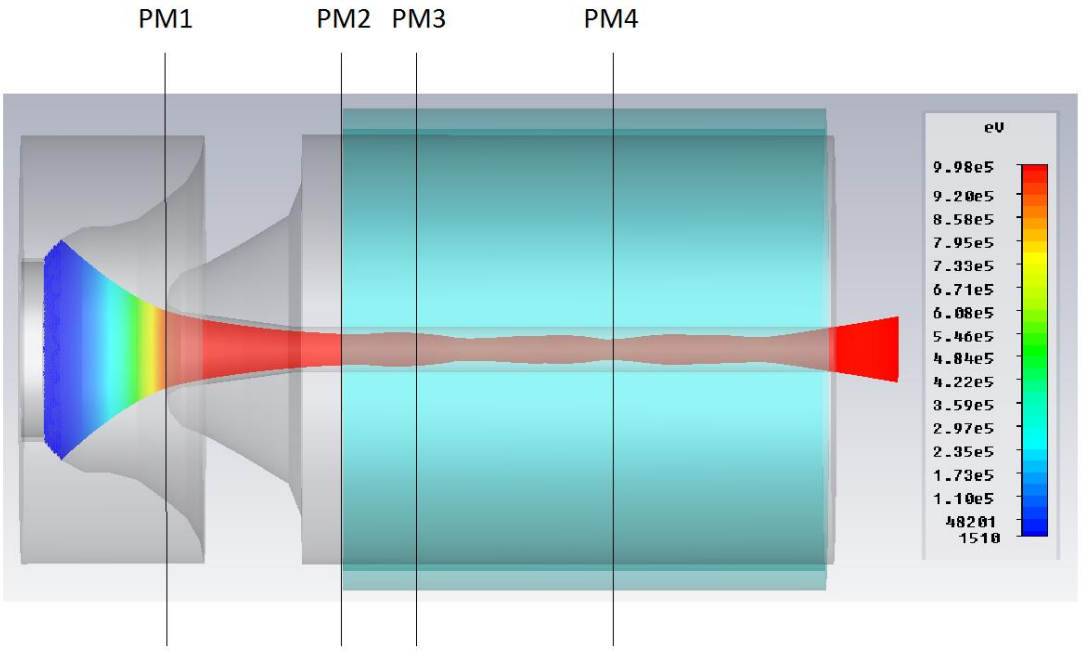

Figure 84 Beam trajectory for annular beam electron gun with permanent magnet

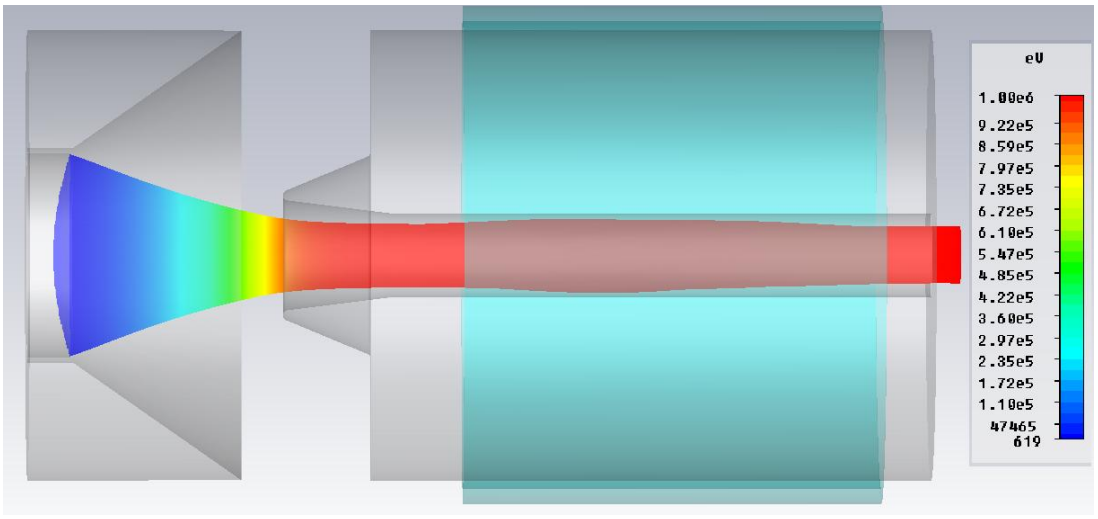

Figure 85 Beam trajectory for solid beam electron gun (Pierce gun) which has same anode extraction gap dimension with annular beam gun Figure 84

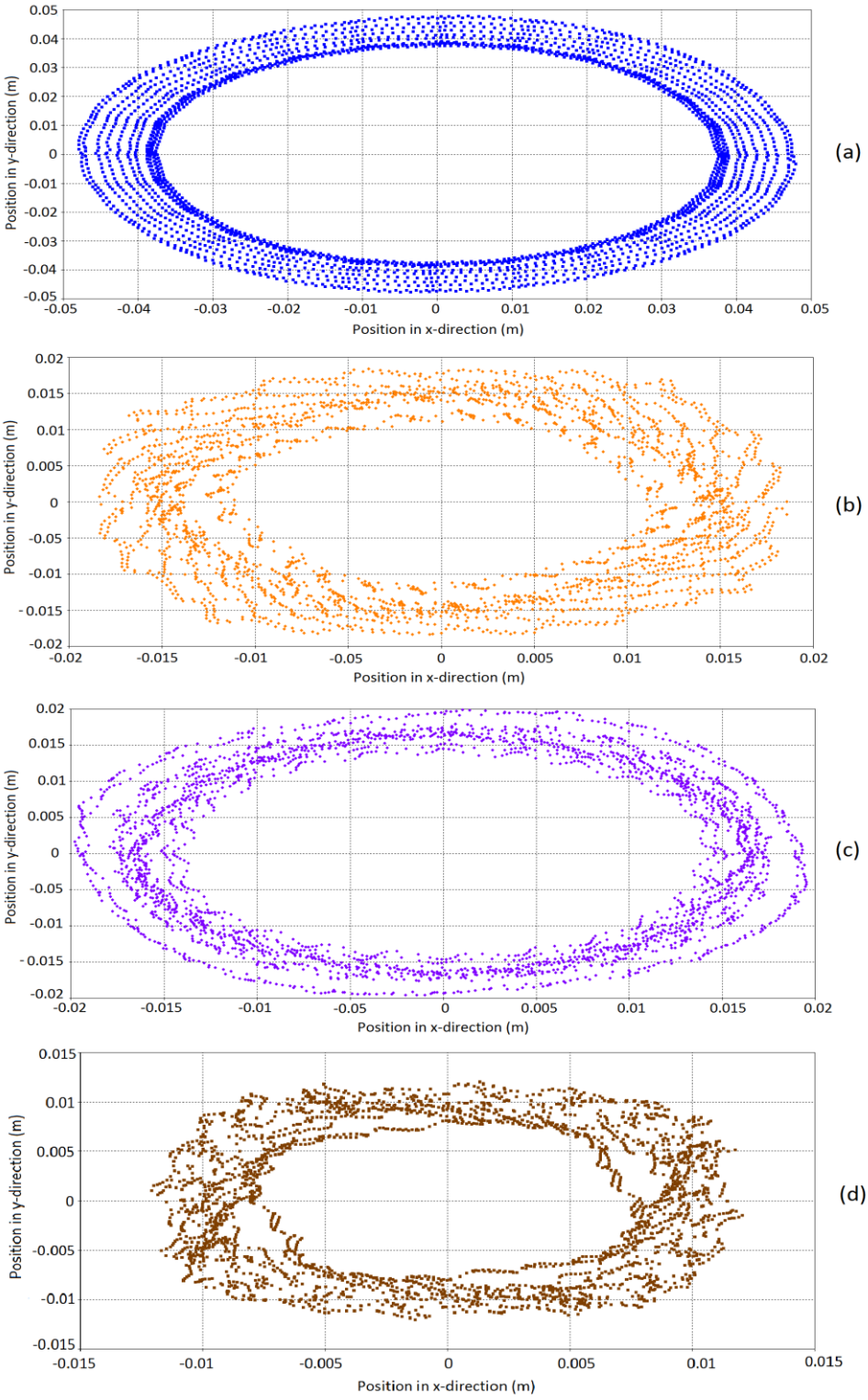

Figure 86 Phase space of planes in z direction for annular beam electron gun with permanent magnet in Figure 84, (a) PM1, distance to origin=178mm, (b) PM2, distance origin=399mm, (c) PM3, distance to origin=481mm, (d) PM4, distance to origin=739mm

In Figure 87, there is another representation of particle monitors such that all particle monitors are plotted on the same graph. Eight particle monitors are placed along the annular electron gun geometry and colored dimension values written right to the plot represents particle monitor distance to beginning of the electron gun and corresponding phase space plot is plotted same color. Annular shape of the electron beam along z direction can be also observed clearly from Figure 87.

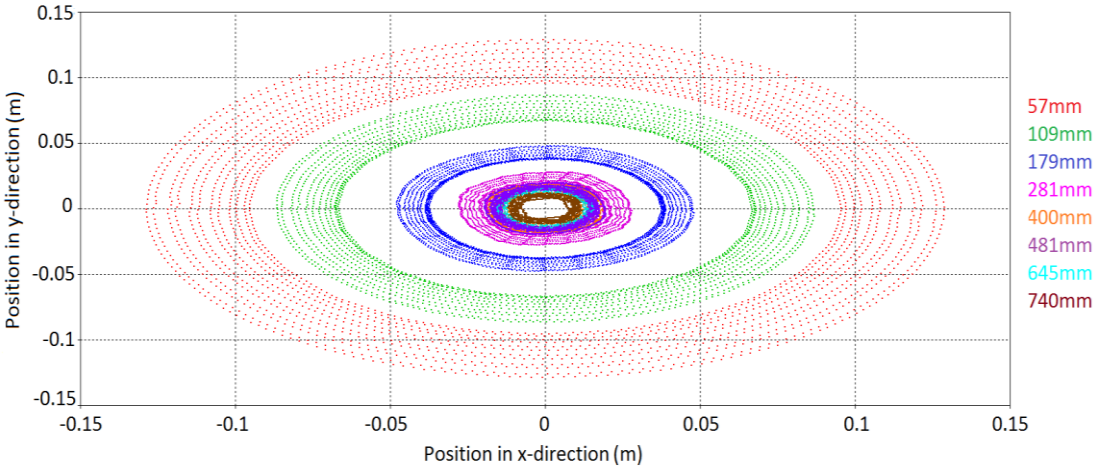

Figure 87 Phase space of planes in z direction for annular beam electron gun in Figure 84

Annular beam geometry in Figure 84 is changed to have greater beam current. First, anode extraction gap is raised to 68.5mm while anode cathode gap is reduced to 123mm. The radius of annular cathode is not changed however electrode consisting of emission area geometry is slightly different from initial geometry. Optimized annular beam electron gun geometry is obtained by these modifications. Magnetic field is applied in this configuration and it is also modified such that peak B field is 0.15T. The applied B field along z-direction is given in Figure 88. Optimized annular beam geometry is illustrated in Figure 89. Beam trajectory and particle monitors locations are also given in Figure 89. Electron beam current is found as 574A; therefore more beam current than initial geometry is achieved. In Pierce gun parametrical analysis, increase of anode extraction gap and decrease of anode cathode gap also help to obtain more beam current.

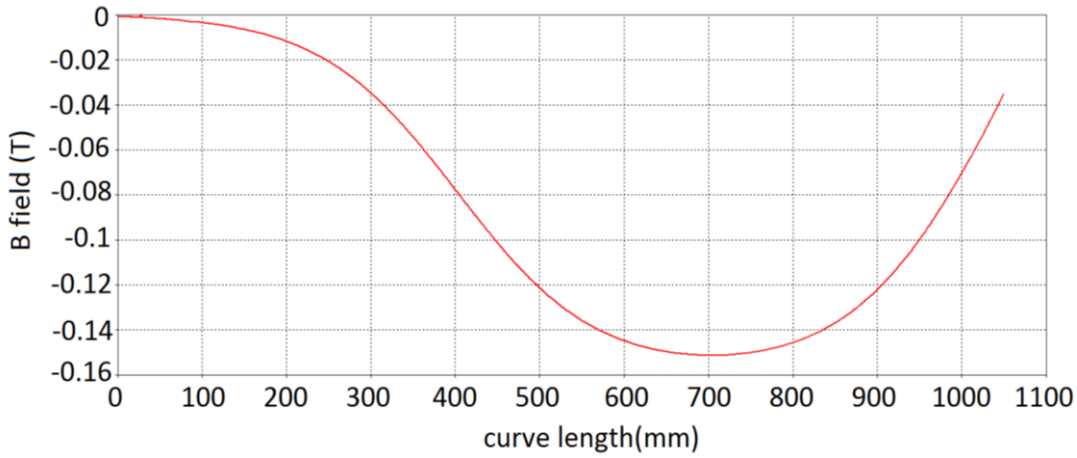

Figure 88 B field along geometry of optimized annular beam electron gun geometry in z direction in Figure 89

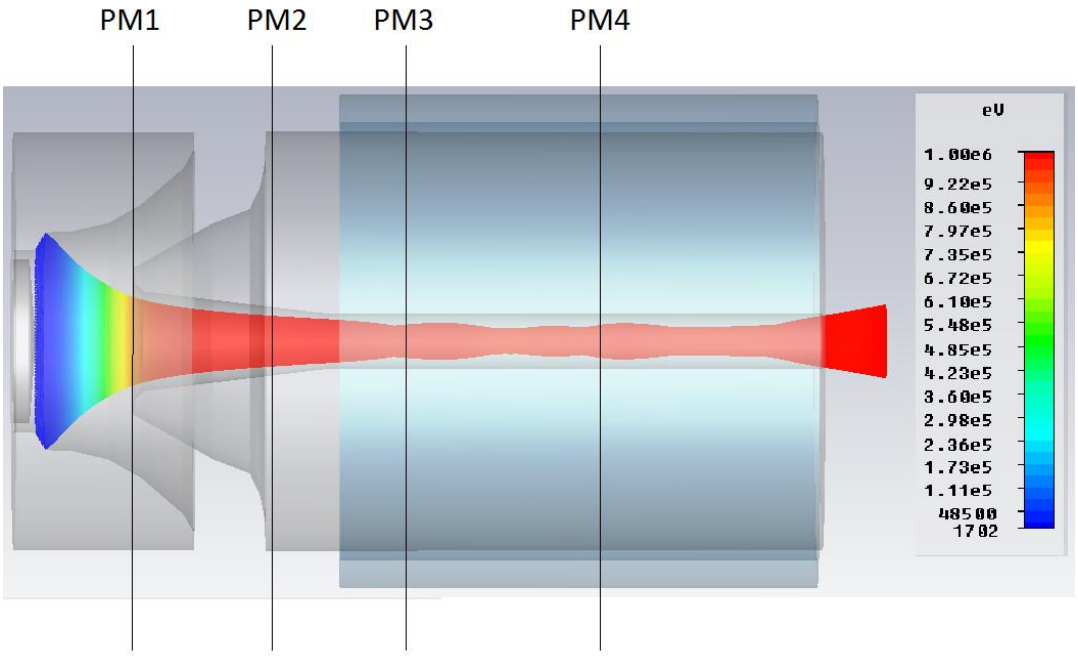

Figure 89 Beam trajectory for optimized annular beam electron gun with permanent magnet

In Figure 90, phase space plots for particle monitors in Figure 89 are shown. The plots are similar to phase space plots of initial geometry as expected. Annular beam shape can be observed for all plots in Figure 90. Moreover, in Figure 91 nine particle monitors results are given and it is understood that annular shape of electron gun is preserved along the optimized annular beam electron gun geometry.

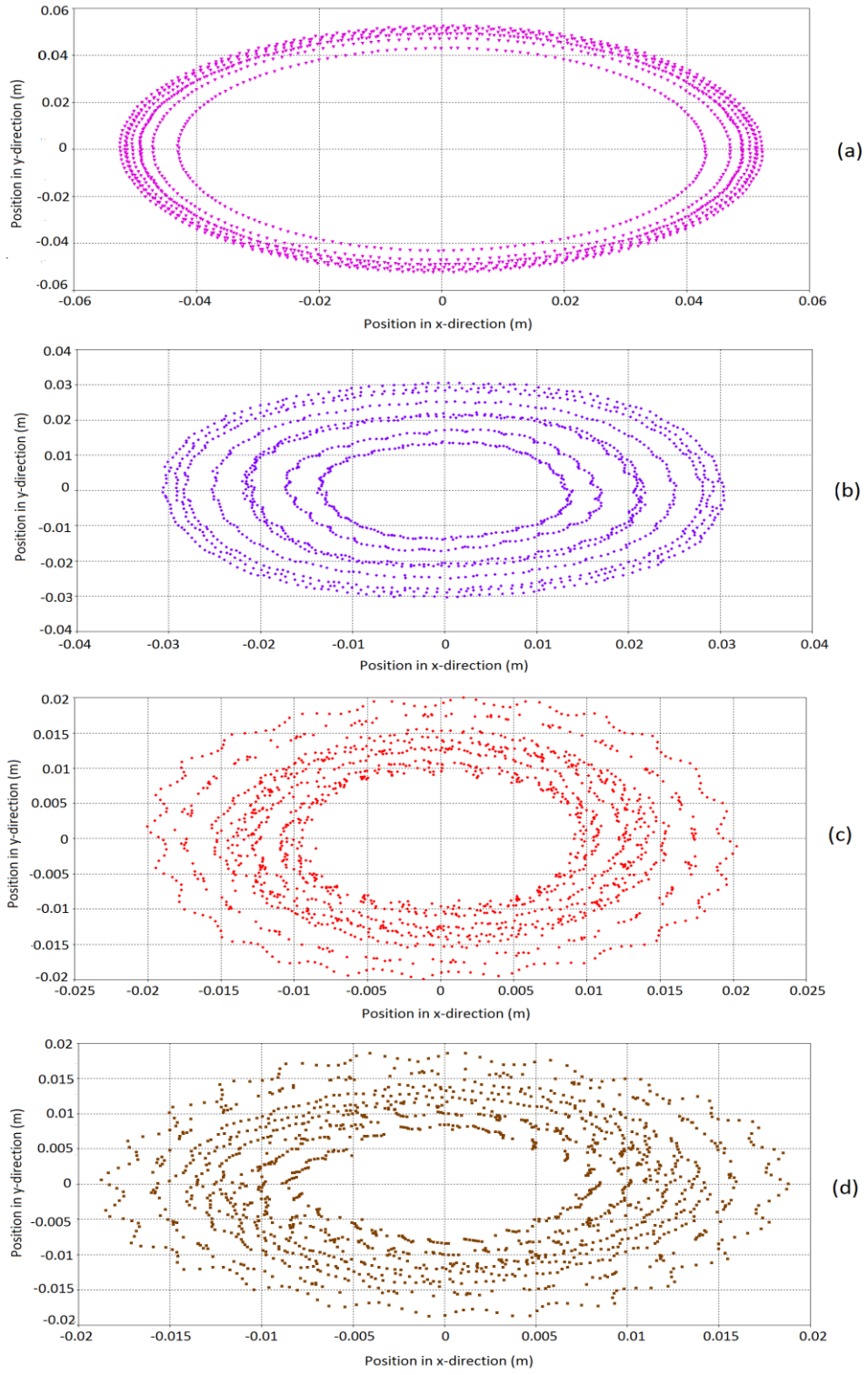

Figure 90 Phase space of planes in z direction for optimized annular beam electron gun with permanent magnet in Figure 89, (a) PM1, distance to origin=157mm, (b) PM2, distance origin=327mm, (c) PM3, distance to origin=495mm, (d) PM4, distance to origin=732mm

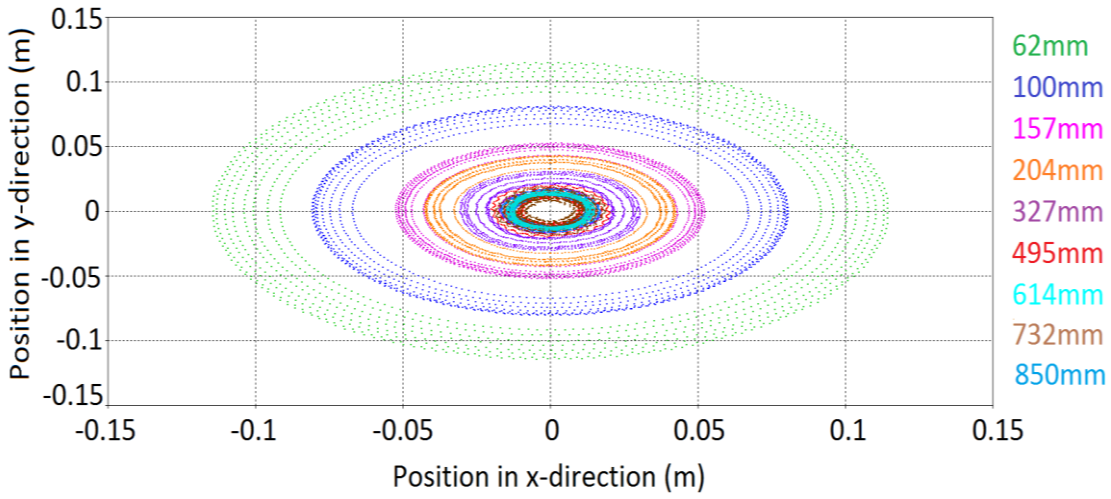

Figure 91 Phase space of planes in z direction for optimized annular beam electron gun in Figure 89

CHAPTER 6

CONCLUSION & FUTURE WORK

The aim of this thesis is to design and simulate specific electrons guns for TWT by PIC code CST PS. According to desired electron beam parameters such as current, perveance and beam shape, various type of electron gun in literature are simulated and optimized.

Simulation tools are very important in charged particle problems. Electron gun simulation includes electron motion under electromagnetic fields in a specific geometry, which is very complicated problem. In order to simulate these problems, simulation tools based on PIC code should be used.

In first part of thesis, analytical solution which describes the charged particles motion under electric and magnetic fields and Pierce gun design procedure were mentioned. Then, Pierce gun parametrical simulation was performed. At the beginning of simulation studies, various PIC codes are mentioned. Also, CST PS Tracking Solver which is used in this thesis was described in detail. The purpose of Pierce gun parametrical analysis is to validate compatibility of computer simulations with analytical solution and to understand effects of geometrical and electrical parameters on beam quality. After the Pierce gun parametrical analysis, relation between beam parameters and analysis parameters was obtained. Moreover, beam controlling method with focus electrode was also validated by this simulation. Furthermore, it is concluded that relation derived from Pierce gun parametrical simulation can be used to optimize not only Pierce gun but also different types of gun.

In order to observe magnetic field effects, a Pierce gun with long anode extraction region was simulated and divergence of electron beam was observed. In order to

confine electron beam inside anode extraction region, axial magnetic field should be applied. In simulation, magnetic field was created with solenoid and its focusing effect was seen. Moreover, change of ripple on electron beam envelope was shown for two different magnetic fields.

In last part of the thesis, specific electron guns were simulated and optimized. First, parametrical analysis Pinto-Xavier-Motta electron gun, which is designed for C-band TWT, was performed and beam parameters according to analysis parameter were obtained. In this simulation, results are similar to Pierce gun parametrical analysis although focus electrode and anode geometry is different than those of Pierce gun. After this analysis, gridded version of Pinto-Xavier-Motta electron gun was simulated. For desired beam current and perveance values for gridded gun, geometrical dimension was chosen from Pinto-Xavier-Motta parametrical analysis, then grid is added to this geometry. This time, grid control technique for beam pulsing were investigated. It is observed that with modulating grid voltage, electron beam can be switched.

The second geometry was dual anode electron gun. The purpose of dual anode is to lengthen the life of electron gun especially in space applications. In this simulation 0.14uP, 75mA electron beam was aimed. In order to have these beam parameters, required configuration of electrode potential was illustrated. Furthermore, optimized geometrical parameters were given and it is shown that desired beam was achieved by these geometrical parameters. Besides, axial magnetic field was applied to the geometry with permanent magnet and beam focusing can be achieved for this geometry.

Final geometry was annular beam electron gun which is used in HPM systems like relativistic magnetron or relativistic BWO. Since annular beam electron gun provides more beam current than solid beam, it is preferred in high power systems. In this section, annular beam and solid beam whose anode extraction region has same dimension, was simulated and compared. Current of annular beam electron gun was almost double of that of solid beam electron gun. Moreover, it is observed that without axial magnetic field, it is impossible to obtain well focused electron beam in

annular beam electron gun. Therefore, beam focusing was accomplished by axial magnetic field by permanent magnet. Then, geometry of annular beam electron gun was optimized to have more beam current. Both first and optimized annular beam electron gun, annular beam shape was represented by particle monitors.

In this thesis, CST PS Tracking Solver was used since this solver is specific tool for design of electron gun and collector. However, time domain analysis of electron gun could not be performed by Tracking Solver. Time domain simulator of CST PS is PIC Solver; however PIC solver is designed to simulate RF and electron beam interaction part of vacuum devices such as TWT interaction circuits. In CST PS, in order to simulate a vacuum tube, electron gun part should be simulated in Tracking Solver and steady state beam parameter should be taken. Then beam parameters are imported to PIC Solver. Therefore, in this thesis, only steady state beam parameter of electron gun could be obtained and transient effects cannot be observed. Transient analysis of electron gun and analysis of formation of electron beam could be subject of future work. In this study, effect of time variant cathode potential or beam controlling technique can be investigated more effectively. However, CST PS is not suitable this kind of study. On the other hand, MAGIC can be useful for this type of simulation, since it is algorithm is based on FDTD and all simulations are done in time domain. Another research topic can be matching one of the electron gun design in this thesis to a vacuum tube device in CST PIC Solver.

REFERENCES

[1] G. Faillon, G. Kornfeld, E. Bosch, and M.K. Thumm, "Microwave Tubes," in *Vacuum Electronics: Components and Devices*, J.A.Eichmeier and M.K. Thumm, Ed. Berlin: Springer, 2008, pp. 1–50.

[2] J. C. Whitaker, *Power Vacuum Tubes Handbook*, 2nd ed., vol. 1. Florida: CRC Press, 2000, pp. 1-12 and pp. 322-330.

[3] A. S. Gilmour, *Principles of Travelling Wave Tubes*. Norwood: Artech House, 1994, pp.1-11 and pp. 123–135.

[4] M. N. Pinto, C.C. Xavier and C.C. Motta, "An Electron Gun Design for a C-Band TWT," *International Microwave and Optoelectronics Conference,* pp. 947-940, Oct. 29, 2011-Nov. 1, 2011.

[5] Shulim E. Tsimring, *Electron Beams and Microwave Vacuum Electronic.* New Jersey: Wiley, 2007, pp. 297-298.

[6] A. S. Gilmour, *Klystrons, Traveling Wave Tubes, Magnetrons, Crossed-Field Amplifiers, and Gyrotrons.* Norwood, 2011, pp. 96 and pp. 114-117.

[7] S. Humphries, *Charged Particle Beams.* New Mexico: Field Precision, 2002, pp. 187-204, pp. 232-239 and pp. 262-283.

[8] Space Charge Particle Optics. Stanford Linear Accelerator Center. [Online]. Available: http://www.egun-igun.com/ (Last accessed on March 12, 2014).

[9] S. Coco, S. Corsaro, A. Laudani, G. Pollicino, R. Dionisio, and R. Martorana "COLLGUN: a 3D FE Simulator for the Design of TWTs Electron Guns and Multistage Collectors," *Scientific Computing in Electrical Engineering Mathematics in Industry*, September 2010.

[10] (2014). CST Particle Studio. Computer Simulation Technologies. [Online]. Available: https://www.cst.com/Products/CSTPS (Last accessed on April 4, 2014).

[11] C.C. Xavier and C.C. Motta, "Design of a Gridded Electron Gun for Traveling-Wave Tubes: an EGUN case study," *IEEE International Vacuum Electronics Conference*, vol. 9, pp. 175-180, 2006.

[12] M.V. Fazio, B. Carlsten, C. Fortgang, K. Habiger, E. Nelson, B. Arfin, G. Caryotakis, A. Haase and G. Scheitrum, "Design for a One Gigawatt Annular Beam Klystrons," *International Linear Accelerator Conference*, pp. 785-787, August 21-25, 2000.

[13] J. E. Han, M. Yoony and S. Y. Parkz, "Design Study of an Electron Gun for a High Power Microwave Source," *Journal of the Korean Physical Society,* vol. 44, no. 5, pp. 1265-1268, May 5, 2004.

[14] D. A. Zavadil, "Dual Beam Dual Mode TWTA," *International Electron Devices Meeting*, pp. 209-211, December 9-11, 1974.

[15] W. Czarczynski and J. Sobanski, "Electron gun design for multiple-beam, coupled-cavity traveling wave tube," *International Conference on Microwave, Radar and Wireless Communications*, pp. 877-880, May 22-24, 2006.

[16] R. K. Sharma, V. S. V. Raju and V. Srivastava, "Design of Dual Anode Electron Gun for Ku Band 140 W Space TWTA," *IEEE International Conference on Vacuum Electronics,* pp. 122-123, May 28-30, 2003.

[17] A. R. Choudhury, R. K Sharma, S. M Sharma, S. Arya, A. Bera and V. Srivastava, "Dual Anode Electron Gun for Ka-Band Helix TWT," *International Conference on Recent Advances in Microwave Theory and Applications*, pp. 192-195, November 21-24, 2008.

[18] R. K. Sharma, P. Sharma, A. R Choudhury, S. M. Sharma, S. Arya and V. Srivastava, "P2-19: Design of Dual Anode Electron Gun and Beam Focusing

for Ku-band 140W Short Length Space TWT," *IEEE International Vacuum Electronics Conference*, pp. 259-260, May 18-20, 2010.

[19] R. K. Sharma, A. R. Choudhury, S. M. Sharma, S. Arya, A. Bera and V. Srivastava, "Dual Anode Electron Gun & PPM Focusing for Ka-Band TWT," *IEEE International Vacuum Electronics Conference*, pp. 185-186, April 28-30, 2009.

[20] Electron beam. (2013). Encyclopedia Britannica. [Online]. Available: http://www.britannica.com/EBchecked/topic/183490/electron-beam (Last accessed on December 21, 2013).

[21] D. Tskhakaya, "The Particle-in-Cell Method," in *Lecture Notes in Physics 739*, H. Feshske, R. Schneider and A. Weiβe, Ed. Berlin: Springer, 2008, pp. 161-163.

[22] W. B. Herrmannsfeldt, "EGUN - an Electron Optics and Gun Design Program," Stanford Linear Accelerator Center and Stanford University, Stanford, California, SLAC-331-UC-28(A), Oct. 1988.

[23] R. Becker and W. B. Herrmannsfeldt, "The Design of Electron and Ion Guns, Beams and Collectors," *Journal of Physics,*Conference Series 2, pp. 152-163, 2004.

[24] K.P Artyomov, V.V Ryzhov, G.A Naumenko and M.V Shevelev, "PIC code KARAT simulation of different types of polarization radiation generated by relativistic electron beam," *Journal of Physics,* Conference Series 357, 2012.

[25] S.V. Samsonova, V.L. Bratmana, G.C. Burtb, A.W. Crossb, G.G. Denisova, A.D.R. Phelpsb and K. Ronaldb, "Generation and Compression of Frequency Modulated Pulses from a Relativistic BWO," *International Conference on High Power Particle Beams*, pp. 430-433, July 18-23, 2004.

[26] MAGIC Description FDTD-PIC Software for EM Design and Simulation. Alliant Techsystems Operations. [Online]. Available:

http://www.mrcwdc.com/magic/description.html (Last accessed on April 8, 2014).

[27] A. J. Woods, L.D. Ludeking and D.L. Rhoades, "Performance Enhancement of FDTD-PIC Beam-wave Simulations Using Multi-core Platforms," *PIERS Proceedings*, pp. 52-55, March 22-26, 2010.

[28] A.J. Woods and L.D. Ludeking, "MAGIC Electromagnetic FDTD-PIC Code Dense Plasma Model Comparison with LSP," *The Open Plasma Physics Journal*, pp. 73-77, April, 2010.

[29] L.D. Ludeking and A.J. Woods, "Well Matched Electromagnetic Boundary in FDTD-PIC for Charged Particle Penetration," *The Open Plasma Physics Journal*, pp. 53-59, January, 2010.

[30] Y.B.Yetkil, F.E. Sağcan, Ş. Demir, "Eş Eksenel Yapıdaki Silindirik Bir Virkatörün Teorik, Ve Sayısal Yöntemlerle İncelenmesi," *SAVTEK Conference*, 2012.

[31] H. Spachmann and U. Becker, "Electron Gun Simulation with CST PARTICLE STUDIO," *Nuclear Instruments and Methods in Physics Research*, sec. A, vol. 558, issue 1, pp. 50-53, March 2006.

[32] F. Hamme, U. Becker and P. Hammes, "Simulation of Secondary Electron Emission with CST PARTICLE STUDIO," *Proceedings of ICAP*, pp. 160-163, 2006.

[33] N.N. Esfahani, M. Tayarani1 and K. SchÄunemann, "Design and 3-D Particle-in-Cell Simulation of a 140GHz Spatial-Harmonic Magnetron," *Progress In Electromagnetics Research*, vol. 133, pp. 443-458, 2013.

[34] C. Nieter and J.R. Cary, "VORPAL: a Versatile Plasma Simulation Code," *Journal of Computational Physics,"* vol. 196, issue 2, pp. 448-473, May 20, 2004.

[35] L. Brieda, "Development of the DRACO ES-PIC Code and Fully-Kinetic Simulation of Ion Beam Neutralization," M.S. thesis, Dept. Aerospace Engineering Eng., Virginia Polytechnic Institute and State University, Blacksburg, Virginia, June 2, 2005.

[36] H. Zhang, J. Wang, and C. Tong, "Particle-in-cell Simulation of a Novel High Power Terahertz Vacuum Electron Device," *Progress in Electromagnetics Research Symposium*, pp. 425-430, July 2-6, 2008.

[37] G. Lapenta, "Particle In Cell Method, A brief description of the PIC Method," Centrum voor Plasma Astrofysica Katholieke Universiteit Leuven, unpublished.

[38] (2009, March). CST Particle Studio, Solvers and Applications. Computer Simulation Technologies. [Online]. Available: https://www.cst.com/Content/Events/UGM2009/6-3-1-CST-PARTICLE-STUDIO-2009.pdf (Last accessed on March 25, 2014).

[39] M. Clemens, S. Drobny, H. Krugert, P. Pindert, O. Podebrad, B. Schillinger, B. Trapp, T. Weiland, M. Wilket, "The Electromagnetic Simulation Software Package MAFIA 4," *International Conference on Computational Electromagnetics and Its Application*, pp. 565-568, 1999.

[40] F. Wolfheimer. Latest Developments in 3D Charged Particle Simulations, Computer Simulation Tool. [Online]. Available: http://accelconf.web.cern.ch/accelconf/icap2012/talks/moaai2_talk.pdf (Last accessed on April 8, 2014).

[41] (2007, October). CST Particle Studio, Features and Application Examples. Computer Simulation Technologies. [Online]. Available: https://www.cst.com/Content/Events/UGM2007/04-Balk.pdf (Last accessed on March 25, 2014).

APPENDIX-A

LANGMUIR FUNCTION VERSUS NORMALIZED RADIUS FOR CONVERGING BEAM

$R = r/R_s$	α^2	$R = r/R_s$	α^2
1.0000	0.0000	0.1923	8.636
0.9524	0.0024	0.1852	9.135
0.9091	0.0096	0.1786	10.01
0.8696	0.0213	0.1724	10.73
0.8333	0.0372	0.1667	11.46
0.8000	0.0571	0.1538	13.35
0.7692	0.0809	0.1429	15.35
0.7407	0.1084	0.1333	17.44
0.7143	0.1396	0.1250	19.62
0.6897	0.1740	0.1176	21.89
0.6667	0.2118	0.1111	24.25
0.6250	0.2968	0.1053	26.68
0.5882	0.394	0.1000	29.19
0.5556	0.502	0.0833	39.98
0.5623	0.621	0.0714	51.86
0.5000	0.750	0.0625	64.74
0.4762	0.888	0.0556	78.56
0.4545	1.036	0.0500	93.24
0.4348	1.193	0.0333	178.2
0.4167	1.358	0.0250	279.6
0.4000	1.531	0.0200	395.3
0.3846	1.712	0.0167	523.6
0.3704	1.901	0.0143	663.3
0.3571	2.098	0.0125	813.7
0.3448	2.302	0.0111	974.1
0.3333	2.512	0.0100	1144
0.3125	2.954	0.0083	1509
0.2941	3.421	0.0071	1907
0.2778	3.913	0.0063	2333
0.2632	4.429	0.0056	2790
0.2500	4.968	0.0050	3270
0.2381	5.528	0.0040	4582
0.2273	6.109	0.0033	6031
0.2174	6.712	0.0029	7610
0.2083	7.334	0.0025	9303
0.2000	7.976	0.0020	13015

APPENDIX-B

LANGMUIR FUNCTION VERSUS NORMALIZED RADIUS FOR CONVERGING BEAM

$R = r/R_s$	α^2	$R = r/R_s$	α^2
1.0	0.0000	6.5	1.385
1.05	0.0023	7.0	1.453
1.1	0.0086	7.5	1.516
1.15	0.0180	8.0	1.575
1.2	0.0299	8.5	1.630
1.25	0.0437	9.0	1.682
1.3	0.0591	9.5	1.731
1.35	0.0756	10	1.777
1.4	0.0931	12	1.938
1.45	0.1114	14	2.073
1.5	0.1302	16	2.189
1.6	0.1688	18	2.289
1.7	0.208	20	2.378
1.8	0.248	30	2.713
1.9	0.287	40	2.944
2.0	0.326	50	3.120
2.1	0.364	60	3.261
2.2	0.402	70	3.380
2.3	0.438	80	3.482
2.4	0.474	90	3.572
2.5	0.509	100	3.652
2.6	0.543	120	3.788
2.7	0.576	140	3.903
2.8	0.608	160	4.002
2.9	0.639	180	4.089
3.0	0.669	200	4.166
3.2	0.727	250	4.329
3.4	0.783	300	4.462
3.6	0.836	350	4.573
3.8	0.886	400	4.669
4.0	0.934	500	4.829
4.2	0.979	600	4.960
4.4	1.022	800	5.165
4.6	1.063	1000	5.324
4.8	1.103	1500	5.610
5.0	1.141	2000	5.812
5.2	1.178	5000	6.453
5.4	1.213	10000	6.933
5.6	1.247	30000	7.693
5.8	1.280	100000	8.523